On a precise check of the standard model in an experiment with a ^{90}Sr beta source

L. A. Mikaélyan, V. V. Sinev, and S. A. Fayans
Kurchatov Institute Russian Science Center, 123182 Moscow, Russia

(Submitted 4 February 1998; resubmitted 24 February 1998)
Pis'ma Zh. Éksp. Teor. Fiz. **67**, No. 7, 435–439 (10 April 1998)

A discussion is given on the prospects for making a precise determination of the value of $\sin^2\theta_W$ (θ_W is the Weinberg angle) and for improving the sensitivity of the search for the antineutrino magnetic moment to $\approx 1.5\times 10^{-11}\mu_B$ and for the $\tilde{\nu}_e \leftrightarrow \tilde{\nu}_x$ mixing parameter to $\sin^2 2\theta \approx 10^{-2}$ by measuring in a single experiment the cross sections for $\tilde{\nu}_e e$ scattering for the reaction $\tilde{\nu}_e p \rightarrow e^+ n$. Such an experiment with $\sim 100\,000$ events/yr detected for each reaction can be carried out, for example, using the BOREXINO detector and an approximately 10 MCi ^{90}Sr source. © *1998 American Institute of Physics.*
[S0021-3640(98)00107-8]

PACS numbers: 12.10.Dm, 14.60.Lm, 14.60.Pq, 13.10+q, 27.60.+j

In this paper we discuss the prospects for checking the standard model of electroweak interactions and the search for phenomena outside the limits of the initial premises of the model in an experiment with electron antineutrinos from a ^{90}Sr beta source and an expected counting rate of more than 100 000 events per year from $\tilde{\nu}_e e$ scattering and from the reaction

$$\tilde{\nu}_e + p \rightarrow e^+ + n. \tag{1}$$

The standard model actually remains unverified in its initial and theoretically well-understood sector of first-generation leptons. In nuclear-reactor experiments the $\tilde{\nu}_e e$ scattering cross section is at present measured with a relative error of $\sim 50\%$ (see, for example, Ref. 1).

A neutrino could possess a magnetic moment of the order of $10^{-11}\mu_B$,[2,3] which is many orders of magnitude larger than the value admitted by the standard model. The discovery of such a moment in a laboratory experiment would have important consequences for particle physics and astrophysics. The limit $\mu \leqslant 2\times 10^{-10}\mu_B$,[4] which is still far from the desired range of values, has been obtained using the reactors in Rovno and Krasnoyarsk.

The new possibilities which are discussing in the present letter are due to a revolution that is now occurring in the technology of detecting the scattering of neutrinos by electrons and the inverse beta decay reaction (1). The crux of this revolution is a large

TABLE I. Number of $\tilde{\nu}_e e$ scattering and inverse beta decay events expected per year in the working volumes of the BOREXINO detector (300 tonnes) and Kam-LAND detector (1000 tonnes) from distant reactors, the Earth's radioactivity (U/Th; Ref. 6) and from a ^{90}Sr source.

Antineutrino source	BOREXINO[1)]		Kam-Land[1)]	
	$\tilde{\nu}_e e$[2)]	$\tilde{\nu}_e p \to e^+ n$	$\tilde{\nu}_e e$[2)]	$\tilde{\nu}_e p \to e^+ n$
Reactors	–	27	–	770
U/Th	–	9–60	–	41–150
^{90}Sr, 10 MCi	250×10^3	190×10^3	350×10^3	270×10^3

Notes: [1)]The distances from the source to the center of the BOREXINO and Kam-Land detectors are 10 m and 15 m, respectively. [2)]In the recoil electron energy interval 250–1500 keV.

increase in the volume of the liquid organic scintillator, serving as the target for neutrinos, together with a decrease of the background level.

The BOREXINO detector, to be built in the underground Gran Sasso Laboratory, is intended for studying the soft part of the solar neutrino spectrum by detecting single electrons from $\tilde{\nu}_e e$ scattering in the recoil energy range >250 keV. It is expected[5] that the background of solitary events will reach the unprecedentedly low level of ~ 10 events per day (for 100 tonnes of scintillator). The plan is to use the BOREXINO detector and the Kam-LAND detector (the useful mass of the liquid scintillator is 1000 tonnes), which is now under construction in Japan, to detect reactor antineutrinos at distances of hundreds of kilometers from the reactors and also to begin studying the uranium and thorium concentrations in the earth by detecting antineutrinos from beta decay of their daughter products. The expected counting rates of the events due to the reaction (1) which were found in Ref. 6 are presented in Table I.

The experiment discussed in the present letter has an important feature: As will become evident from the discussion below, its results will be, to a first approximation, independent of the source activity, the geometry of the experiment, and even the absolute electron and proton densities in the target.

DETECTOR AND SOURCE

In the BOREXINO detector (see Fig. 1) the target for antineutrinos is a liquid organic scintillator which is viewed by photomultipliers through a 2-m layer of oil separated from the scintillator by a transparent film. The $\tilde{\nu}_e e$ scattering events will be detected from the solitary recoil electrons, while the inverse beta decay events will be detected from positron–neutron pairs which are correlated in time and space. The construction of the Kam-LAND detector is close to that shown in Fig. 1, but there is still some question as to whether or not $\tilde{\nu}_e e$ scattering can be detected. ^{90}Sr ($E_{\nu\,\max}=546$ keV, $T_{1/2}=28.6$ yr) decays to the ground state of ^{90}Y ($E_{\nu\,\max}=2279$ keV, $T_{1/2}=64$ h), which with a 99.988% probability populates the ground state of the stable ^{90}Zr nucleus, so that there are two antineutrinos per ^{90}Sr decay.

Two circumstances make this source especially attractive. First, it can be used to generate both $\tilde{\nu}_e e$ scattering and inverse beta decay events, and, second, such sources are produced commercially in Russia and some other countries and are used as a source of heat in radioisotope thermoelectric generators. This latter circumstance is very important

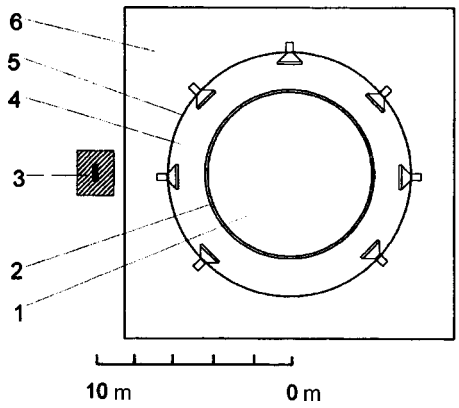

FIG. 1. BOREXINO detector (diagram): *1* — liquid organic scintillator (300 tonnes), *2* — transparent film, *3* — shielded source, *4* — oil, *5* — metal sphere holding photomultipliers, *6* — water.

for practical realizability of the experiment which we are discussing here. To produce a 10 MCi source it is necessary to assemble a bank of ~80 standard 2-liter containers with a total energy release of about 75 kW. The source in the working position at the detector must be surrounded with an approximately 500 g/cm^2 thick shield in order to absorb the bremsstrahlung. We note the possibilities of producing a ^{90}Sr source and utilizing it in neutrino physics experiments were studied earlier in Refs. 7.

WEINBERG ANGLE, NEUTRINO MAGNETIC MOMENT OSCILLATIONS

1. We shall use the following expression for the differential cross section of the weak $\tilde{\nu}_e e$ scattering (see, for example, Ref. 2):

$$\frac{d\sigma^W}{dT}=g_F^2\frac{m}{2\pi}\left[(1+2x^2)^2(1-T/E)^2+4x^2-2x^2(1+2x^2)\frac{mT}{E^2}\right], \tag{2}$$

where E and T are the antineutrino energy and the electron kinetic energy, $g_F^2(m/2\pi)=4.31\times10^{-45}$ cm^2/MeV, $x^2=\sin^2\theta_W=0.232$, and m is the electron mass.

The cross section of the reaction (1) is given by[8]

$$\sigma(E)=9.556\times10^{-44}\frac{886}{\tau_n}[(E-\Delta)^2-m^2]^{1/2}(E-\Delta)(1+\delta)\text{cm}^2, \tag{3}$$

where E, $\Delta=1.293$, and m are expressed in MeV, the correction $\delta\ll1$ takes into account the effects of recoil and weak magnetism and a radiation correction, and τ_n is the lifetime of a free neutron in seconds. The numerical coefficient in Eq. (3) is now known to within ~0.15%. It can be expressed in terms of the combination $G_V^2+3G_A^2$ of vector and axial beta-decay constants.

In the spectrum of the Sr–Y source the detected energy of the positrons from the reaction (1) lies in the range 1.02–1.48 MeV. The netrons upon capture in hydrogen release an energy of 2.23 MeV.

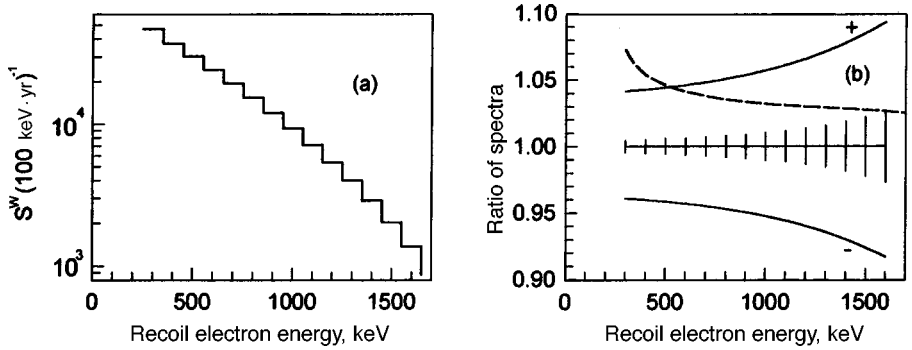

FIG. 2. a — Expected recoil-electron spectrum from scattering of antineutrinos from a ^{90}Sr–^{90}Y source. b — Relative change produced in the spectrum by a $\pm 5\%$ variation of the parameter $\sin^2\theta_W$ (solid lines) and by including a neutrino magnetic moment $\mu = 2.5\times 10^{-11}\mu_B$ (dashed line).

The recoil-electron spectrum S^W for $\tilde{\nu}_e e$ scattering due to the weak interaction and the number $N_{\nu p}$ of events from the reaction (1) which are measured in the experiment can be written as

$$S^W = C^W n_e g_F^2 F(T, \sin^2\theta_W), \quad N_{\nu p} = C^{\nu p} n_p (G_V^2 + 3G_A^2) s, \tag{4}$$

where C^W and $C^{\nu p}$ are coefficients which depend on the source strength and the geometry and n_e and n_p are, respectively, the number of electrons and protons in the volume. The function $F(T, \sin^2\theta_W)$ and the factor s are obtained by convolving the cross sections (2) and (3) with the antineutrino spectrum of the source. Hence one can see that the spectrum S^W normalized to the number of events due to the reaction (1),

$$S^W/N_{\nu p} \sim \frac{g_F^2}{G_V^2 + 3G_A^2} F(T, \sin^2\theta_W) \frac{n_e}{n_p}, \tag{5}$$

can be expressed in terms of the fundamental constants of the weak interaction and the ratio of the number of electrons and protons in the volume and is independent of the source activity and the geometry of the experiment.

2. The expected number of recoil electrons from $\tilde{\nu}_e e$ scattering in the energy interval 250–1500 keV is presented in Table I, while their energy spectrum is presented in Fig. 2a. The relative distortion produced in the spectrum by a $\pm 5\%$ change in the value of $\sin^2\theta_W$ used in Eq. (2) is shown in Fig. 2b.

The statistical error in determining $\sin^2\theta_W$ will equal $\sim 0.5\%$. However, if the normalization (5) is used and it is assumed that the ratio n_e/n_p will be known to within 0.5%, then the error in determining $\sin^2\theta_W$ will increase to $\sim 1\%$. Here it is pertinent to present a result obtained in the CHARM-II experiment, studying the scattering of muon neutrinos by electrons, where 5.5 thousand events were detected: $\sin^2\theta_W = 0.2324 \pm 2.5\%$ (stat.) $\pm 2.5\%$ (syst.).[9]

3. The existence of a neutrino magnetic moment $\mu = 2.5\times 10^{-11}\mu_B$ would change the spectrum in the manner shown by the dashed curve in Fig. 2b. Estimates show that when the normalization (5) is used, the limit of detection of μ should be ~ 1.3

$\times 10^{-11}\mu_B$, which should lower the existing limit for the electron neutrino by a factor of 15. For muon neutrinos the best limit on the magnetic moment was obtained in Ref. 10: $\mu < 7.4 \times 10^{-10}\mu_B$.

The question of the search for a neutrino magnetic moment with the aid of the BOREXINO detector and a ^{51}Cr neutrino source was studied in Ref. 11. With the expected sample of 1400 events the authors anticipate a sensitivity of $5 \times 10^{-11}\mu_B$.

4. The survival probability of a neutrino with energy E at a distance R from the source is given by the expression

$$P(\tilde{\nu}_e \to \tilde{\nu}_e) = 1 - \sin^2 2\theta \cdot \sin^2\left(\frac{1.27\Delta m^2(\mathrm{eV}^2)R(\mathrm{m})}{E(\mathrm{MeV})}\right), \tag{6}$$

where $\sin^2 2\theta$ is the mixing parameter, $\Delta m^2 = |m_1^2 - m_2^2|$, and m_1 and m_2 are the masses of the interfering states. The second term in Eq. (6) gives the probability of the appearance of next-generation neutrinos $\tilde{\nu}_{\mu,\tau}$ or sterile neutrinos. The neutrinos $\tilde{\nu}_{\mu,\tau}$ that appear are scattered by electrons on account of the neutral current, but they vanish completely from the inverse beta decay detection channel. Analysis of this situation could yield rich information and will be performed elsewhere.

Here we shall consider the case where oscillations can appear in the form of a periodic spatial modulation of the smoothly decaying (with increasing distance from the source) field of detected inverse beta decay reaction events. The distance between the neighboring maxima is determined from the condition $1.27\Delta m^2 l_\nu / E = \pi$ and the degree of modulation equals $\sin^2 2\theta$. For estimates, we can take $E \approx 2.1$ MeV, which corresponds to a narrow range of energies from the threshold of the $\tilde{\nu}_e$ reaction to the ^{90}Y spectrum limit, so that $l_\nu \approx 5.2/\Delta m^2$ m. In the region $\Delta m^2 > 4$ eV^2, or $l_\nu < 1.3$ m, the periodic structure starts to broaden on account of the spatial resolution, while for $\Delta m^2 < 0.7$ eV^2 the structure no longer fits within the working volume. We note that the characteristics of this structure — the period and amplitude — are determined only by the parameters of the oscillations.

The problem of the interaction of an electron neutrino with an electron arose, as is well known, in the mid-1930s and it has never been studied experimentally. Only now has it become possible to study this problem at the modern level of understanding. As far as neutrino oscillations are concerned, it seems that the approach discussed here can greatly increase the sensitivity to the mixing parameter in the region $\Delta m^2 > 0.3$ eV^2 as compared with nuclear-reactor experiments[12] and accelerator experiments, excluding in the latter case only the ''appearance'' experiments on $\tilde{\nu}_\mu \to \tilde{\nu}_e$ (Ref. 13).

We thank O. Zaĭmidorog and A. Starostin for helpful discussions and I. Machulin for assistance. This work was supported by the Russian Fund for Fundamental Research, Grants 97-02-16031 and 96-15-96640.

[1] G. S. Vidyakin, V. N. Vydorov, I. I. Gurevich *et al.*, JETP Lett. **55**, 206 (1992).
[2] M. Voloshin, M. Vysotskiĭ, and L. Okun', Zh. Éksp. Teor. Fiz. **91**, 754 (1996) [Sov. Phys. JETP **64**, 446 (1986)].
[3] D. Oakley *et al.*, Astrophys. J. **437**, 437 (1994).
[4] A. V. Derbin, Yad. Fiz. **57**, 236 (1994) [Phys. At. Nucl. **57**, 222 (1994)].
[5] G. Ranucci, TAUP-97 Conf., Nucl. Phys. B, Proc. Suppl., 1998, to be published.

[6] R. S. Raghavan, S. Schoenert, S. Enomoto *et al.*, Phys. Rev. Lett. **80**, 635 (1998); F. Suekane, Talk at Tohoko Univ., August 26, 1997; S. Schoenert, S. Enomoto, Sendai, Japan, unpublished.
[7] A. Borovoĭ, L. Mikaélyan, and Yu. Chushkin, IAE Report No. 12/1244 [in Russian], Kurchatov Institute of Atomic Energy, 1974; C. Arpesella *et al.*, Borexino Proposal, INFN Report, Milano, 1991; O. Zaimidoroga, JINR Rapid Communications, 5/56/-92; L. Mikaelyan and I. Machulin, IAE Report 50.05-17/9, 1997.
[8] P. Vogel, Phys. Rev. D **29**, 1918 (1984); S. Fayans, Yad. Fiz. **42**, 929 (1985) [Sov. J. Nucl. Phys. **42**, 590 (1985)].
[9] P. Villian *et al.*, Phys. Lett. B **335**, 246 (1994).
[10] D. A. Krakauer, R. L. Talga, R. C. Allen *et al.*, Phys. Lett. B **252**, 177 (1990).
[11] N. Ferrary, G. Fiorentini, and B. Ricci, Phys. Lett. B **387**, 427 (1996).
[12] Y. Declais *et al.*, Phys. Lett. B **338**, 383 (1994); B. Achkar *et al.*, Nucl. Phys. B **534**, 503 (1995).
[13] J. Kleinfeller *et al.*, in *Neutrino-96, Proceedings of the 17th Conference on Neutrino Physics and Astrophysics*, Helsinki, June 13–19, 1996, edited by K. Enqvist *et al.*, World Scientific (1997), p. 193; C. Athanassopoulos, L. B. Auerbach, D. A. Bauer *et al.*, Phys. Rev. Lett. **75**, 2650 (1995).

Translated by M. E. Alferieff

Search for anomalous transmission of ultracold neutrons through metal foils

Al. Yu. Muzychka and Yu. N. Pokotilovskiĭ[a)]
Joint Institute for Nuclear Research, 141980 Dubna, Moscow Region, Russia

P. Geltenbort
Institute Laue–Langevin, B. P.156 F-38042, Grenoble, France

(Submitted 23 February 1998)
Pis'ma Zh. Éksp. Teor. Fiz. **67**, No. 7, 440–444 (10 April 1998)

Results are presented on the search for anomalous transmission of ultracold neutrons (UCNs) through beryllium (thickness ~ 0.14 mm), stainless steel (0.05 and 0.015 mm), and copper (0.01 and 0.018 mm) foils. This anomalous transmission is considered to be a possible reason for the disappearance of UCNs from beryllium bottles, an effect which was discovered in experiments at the St. Petersburg Nuclear Physics Institute and which was recently observed in the experiment of V. E. Varlamov *et al.*, JETP Lett. **66**, 336 (1997). No transmission was found in our measurements at the 10^{-7} level except in the case of copper foils, which we attribute to the presence in the UCN flux of an admixture of neutrons with energies higher than the boundary energy for copper.
[S0021-3640(98)00207-2]

PACS numbers: 25.40.Dn

1. INTRODUCTION

The storage times of ultracold neutron (UCNs) in closed volumes or, equivalently, the anomalous losses of UCNs upon reflection from the inner surfaces of UCN traps present a well-known and long-standing puzzle. The most surprisingly large discrepancy in the experimental and predicted loss coefficients was observed for the most promising materials for high UCN storage times: cold beryllium[1] and solid oxygen.[2] The anomaly observed in Refs. 1 and 2 consists in an almost temperature-independent (in the temperature interval 10–300 K) wall loss coefficient ($\sim 3\times 10^{-5}$), corresponding to an extrapolated inelastic thermal neutron cross section $\sigma^* \sim 0.9$ b. This experimental figure for Be is two orders of magnitude greater than the theoretical one, the latter being completely determined at a low temperature by the neutron capture in Be (0.008 b). The experiment/theory ratio for a very cold oxygen surface achieves three orders of magnitude.[2] The approximate universality of the loss coefficient for beryllium and oxygen, and the independence of the Be figures of temperature, forces one to suspect a universal reason for this anomaly. A series of experiments to find the channel by which UCNs leave the trap are described in Ref. 1. None of the suspected reasons has been confirmed: surface contamination by dangerous elements with large absorption cross sections, penetration of

UCNs through possible microcracks in the surface layers of Be, the hypothetical process of milliheating of UCNs due to collisions with a low frequency vibrating surface, and the upscattering of UCNs due to thermal vibrations of the wall nuclei.

Recently an experiment was published[3] describing the observation of subbarrier penetration of UCNs in the energy interval $\sim(0.5\text{–}1.8)\times10^{-7}$ eV through a rolled beryllium foil. The thickness of the foil was 56 μm, and the calculated boundary energy E_b for beryllium according to the usual formula $E_b=2\pi\hbar^2Nb/m$, where N is the atomic density and b is the coherent scattering length, is 2.4×10^{-7} eV. The measured penetration probability per UCN collision with the foil surface was found to be $(5\pm1)\times10^{-7}$, which is in serious contradiction (is many orders of magnitude greater) with the simple quantum mechanical calculation of the probability of subbarrier penetration. The authors[3] think that the observed phenomenon may have close relation to the aforementioned anomaly in the measured UCN loss coefficients.

There are several possible causes of the observed effect.

1. Penetration through the foil by UCNs with energies higher than the boundary energy for beryllium. These UCNs could survive in the storage chamber for comparatively long times on some trajectories. While interesting in itself, this phenomenon can hardly be regarded as radically new.

2. Subbarrier UCN penetration through matter due to some new mechanism, e.g., of the type proposed recently in Ref. 4. According to this mechanism the subbarrier quantum particles diffuse through a very long (in comparison with the wavelength) distance as a result of neutron incoherent scattering inside the matter (in Ref. 3 the product $kL\geqslant5\times10^3$, where k is the neutron wave vector in vacuum, and L is the foil thickness). This phenomenon is new, and unusual, and hitherto inexplicable in the framework of the now accepted (see Ref. 5 and references therein) quantum theory of multiple scattering of waves and particles in application to neutrons.

3. Weak UCN heating (acquiring of energy of the order of the UCN energy or less) during collisions with the chamber walls. In this case the measured effect has unexpectedly high probability, since numerous calculations show that with a probability that is orders of magnitude greater the UCNs must be heated to an energy range close to the wall temperature. The trivial effect of acquisition of energy due to wall mechanical vibrations was excluded according to the arguments of Nesvizhevsky.[b)]

2. EXPERIMENTAL METHOD

The measurements were performed on the test channel of the UCN turbine source at the Laue–Langevin Institute (ILL).[6] The layout of the experiment is shown in Fig. 1. UCNs spread over the stainless steel cylindrical neutron guides *1* (60 mm in diameter) and collided with the surface of the foil *3*, which tightly seals off the UCN path to the UCN detector *4*. It was possible to change the UCN spectrum at the foil by the changing the height h of the part of the guide containing the foil. In some experiments an additional UCN scatterer *5* ($\sim$0.1 μm Be layer deposited on the surface of a 50 μm Al foil) was placed near the foil. It was supposed that if the anomalous transmission is the result of weak (of the order of UCN energy) upscattering, the insertion of the scattering specimen with the enlarged surface would increase the transmission effect. The scatterer had the form of a corrugated ribbon rolled into a spiral with an overall area of ~600 cm^2.

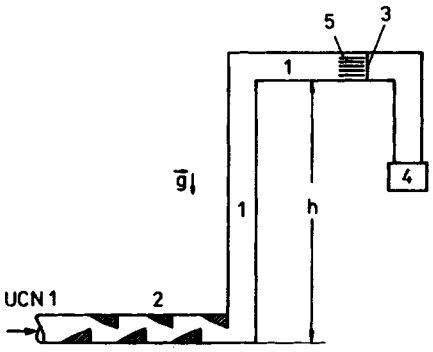

FIG. 1. The scheme of the experiment for the search for the anomalous transmission of UCNs through metal foils: *1* — vacuum stainless steel neutron guides, 60 mm in diameter, *2* — spectral filter for UCNs *3* — foil *4* — detector of UCNs (^{3}He proportional counter) *5* — additional UCN scatterer.

The density of the UCN flux at the foil was measured with the ^{3}He proportional counter *4* through a small 0.5 cm^2 hole in the membrane placed in the foil position. The counter background count rate depended on the width of the pulse amplitude window and was equal to $(6.5\pm 1.8)\times 10^{-5}$ s^{-1} when only the total energy peak in the counter spectrum is taken into account (64% of the counter neutron response total pulse spectrum), and to $(1.12\pm 0.22)\times 10^{-4}$s^{-1} for a part of the pulse spectrum $\sim$2.5 times wider.

The UCN spectrum in the chamber in the vicinity of the foils was not measured directly but was estimated from height–energy considerations: i.e., after passing through the vertical (or inclined) section of the neutron guide all the UCNs have a change in energy of gh, where g is the acceleration of gravity and h is the height difference. The important feature of experiments with UCNs is the fact that the spectra of neutrons emerging from the neutron guides transporting the UCNs from the moderators to the experimental installations usually contain a significant admixture of neutrons with higher energies. This unwanted flux of more energetic neutrons is often many times greater than the flux of UCNs. There are some cases in which the presence of neutrons with energies higher than some strictly determined critical energy (superbarrier neutrons) is detrimental to the correct interpretation of the experiment. The experiments described here belong to this class — it is important to be confident that the measured flux of transmitted neutrons is not caused by the transmission of UCNs which have energies higher than the boundary energy of the reflecting surface and which penetrate deeply into the bulk of the wall substance. The same applies to experiments searching for the anomalous upscattering of subbarrier UCNs. In both of these cases superbarrier neutrons might imitate the effect being sought. For example, a 1% admixture of the superbarrier neutrons with energies surpassing the boundary energy by 1% percent gives, for an isotropic angular distribution of incoming neutrons, a probability of penetration into the bulk as high as 1×10^{-4}.

Over the years, different devices have been used for preliminary preparation of the UCN spectrum before allowing neutrons to enter the experimental chambers. The task of such devices was to restrict, as much as possible, the access of UCNs with energies higher than some critical energy into the irradiation chamber and to let UCNs with lower energies pass with the smallest losses. The general idea of such devices consists in arranging some kind of geometric labyrinth or trap for UCNs, in which the more ener-

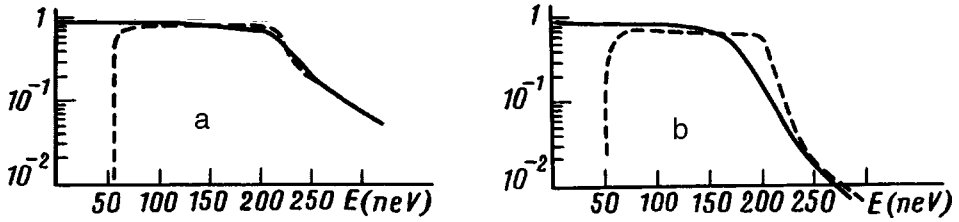

FIG. 2. Results of Monte Carlo simulations of UCN detector (^{3}He counter with aluminum membrane) efficiency for two different positions of the detector in respect to the foil position: dashed line — horizontal one, and solid line — at a level 60 cm lower, and for two different probabilities η of diffuse reflection of UCNs during their transport from the foil to detector through the stainless steel neutron guide of diameter 60 mm: a — $\eta=0.1$; b — $\eta=0.5$.

getic neutrons will ''die out'' at a higher rate due to their larger probability of penetrating the bulk and being captured in the wall. A quantitative analysis of the merits and demerits of different kinds of such devices has been published Ref. 7. In the experiments described we used one of these UCN ''filters'' (*2* in Fig. 1).

3. EXPERIMENTAL RESULTS

We obtained the following results for the penetration probability T of subbarrier UCNs through foils. For the UCN spectra in the energy range $[0,\sim 90$ neV$]$: $T=(-0.8\pm 1.6)\times 10^{-7}$ for Be foil, $T=(1.05\pm 1.6)\times 10^{-7}$ for stainless steel foil 15 μm thick, and $T=(-1.18\pm 1.4)\times 10^{-7}$ for stainless steel foil 50 μm thick.

For the UCN spectra in the energy range $[0,\sim 160$ neV$]$: $T=(1.0\pm 1.2)\times 10^{-7}$ for Be foil, and $T=(-2.7\pm 1.5)\times 10^{-7}$ for stainless steel foil 15 μm thick.

The transmission measurements for copper foils gave the following results for the UCN spectrum in the energy range $[0,\sim 90$ neV$]$: $T=(2.6\pm 0.4)\times 10^{-5}$ for copper foil 10 μm thick, and $T=(1.19\pm 0.09)\times 10^{-5}$ for copper foil 18 μm thick.

For the UCN spectrum in the energy range $[0,\sim 160$ neV$]$: $T=(7.5\pm 0.6)\times 10^{-5}$ for the copper foil 10 μm thick.

The placing of the additional UCN scatterer 5 in the UCN flux in the vicinity of the copper foil decreased the measured transmission. For the UCN energy interval $[0,\sim 90$ neV$]$: $T=(1.67\pm 0.28)\times 10^{-5}$ for copper foil 10 μm thick, and for the UCN energy interval $[0,\sim 160$ neV$]$: $T=(5.8\pm 0.8)\times 10^{-5}$ for copper foil 10 μm thick. At this stage we are unable to rule out the possible presence in the neutron flux of UCNs with energies higher than the boundary energy for copper (~ 165 neV), which could propagate through the copper foils.

One of the possible reasons for nonobservation of UCN transmission through Be and stainless steel foils in our measurements (if this phenomenon does exist at all) may be the higher UCN loss probability in our foils. The other difference consisting in the lower detector position in our measurement (in Ref. 3 the UCN detector was placed at the same level as the foil) does not seem essential.

Figure 2 shows the results of Monte Carlo simulations of the UCN detector (^{3}He counter with aluminum membrane) efficiency for two different positions of the detector

in respect to the foil position: a horizontal one, and one at a level 60 cm lower, and for two different probabilities of diffuse reflection of UCNs during their transport from the foil to detector through the stainless steel neutron guide of diameter 60 mm. It is seen that the efficiencies do not differ significantly over all the energy interval except for the low energy part (below ~ 60 neV), where the lowered detector has higher efficiency.

We are grateful to V. V. Nesvizhevsky, V. N. Shvetsov, and V. E. Varlamov for informing us of some of the details of their experiment.[3] The authors thank H. Yust of ILL for his valuable technical help during the performance of the measurements. We also express our appreciation to the ILL reactor staff.

[a)]e-mail: pokot@nf.jinr.ru
[b)]V. V. Nesvizhevsky, private communication.

[1] V. P. Alfimenkov, V. V. Nesvizhevsky, A. P. Serebrov *et al.*, LNPI Preprint No. 1729, Gatchina, Russia (1991); V. P. Alfimenkov, A. V. Strelkov, V. N. Shevtsov *et al.*, JETP Lett. **55**, 84 (1992).
[2] V. P. Alfimenkov, V. V. Nesvizhevski, A. P. Serebrov *et al.*, LNPI Preprint No. 1629 (1991), PNPI Preprint No. 1756 (1992), Gatchina, Russia.
[3] V. E. Varlamov, P. Geltenbort, V. V. Nesvizhevskiĭ, *et al.*, JETP Lett. **66**, 336 (1997).
[4] A. P. Serebrov, Report at ISINN-5, Dubna, May 1997.
[5] V. F. Sears, Phys. Rep. **82**, 1 (1982); V. K. Ignatovich, *Ultracold Neutrons*, Clarendon Press, Oxford, 1990 [Russian original, Nauka, Moscow, 1986].
[6] A. Steyerl, H. Nagel, F.-X. Schreiber *et al.*, Phys. Lett. **116**, 347 (1986).
[7] Al. Yu. Muzychka and Yu. N. Pokotilovski, JINR Commun. E3-95-282, Dubna, 1995.

Published in English in the original Russian journal. Edited by Steve Torstveit.

Comments on preliminary data on the reactions $e^+e^- \to \phi \to \gamma f_0(980) \to \gamma \pi^0 \pi^0$

N. N. Achasov[a)] and V. V. Gubin[b)]
S. L. Sobolev Institute of Mathematics, Siberian Branch of the Russian Academy of Sciences, 630090 Novosibirsk, Russia

(Submitted 20 February 1998)
Pis'ma Zh. Éksp. Teor. Fiz. **67**, No. 7, 445–449 (10 April 1998)

Preliminary data on the reactions $e^+e^- \to \phi \to \gamma f_0(980) \to \gamma \pi^0 \pi^0$ together with data on $\pi\pi$ scattering and the reactions $J/\psi \to \phi \pi^+ \pi^-$ and $K^- p \to \pi^+ \pi^- (\Lambda, \Sigma)$ are analyzed. The analysis shows that the mass of the $f_0(980)$ meson is $m_{f_0} = 950$ MeV, and $BR(\phi \to \gamma f_0 \to \gamma \pi^0 \pi^0) \simeq 1 \times 10^{-4}$, indicating that the $f_0(980)$ resonance is of a four-quark nature.
 [S0021-3640(98)00307-7]

PACS numbers: 13.65.+i, 14.40.Cs, 13.25.Ft, 13.85.Hd

The unusual properties of $a_0(980)$ and $f_0(980)$ mesons have been attracting intense attention for decades. It is well known that the standard quark model does not describe the properties of these scalar mesons (see, for example, Ref. 1). At the same time, all of their unusual properties can be naturally explained on the basis of the four-quark $q^2\overline{q^2}$ MIT bag model[2] (see Ref. 1). Moreover, in addition to the $q^2\overline{q^2}$ model other possibilities are being discussed in the literature: the $K\overline{K}$ molecule model[3] and the $s\overline{s}$ model for the f_0 meson.[4] As was shown in Refs. 5–8, radiative decays of the ϕ meson $\phi \to \gamma f_0 \to \gamma \pi\pi$ and $\phi \to \gamma a_0 \to \gamma \eta \pi$ can serve as an excellent criterion for selecting different models of the f_0 and a_0 meson structure. In this connection, an active experimental investigation of these decays is already being conducted at the operational VEPP-2M accelerator complex (Novosibirsk) with a spherical neutral detector (SND) and a cryogenic magnetic detector (KMD-2), and plans are being made for such investigations at the ϕ factory DAΦNE (Frascati) and at CEBAF (USA). Preliminary data on these decays have already been obtained (see Ref. 9). It follows from experiments that $BR(\phi \to \gamma \pi^0 \pi^0) = (1.1 \pm 0.2) \times 10^{-4}$ and $BR(\phi \to \gamma \pi \eta) = (1.3 \pm 0.5) \times 10^{-4}$ for photon energies $\omega < 200$ MeV, indicating a $q^2\overline{q^2}$ nature of the a_0 and f_0 mesons.[5,8] The quite large statistical sample made it possible to construct the spectrum of pions in the reaction $e^+e^- \to \phi \to \gamma \pi^0 \pi^0$. The experimental data for this reaction were analyzed[9] with the aid of the formula (see $g(m)$ and details in Refs. 5 and 8)

$$\frac{d\sigma_\phi}{dm} \sim \frac{\omega |g(m)|^2}{|D_{f_0}(m)|^2} \sqrt{1 - \frac{4m_\pi^2}{m^2}}, \tag{1}$$

where m is the mass of the $\pi\pi$ system, s is the square of the total energy of the e^+e^- beams, the photon energy $\omega = (s - m^2)/2\sqrt{s}$, and $1/D_{f_0}(m)$ is the f_0 meson propagator:

$$D_{f_0}(m)=m_{f_0}^2-m^2+\sum_{ab}\,[\mathrm{Re}\;P_{f_0}^{ab}(m_{f_0}^2)-P_{f_0}^{ab}(m)]. \tag{2}$$

The sum $\Sigma_{ab}[\mathrm{Re}\;P_{f_0}^{ab}(m_R^2)-P_{f_0}^{ab}(m)]$ contains corrections for the finite decay width of the resonance which are due to the $\pi\pi$, $K\overline{K}$, $\eta\eta$, $\eta\eta'$, etc. channels. For ab pseudoscalar mesons and $m_a \geqslant m_b$, $m^2 > m_+^2$ we have

$$P_{f_0}^{ab}(m)=\frac{g_{f_0ab}^2}{16\pi}\left[\frac{m_+m_-}{\pi m^2}\;\ln\frac{m_b}{m_a}+\rho_{ab}\left(i+\frac{1}{\pi}\;\ln\frac{\sqrt{m^2-m_-^2}-\sqrt{m^2-m_+^2}}{\sqrt{m^2-m_-^2}+\sqrt{m^2-m_+^2}}\right)\right]. \tag{3}$$

An expression for $P_{f_0}^{ab}(m)$ for other values of m can be obtained by analytical continuation.

Fitting the formulas written out above to the experimental data on the reaction $e^+e^-\to\phi\to\gamma\pi\pi$ gave the following parameters for the f_0 meson:[9]

$$m_{f_0}=950\pm 8\ \mathrm{MeV},\quad g_{f_0K^+K^-}^2/4\pi=(2.3\pm 0.5)\mathrm{GeV}^2,$$

$$g_{f_0\pi^+\pi^-}^2/4\pi=(0.4\pm 0.1)\ \mathrm{GeV}^2, \tag{4}$$

which corresponds to the $q^2\overline{q^2}$ model.[5,8] The effective width of the f_0 meson for these parameters is $\Gamma_{\mathrm{eff}}\simeq 60$ MeV (see Ref. 8 for the definition of the effective width). We note that for this fit $\chi^2=4.6$ with 7 degrees of freedom.

The comparatively low f_0 meson mass obtained from the fit elicited debate at the HADRON-97 conference, where it was noted that the value $m_{f_0}=950$ MeV is much lower than the value given by the Particle Data Group.[10] However, it should be remembered that in contrast to the Particle Data Group value, the mass presented in Eq. (4) is determined in the spirit of field theory, i.e., as a zero of the real part of the inverse propagator (just as, for example, is the mass of the Z_0 boson) and, accordingly, it is a physical mass resonance. At the same time, for the fit (4) the position of the pole of the propagator lies at the point $m_{f_0}^p=0.988-i0.08$ GeV, which is in excellent agreement with the Particle Data Group data.[10]

However, there is a different problem. An isolated resonance with mass $m_{f_0}=950$ MeV, as represented in the fit (4), cannot describe the $\pi\pi$ scattering data, even if an elastic background with an additional phase $\theta\simeq 80-90°$ is taken into account. A ''heavy'' f_0 meson with mass $m_{f_0}=980$ MeV can describe the $\pi\pi$ scattering data in the interval $0.7<m<1.1$ GeV, with only the elastic background taken into account. In order to describe the $\pi\pi$ scattering data with a lighter f_0 meson, an additional resonance — a σ meson — must be introduced.

On this basis we present the results of an analysis of the spectrum in the reaction $e^+e^-\to\phi\to\gamma\pi\pi$, including a concurrent two-channel description of the spectrum in the reaction $e^+e^-\to\phi\to\gamma(f_0+\sigma)\to\gamma\pi\pi$, and the $\pi\pi$ scattering data. Moreover, we shall analyze the agreement between the parameters of the f_0 meson and other known experimental data — data on the production of the f_0 mesons in J/ψ decays and data on the reaction $K^-p\to\pi^+\pi^-(\Lambda,\Sigma)$.

Our analysis is based on previous work (see Refs. 1 and 8). We describe the $\pi\pi$ scattering data by a two-channel model where, besides the f_0 meson, a wide ($\Gamma_\sigma \simeq 300$ MeV) relatively heavy ($m_\sigma \simeq 1.5$ GeV) resonance is present. To fit the $\pi\pi$ scattering data we represent the s-wave amplitude of the reaction $\pi\pi \to \pi\pi$ with $I=0$ as the sum of an inelastic resonance amplitude $T^{\rm res}_{\pi\pi}$, in which we shall take into account the contributions of f_0 and σ mesons, and the elastic background amplitude[1,8]

$$T(\pi\pi \to \pi\pi) = \frac{\eta_0^0 e^{2i\delta_0^0} - 1}{2i\rho_{\pi\pi}} = \frac{e^{2i\delta_B} - 1}{2i\rho_{\pi\pi}} + e^{2i\delta_B} T^{\rm res}_{\pi\pi}, \tag{5}$$

where

$$T^{\rm res}_{\pi\pi} = \sum_{RR'} \frac{g_{R\pi\pi} g_{R'\pi\pi}}{16\pi} G^{-1}_{RR'}(m). \tag{6}$$

The phase δ_B of the elastic background is taken in the form $\delta_B = \theta\rho_{\pi\pi}$, where $\theta \simeq 60°$. The matrix of the inverse propagator $G_{RR'}$ has the form

$$G_{RR'}(m) = \begin{pmatrix} D_{f_0}(m) & -\Pi_{f_0\sigma}(m) \\ -\Pi_{\sigma f_0}(m) & D_\sigma(m) \end{pmatrix}.$$

The off-diagonal elements of $G_{RR'}(m)$ are transitions due to mixing of resonances as a result of a final-state interaction, arising in the presence of the common decay channels, $R \to ab \to R'$. We shall write them in the form[1,8]

$$\Pi_{RR'}(m) = \sum_{ab} \frac{g_{R'ab}}{g_{Rab}} P^{ab}_R(m) + C, \tag{7}$$

where the constant C effectively takes into account the contributions from the intermediate states VV, 40^-, etc. and also includes the subtraction constant for the transitions $R \to (0^-0^-) \to R'$. In the four-quark model we assume that these constants are free parameters. In the present work, we take into account only the $\pi\pi$ and $K\overline{K}$ intermediate channels in the inverse propagator matrix; the other channels have virtually no effect on the results.

A concurrent fit of the $\pi\pi$ scattering data and the mass spectrum in the reaction $e^+e^- \to \phi \to \gamma(f_0 + \sigma) \to \gamma\pi\pi$ (see Fig. 1) gave for the mass spectrum in the reaction $e^+e^- \to \phi \to \gamma\pi\pi$ the best fit $\chi^2 = 6.2$ and the f_0 meson parameters

$$m_{f_0} = 950 \text{ MeV}, \quad g^2_{f_0K^+K^-}/4\pi = 2.25 \text{ GeV}^2,$$

$$R = g^2_{f_0K^+K^-}/g^2_{f_0\pi^+\pi^-} = 3.5, \tag{8}$$

and an effective width of the f_0 meson $\Gamma_{\rm eff} \simeq 80$ MeV. The relative decay probability $BR(\phi \to \gamma(f_0 + \sigma) \to \gamma\pi^0\pi^0) = 1.03$ in the interval $\omega < 200$ MeV. The position of the pole in the propagator for the parameters (8) is $m^p_{f_0} = 0.998 - i0.14$ GeV. We note that we were not able to achieve a satisfactory concurrent description of the data for the masses $m_{f_0} > 960$ MeV. For $m_{f_0} = 960$ MeV (in this case $R = 4.0$, while all other parameters are the same) we obtained $\chi^2 = 8.6$. The total number of parameters in our model is 7, and we perform a fit of three characteristics — phase and inelasticity of the $\pi\pi$ scattering and

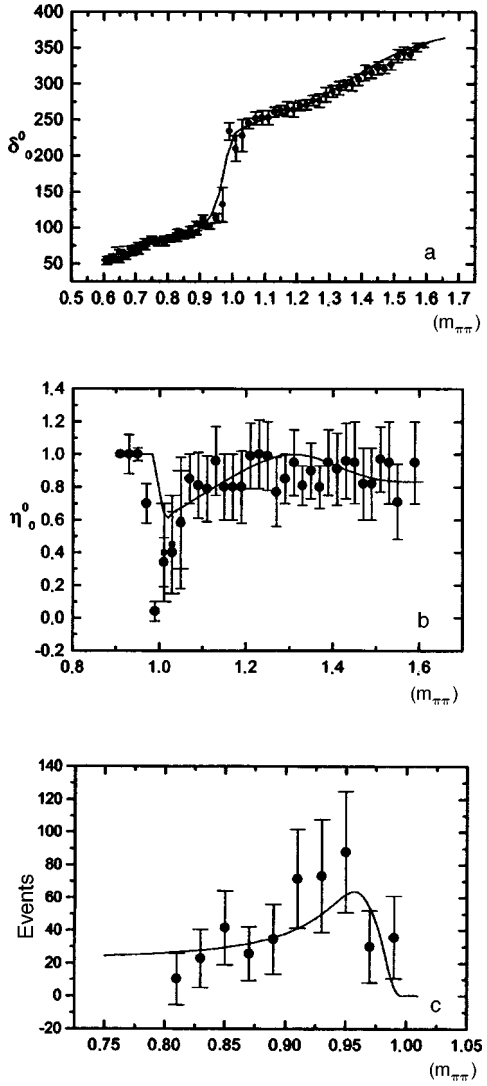

FIG. 1. Result of the fit for the parameters $m_{f_0}=0.950$ GeV, $m_\sigma=1.38$ GeV, $g^2_{f_0K^+K^-}/4\pi=2.25$ GeV^2, $g^2_{\sigma\pi\pi}/4\pi=1.8$ GeV^2, $C=-0.34$, $R=3.5$, and $\theta=43°$: a — phase δ_0^0; b — inelasticity η_0^0; c — mass spectrum in the reaction $e^+e^-\to\gamma\pi\pi$.

the mass spectrum in the reaction $e^+e^-\to\phi\to\gamma\pi\pi$ (the total number of points is 110). The quantity χ^2 is presented only for the $\pi\pi$ spectrum in the reaction $\phi\to\gamma\pi\pi$. Therefore our analysis gives virtually the same parameters as Eq. (4).

Moreover, in order to clarify the question of whether or not the data obtained from our fit agree with other experiments we analyzed the mass spectrum in the region of the f_0 meson in the decay $J/\psi\to\phi\pi^+\pi^-$ (Ref. 11). In this decay the mass spectrum is determined by the expression[8]

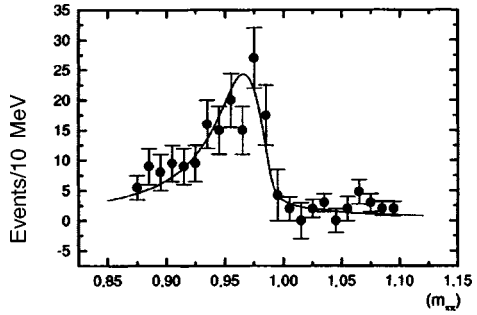

FIG. 2. Mass spectrum in the reaction $J/\psi\to\phi\pi^+\pi^-$, $C=9.0$, $\xi=0.1$; all other parameters are the same as in Fig. 1.

$$\frac{dN_{\pi\pi}}{dm}=C\frac{m^2\Gamma_{f_0\pi\pi}(m)}{|D_{f_0}(m)|^2}\left|\frac{D_\sigma(m)+(1+\xi)\Pi_{f_0\sigma}(m)+\xi(g_{\sigma\pi\pi}/g_{f_0\pi\pi})D_{f_0}(m)}{D_\sigma(m)-\Pi^2_{f_0\sigma}/D_{f_0}(m)}\right|^2 \tag{9}$$

and contains only two unknown parameters: ξ — the relative weight of the direct production of the σ meson and C — the overall normalization constant. Making the fit according to these parameters we found that the mass spectrum is described satisfactorily by the parameters found from the preceding fit (Fig. 2). For the set of parameters corresponding to the mass $m_{f_0}=950$ MeV we obtained $\chi^2=19.7$ (23 points) with $\xi=0.1$ and $C=9.0$. For the set of parameters corresponding to the mass $m_{f_0}=960$ MeV we have $\chi^2=27.3$.

Thus the $J/\psi\to\phi\pi^+\pi^-$ decay data confirm the value $m_{f_0}=950$ MeV. We note that the $J/\psi\to\phi\pi^+\pi^-$ decay data are not described by a single f_0 meson with the mass $m_{f_0}=980$ MeV, but they are described by an f_0 resonance with mass $m_{f_0}=950$ MeV.

We performed a similar analysis of the $\pi\pi$ spectrum in the reaction $K^-p\to\pi^+\pi^-(\Lambda,\Sigma)$.[12] The mass spectrum in this reaction is also determined by expression (9). There are fewer data for the reaction $K^-p\to\pi^+\pi^-(\Lambda\Sigma)$ than for the decay $J/\psi\to\phi\pi^+\pi^-$, and for this reason they are not sensitive to the mass of the f_0 meson. For example, we obtained the same value $\chi^2=29$ for the parameters corresponding to both $m_{f_0}=950$ MeV and for $m_{f_0}=985$ MeV. We note that for a single f_0 resonance the $K^-p\to\pi^+\pi^-(\Lambda\Sigma)$ data are likewise insensitive to the mass of the f_0 meson.

In summary, the spectrum obtained for $\pi\pi$ mesons in ϕ decay, $\phi\to\gamma\pi^0\pi^0$, agrees well with other experiments, while the relative decay probability confirms the hypothesis that the f_0 meson is of a four-quark nature.

[a)]e-mail: achasov@math.nsc.ru
[b)]e-mail: gubin@math.nsc.ru

[1] N. N. Achasov, S. A. Devyanin, and G. N. Shestakov, Usp. Fiz. Nauk **142**, 361 (1984) [Sov. Phys. Usp. **27**(6), 161 (1984)]; N. N. Achasov and G. N. Shestakov, Usp. Fiz. Nauk **161**, 53 (1991) [Sov. Phys. Usp. **34**, 471 (1991)].
[2] R. L. Jaffe, Phys. Rev. D **15**, 267, 281 (1977).

[3] J. Weinstein and N. Isgur, Phys. Rev. D **27**, 588 (1983).
[4] N. A. Tornqvist, Phys. Rev. Lett. **49**, 624 (1982).
[5] N. N. Achasov and V. N. Ivanchenko, Nucl. Phys. B **315**, 465 (1989).
[6] F. E. Close, N. Isgur, and S. Kumano, Nucl. Phys. B **389**, 513 (1993).
[7] N. N. Achasov, V. V. Gubin, and V. I. Shevchenko, Phys. Rev. D **56**, 203 (1997).
[8] N. N. Achasov and V. V. Gubin, Phys. Rev. D **56**, 4084 (1997).
[9] N. N. Achasov *et al.*, Preprint Budker INP 97-78, (1997); http://xxx.lanl.gov/abs/hep-ex/9710017.
[10] Particle Data Group, Phys. Rev. D **54**, (1996).
[11] A. Falvard *et al.*, Phys. Rev. D **38**, 2706 (1988).
[12] G. W. Brandenburg *et al.*, Nucl. Phys. B **104**, 413 (1976).

Translated by M. E. Alferieff

Photoselective laser photo-ion microscopy with 5 nm resolution

S. K. Sekatskiĭ,[a] D. V. Serebryakov, and V. S. Letokhov
Institute of Spectroscopy, Russian Academy of Sciences, 142092 Troitsk, Moscow Region, Russia

(Submitted 19 February 1998)
Pis'ma Zh. Éksp. Teor. Fiz. **67**, No. 7, 450–454 (10 April 1998)

Spectral selectivity has been attained in the method of field-ion microscopy with a spatial resolution of about 5 nm and time-of-flight determination of the photo-ion masses. Light-absorbing CdS_xSe_{1-x} nanocrystals in a transparent glass matrix are detected by irradiating field tips made from red light filters with copper-vapor laser radiation. The nanocrystals appeared in the photo-ion images as bright spots on a dark background. © *1998 American Institute of Physics.* [S0021-3640(98)00407-1]

PACS numbers: 07.79.Lh

The method of field-ion atom probe microscopy, which makes it possible not only to investigate with atomic resolution tips made of different metals and alloys but also to identify single atoms evaporated from a tip by their time-of-flight to a detector, is now a generally recognized and, in many ways, an unique method for analyzing different problems in materials science, metallurgy, semiconductor physics, and so on (see, for example, Ref. 1 and reference cited there). The possibilities of this method have been greatly expanded by the use, since the 1980s, of pulsed lasers for irradiating the tips of interest: pulsed heating of tips by laser irradiation induces pulsed field evaporation and desorption from them, which makes it possible both to improve the temporal (and therefore mass) resolution of the method and to extend the range of samples accessible to investigation.

However, all works performed by the atomic probe method using pulsed lasers were conducted with strongly and ''nonselectively'' absorbing samples (metals, alloys, semiconductors which strongly absorbing the radiation employed, thick films of dye deposited on the metal tips, and so on), whose heating leads to ''structurally and elementally nonselective'' field desorption (evaporation) of the sample material. The old and much-promising idea of laser-selective photo-ion projection microscopy, based on selective single- or multistep photoionization and photodetachment of selected molecules or even light-absorbing fragments of large molecules (chromophores)[2] has remained unrealized.

In the present letter we report the attainment of real spectral (laser) selectivity in the method of laser projection photo-ion microscopy. The photo-ion images were obtained by irradiating tips, prepared from red light filters, with pulsed copper-vapor laser radiation. Local heating of light-absorbing CdS_xSe_{1-x} nanoparticles in a transparent glass matrix

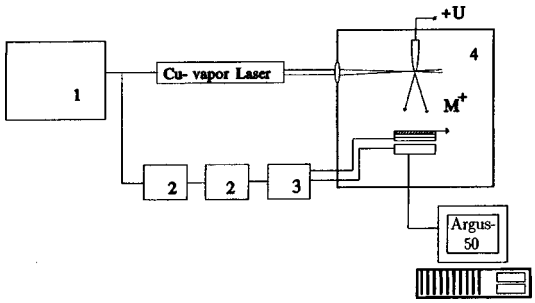

FIG. 1. Diagram of a laser photo-ion projection microscope: *1* — Power supply for the copper-vapor laser, *2* — pulse generators, *3* — pulsed power supply for the detector.

resulted in a local field evaporation of atoms from neighborhoods of these particles, making it possible to observe individual nanoparticles in the form of bright spots on a dark quasiuniform background.

The layout of the laser photo-ion microscope is presented in Fig. 1. The same microscope that we used previously for observing single F_2 color centers at the points of LiF tips was used.[3,4] The main differences were that in the present work we employed a pulsed copper-vapor laser (pulse repetition frequency 8.8 kHz, pulse duration 18 ns, power up to 5 W, lasing wavelengths 511 nm (60%) and 572 nm (40%)), that photo-ions rather than photoelectrons were detected, and that a simple scheme was developed for recording the tip-to-detector time of flight of the ions. The experimental tips were prepared by etching fragments of red light filters (KS-11 and KS-15 optical colored glass) in concentrated or diluted (to a concentration of 10–20%) hydrofluoric acid. Prior to etching, the samples of light filters were subjected to thermal heating in a muffle furnace at a temperature of 700–800 °C for 5–7 h in order to obtain a sample with a known average radius of CdS_xSe_{1-x} microcrystallites — it is known that such annealing makes it possible to bring the average radius up to 10–20 nm and larger.[5,6]

The laser radiation was focused into an area $S \simeq 0.1$ mm^2 on a tip. The input of the detector, an assembly consisting of a microchannel plate (MCP) and phosphorescent screen, provided by the Hamamatsu Photonics Company (Japan), was grounded, and a constant voltage U in the range 0 + 20 kV was applied to the tip. The images obtained were photographed with a CCD camera and analyzed in a specialized Argus-50 processor manufactured by the Hamamatsu Photonics Company.

The radial electric field directs the emitted particles of mass M toward the detector, where an image of the tip enlarged by a factor $K = L/\gamma r$ is formed[1] (L is the tip–detector distance, r is the radius of curvature of the tip, and γ is a numerical factor equal to 1.5–2). The spatial resolution d of the microscope is determined by the average kinetic energy of the emitted particles in a direction transverse to E_0 and equals[1]

$$d \simeq 4\gamma r \sqrt{\frac{E_0}{eU}}. \tag{1}$$

For field-ionization images E_0 is determined by the tip temperature kT, $E_0 \simeq kT$,[1] so that

for $T \simeq 400$ K (see below), $r = 400$ nm, and $U = 10$ kV we obtain $d \simeq 5$ nm. The time of flight t of a particle of mass M from tip to detector equals,[1] to a high degree of accuracy,

$$t = L\sqrt{\frac{M}{2eU}}. \tag{2}$$

To record the time of flight of the ions we employed for the MCP a pulsed power supply, provided by the Hamamatsu Photonics Company, that made it possible to open the MCP for a time as short as 100 ns in order to detect a signal. Using delay generators, the moment at which the MCP was opened was set with a controllable delay with respect to the start of the laser pulse to an accuracy not worse than 100 ns.

The photo-ion image of the point of a needle made from a fragment of KS-11 glass is displayed in Fig. 2a. The photo-ion flux $N_{\text{ph.ion}}$ increased rapidly and nonlinearly with increase of both the irradiation intensity I and the tip voltage U, and in the absence of laser radiation it was not detected in the entire range of tip voltages. Figures 3a and 3b show $N_{\text{ph.ion}}(I)$ and $N_{\text{ph.ion}}(U)$, respectively. The indicated nonlinear dependences are typical for experiments on field-ion atom probe microscopy and can be explained by stimulation of field evaporation/desorption from the tip as a result of heating of the tip by laser radiation.[1]

Figure 2b shows the photo-ion image obtained of the same tip in the pulsed regime with the following parameters: The MCP was opened for 300 ns to detect a signal 700 ns after the laser pulse. One can see that a large fraction of the clearly distinguished spots seen in Fig. 2a are present in this image.

No sharp structure was seen in the images obtained in the detection window with a delay from 0 to 600 ns with respect to the laser pulse and in windows opened for 1 μs and longer after the laser pulse, though a weak structureless photo-ionic image could be identified against a noise background with long-time accumulation in these detection windows also. Proceeding from Eqs. (2), this attests to the fact that the image obtained was formed by relatively heavy ions with masses in the range 100–200 amu, while the light ions, such as Na, Si, SiO, and SiO_2, observed previously in field-ion microscopy of transparent optical (chromium coated) glasses and giving rise to their photo-ion images,[7] did not make a large contribution to the photo-ion images of the red light filters. Heavy Cd ions (112 amu, time of flight 760 ns), CdS (144 amu, 860 ns), and CdSe (191 amu, 1 μs), whose field evaporation can be expected in our case by analogy to many well-known works on laser desorption from CdS, CdSe, and similar materials (see, for example, Ref. 8 and the references cited therein), should reach the detector in the indicated range of delay times. The ''background'' photo-ion images can be explained, in all probability, by a steady heating of the sample by the copper-vapor laser, which has a very high pulse repetition frequency.

The works devoted to analysis of the temperature increase of absorbing impurities heated by laser pulses (see, for example, Ref. 9) give the following estimate of the maximum heating of an inclusion with radius R as a function of the irradiation intensity I:

$$\Delta T = \frac{I\sigma}{4\pi R\chi}. \tag{3}$$

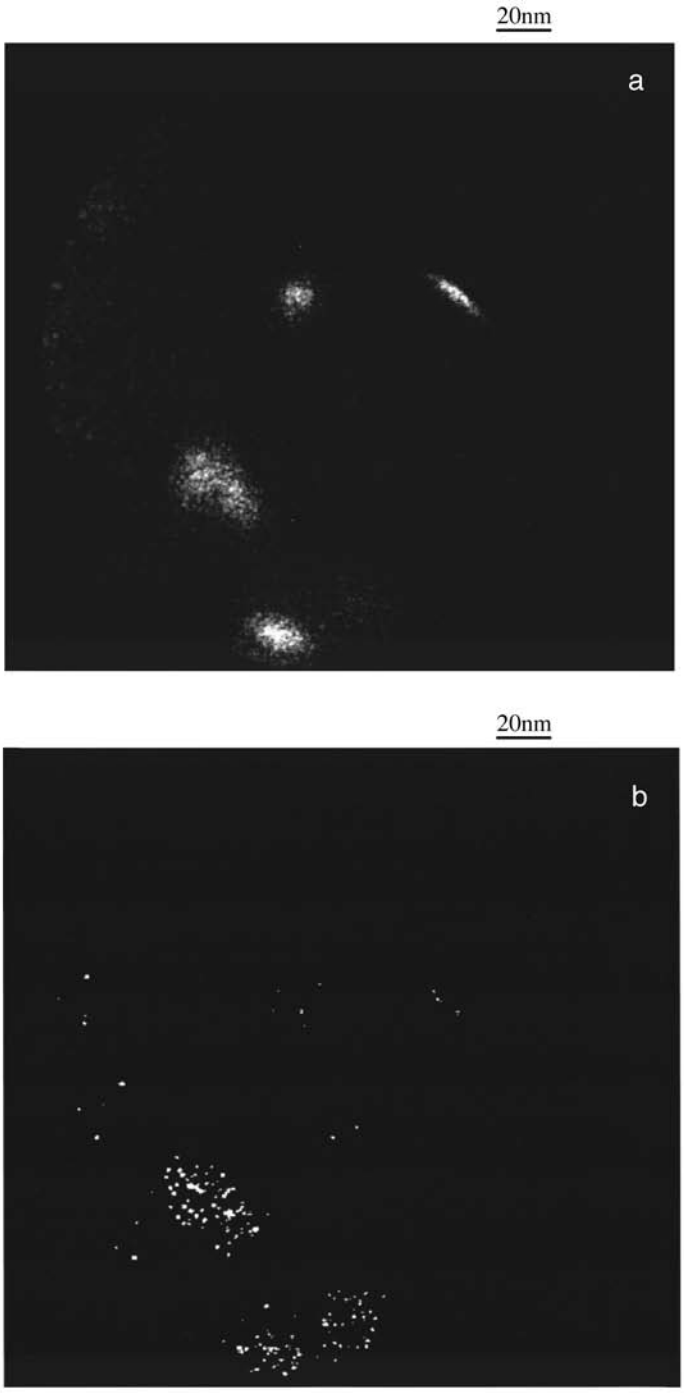

FIG. 2. Laser-stimulated photo-ion image of a KS-11 glass tip with a radius of curvature of the order of 400 nm: a — obtained in the entire range of delay times with respect to the laser pulse, b — obtained in the range of delay times 700–1000 ns.

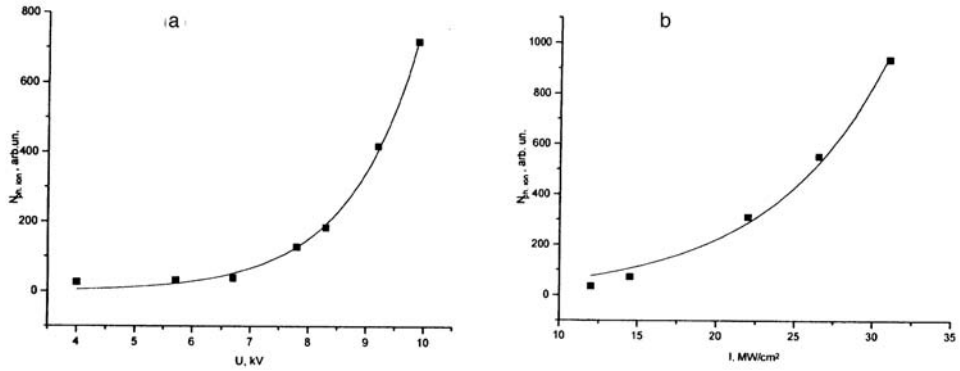

FIG. 3. Photo-ion current $N_{\text{ph.ion}}$ versus: a — the tip potential (irradiation intensity 3×10^7 V/cm^2) and b — irradiation intensity (tip voltage 9.9 kV).

Here σ is the light absorption cross section of the impurity and χ is the thermal conductivity of the transparent matrix. If the quantity σ is estimated by the simplest formula

$$\sigma \simeq \pi R^2 \cdot kR = \pi k R^3, \tag{4}$$

then for an inclusion with of radius of 10 nm we obtain $\sigma \simeq 3\times10^{-13}$ cm^2 (here $k \simeq 10^5$ cm^{-1} is the linear absorption coefficient of the impurity material). Substituting the average data[9] for glasses $\chi \simeq 0.01$ V/cm·K, we obtain for $I=3\times10^7$ V/cm^2 and $\Delta T=80$ K. We note that the estimate (4) is valid if the pulse duration t_{pulse} is greater than the time required to establish the temperature in the matrix[9] $\tau=\rho c R^2/\pi\chi=60$ ps, which certainly holds under our conditions. (Here $\rho\sim3$ g/cm^2 and $c\sim0.6$ J/g·K are typical ''average'' values of the density and specific heat of glass.[10])

Thus, the heating of relatively large absorbing CdS_xSe_{1-x} nanocrystals is not very large. Nonetheless, as follows from the practice of field ion atom probe microscopy,[1] it is sufficient to stimulate field evaporation of atoms from impurities. It should also be noted that since the geometry of our problem is substantially different from the case of an ''absorbing inclusion in an infinite volume,'' the heating can also be much greater than that given by Eq. (3) — see Ref. 11. Since the heating of inclusions is all the greater the larger their diameter R (from Eqs. (3) and (4) follows $\Delta T\sim R^2$), evidently, only relatively large CdS_xSe_{1-x} nanocrystals will be clearly seen in our projection photo-ion microscope, just as happens in reality.

In summary, the data presented attest to the fact that laser (spectral) selectivity in the method of field ion atom probe microscopy has indeed been achieved — only light-absorbing CdS_xSe_{1-x} inclusions were visualized by irradiating the experimental samples.

In closing, we thank N. S. Kopylov for assisting in the heat treatment of the samples of red light filters, A. L. Ivanov and V. O. Kompants for assisting in the work with the lasers, and the Hamatsu Photonics Company (Japan) for providing the experimental equipment. This work was supported by the Russian Fund for Fundamental Research and the US Department of Defense.

[a)]e-mail: sekats@isan.troitsk.ru

[1] T. T. Tsong, *Atom-Probe Field Ion Microscopy*, Cambridge Univ. Press, New York, 1990.
[2] V. S. Letokhov, Kvantovaya Élektron. (Moscow) **2**, 930 (1975) [Sov. J. Quantum Electron. **5**, 506 (1975)].
[3] V. N. Konopsky, S. K. Sekatskii, and V. S. Letokhov, Appl. Surf. Sci. **94/95**, 148 (1996).
[4] S. K. Sekatskiĭ and V. S. Letokhov, JETP Lett. **65**, 465 (1997).
[5] V. V. Golubkov, A. I. Ekimov, A. A. Onushchenko, and V. A. Tsekhomskiĭ, Fiz. Khim. Stekla **7**, 397 (1981).
[6] H. Shinojima, J. Yumoto, N. Uesugi *et al.*, Appl. Phys. Lett. **55**, 1519 (1989).
[7] G. L. Kellog, J. Appl. Phys. **53**, 6383 (1982).
[8] É. F. Laznev, *Laser Desorption* [in Russian], Leningrad State University Press, Leningrad, 1990.
[9] M. F. Koldunov, A. A. Manenkov, and I. L. Pokotilo, Izv. Ross. Akad. Nauk, Ser. Fiz. **59**, 72 (1995).
[10] L. I. Demkina, *Physicochemical Principles of the Production of Optical Quality Glass* [in Russina], Khimiya, Leningrad, 1976, Chap. 7.
[11] M. F. Koldunov, A. A. Manenkov, and I. L. Pokotilo, Kvantovaya Élektron. (Moscow) **17**, 523 (1990) [Sov. J. Quantum Electron. **20**, 456 (1990)].

Translated by M. E. Alferieff

On the interrelation of the characteristic scales of depolarization and decorrelation of optical fields under multiple-scattering conditions

D. A. Zimnyakov and V. V. Tuchin[a)]
Sarotov State University, 410026 Saratov, Russia

(Submitted 27 February 1998)
Pis'ma Zh. Éksp. Teor. Fiz. **67**, No. 7, 455–460 (10 April 1998)

The interrelation of depolarization and decorrelation of optical fields in multiply scattering Brownian media is studied on the basis of the notion of the probability density of optical path lengths of the partial components of the scattered field under multiple-scattering conditions. To describe such media a universal parameter that is independent of the density (concentration) of scattering particles is introduced — the characteristic correlation time. Experimental results obtained with aqueous suspensions of polystyrene beads as model media are presented which demonstrate the constancy of this parameter at different concentrations of scattering particles. © *1998 American Institute of Physics.* [S0021-3640(98)00507-6]

PACS numbers: 42.25.Fx, 42.25.Ja

Stochastization of the space–time fluctuations of coherent optical fields in inhomogeneous media under multiple-scattering conditions is manifested in the existence of specific effects (coherent backscattering as well as angular and temporal correlations of amplitude and intensity fluctuations of the scattered fields). Some of these effects (for example, coherent backscattering) can be interpreted as classical analogs of the quantum-mechanical phenomenon of weak localization.[1] The spatial and temporal correlations of amplitude and intensity fluctuations describe the statistical properties of random interference structures, or speckle fields, formed as a result of superposition of the partial components of the scattered field during the propagation of coherent beams in static and dynamic multiply scattering media. The depolarization of scattered radiation observed under multiple-scattering conditions and manifested as a decrease in the degree of polarization of the scattered field as compared with the initial degree of polarization of the probe beam is due, just as the decorrelation of the spatial-temporal fluctuations of the amplitude and intensity, to stochastization of the directions of the wave vectors for partial components of the fields which are formed as a result of a large number of scattering events.

The interrelation of the processes of decorrelation and depolarization of optical fields during their propagation in multiply scattering media can be analyzed using the notion of the probability density $\rho(s)$ of the optical path lengths of the partial components of the scattered fields. This probability density is introduced on the basis of a

random walk model describing the statistical properties of the scattered fields.[2] In the limiting case when the source and detector of the radiation are isotropic and pointlike and the radiation propagates diffusively in the scattering medium, $\rho(s)$ can be represented[2] in the simple analytical form $\rho(s)=(3/4\pi s l^*)^{3/2}\exp(-3|\mathbf{r}-\mathbf{r}'|^2/4sl^*)$, where l^* is the transport length determined as the characteristic spatial scale of stochastization of the propagation directions of the partial components of the optical field, and $|\mathbf{r}-\mathbf{r}'|$ is the source–detector distance. The diffusion approach neglects the anisotropy of the angular distributions of the components of the scattered field for a single scattering event as well as the contribution to the resultant filed from the unscattered component and the components formed as a result of a small number of scattering events. In consequence, the expression presented is inapplicable in the case when $l^*\sim|\mathbf{r}-\mathbf{r}'|$. At the same time, the increase in the contribution of the unscattered component and the components characterized by small numbers of scattering events to the formation of the scattered field in the intermediate region $l^*\neq|\mathbf{r}-\mathbf{r}'|$ can be taken into account by making a certain modification of the function $\rho(s)$. Specifically, a variant of such a modification, in which an expansion of the probability density $\rho(s)$ in spherical harmonics is used to take account of the effect of the anisotropy of the angular characteristics of the single-scattering process on the formation of the scattered field under conditions when the transport length l^* is comparable to the dimensions of the scattering medium, was studied in Refs. 2 and 3.

For multiply scattering ensembles of moving noninteracting particles it can be shown in the random walk model that the normalized temporal autocorrelation function of fluctuations of the scattered field at a fixed observation point can be represented as a modified Laplace transform of the probability density $\rho(s)$:

$$g_1(\tau)=\int_0^\infty \exp\{-2B(\tau)k_0^2 s/l^*\}\rho(s)ds, \tag{1}$$

where the function $B(\tau)$ determines the mean-squared displacement of the scattering particles over the observation time τ, and k_0 is the wave number of the probe beam. In the particular case of ensembles of Brownian particles $g_1(\tau)$ can be represented as follows (see, for example, Ref. 4):

$$g_1(\tau)=\int_0^\infty \exp\{-2\tau s D_s k_0^2/l^*\}\rho(s)ds, \tag{2}$$

where D_s is the diffusion coefficient of the scattering particles.

Proceeding from general notions about the process of depolarization of radiation as a result of multiple scattering, the degree of polarization of the scattered field can also be represented as an integral transform of the probability density $\rho(s)$ of the optical path lengths of the partial components:

$$P=\int_0^\infty \varphi(s)\rho(s)ds. \tag{3}$$

Using as a basis the results presented in Refs. 5 and 6, in the analysis below we shall employ an exponential kernel in the integral transform (3): $\varphi(s)\sim\exp(-s/\zeta_i)$, where the

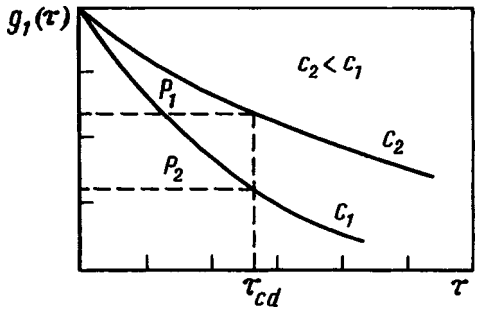

FIG. 1. Method for determining the characteristic correlation time for multiply scattering Brownian media.

parameter ζ_i $(i=C, L)$ is determined by the characteristic scale of the depolarization of a probe beam with initial linear (L) or circular (C) states of polarization. As a result, the expression for the degree of polarization assumes the form

$$P_i = \int_0^\infty \exp(-s/\zeta_i)\rho(s)ds. \tag{4}$$

Comparing expressions (2) and (4), we can introduce the quantity $\tau_{cd} = l^*/2\zeta_i D_s k_0^2$, the value of τ at which, if it is assumed that the kernels of the integral transforms (2) and (4) are exponential, the values of the normalized autocorrelation function of the fluctuations and the degree of polarization of the scattered field are equal to each other. It is easy to see that the quantity $\tau_{cd} = l^*/2\zeta_i D_s k_0^2$, which can be loosely designated as the characteristic correlation time, is a universal parameter of a multiply scattering Brownian medium which does not depend on the concentration c of the scattering particles (since $l^* \sim c^{-1}$ and $\zeta_i \sim c^{-1}$ simultaneously) and is determined only by the optical properties of the scatterers. As a consequence of the hypothesis that the kernels of the integral transforms in expressions (2) and (4) are identical functions of s, the universality of the parameter τ_{cd} should also be manifested in its independence, within wide limits, of the conditions under which the correlation–polarization experiment is performed (geometry of the scattering medium, angle of introduction of the probe beam and detection of the scattered radiation, and so on), which influence only the form of $\rho(s)$. Figure 1 illustrates the method of determining τ_{cd} for multiply scattering Brownian media with different concentrations of scattering particles.

The absence of a concentration dependence of the characteristic correlation time for multiply scattering Brownian ensembles of noninteracting particles was checked in experiments with model media — aqueous suspensions of polystyrene beads with diameters of 0.46 and 1.07 μm. A plane-parallel cylindrical glass cell, 10 mm thick and 70 mm in diameter, was filled with the experimental aqueous suspension and used as the scattering object. An single-mode argon laser (wavelength 514 nm) was used as the source of the linearly polarized probe beam. A laser beam 0.7 mm in diameter was introduced into the experimental medium perpendicular to the flat surface of the cell. The forward-scattered radiation was detected in the paraxial region of the illuminating beam with the aid of a single-mode optical fiber (5 μm in diameter, numerical aperture 0.16). The distance between the fiber end and the exit surface of the cell was equal to 10 mm. A polarizer was inserted between the cell and the end of the optical fiber in order to measure the

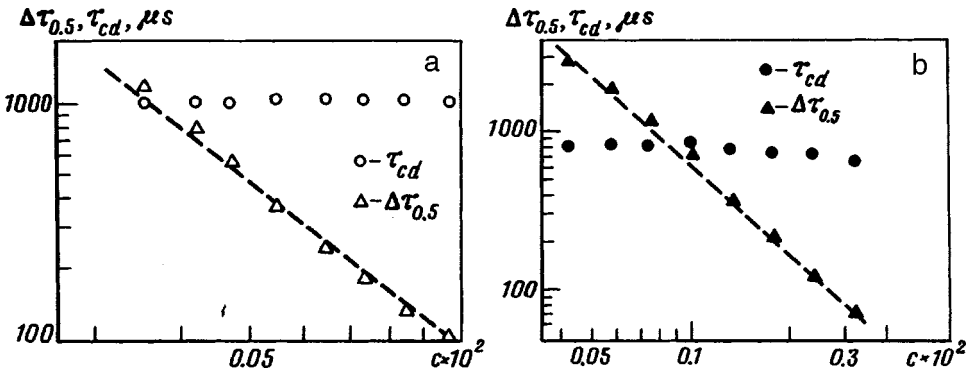

FIG. 2. Concentration dependences of the characteristic correlation time and half-width of the autocorrelation function of intensity fluctuations for aqueous suspensions of polystyrene beads: a — bead diameter 0.46 μm; b — bead diameter 1.07 μm.

degree of polarization of the scattered radiation. In the experiments, a Hamamatsu HC-120 photomultiplier operating in the photon-counting mode was used as a photodetector. The correlation analysis of the intensity fluctuations was performed with a BIC-9000 digital correlator (Brookhaven Instruments, USA). The values of the modulus of the normalized autocorrelation function of the field were reconstructed using the Siegert relation[7] from the normalized autocorrelation functions of the intensity fluctuations measured without a polarizer between the cell and the end of the fiber. The degree of polarization P_L of the scattered field for a fixed concentration of scattering particles was determined from the experimentally measured average values $\langle I_{\parallel}\rangle$ and $\langle I_{\perp}\rangle$ of the intensity of the linearly polarized components of the scattered field with mutually orthogonal directions of polarization (the direction of polarization $\langle I_{\parallel}\rangle$ is the same as that of the beam introduced): $P_L=(\langle I_{\parallel}\rangle-\langle I_{\perp}\rangle)/(\langle I_{\parallel}\rangle+\langle I_{\perp}\rangle)$. The maximum concentrations of the aqueous suspensions investigated in our experiments were determined on the basis of a maximum admissible error of 20% for determining the degree of polarization of the scattered field for $P_L>0.07$–0.08. The values of τ_{cd} were determined by the method illustrated in Fig. 1 for the dependences $|g_1(\tau)|$ reconstructed according to the Siegert relation using the measured values of the degree of polarization P_L. Moreover, measurements of the half-width $\Delta\tau_{0.5}$ of the normalized autocorrelation function of the fluctuations were performed. Figure 2 shows a logarithmic plot of the experimentally measured concentration dependences of τ_{cd} and $\Delta\tau_{0.5}$.

Analysis of the experimental data shows that in the experimental range of concentrations of the aqueous suspensions of polystyrene beads the concentration dependences are close to power-law functions $\Delta\tau_{0.5}\sim c^{-\alpha}$. The exponents α in the power-law functions approximating the experimental values of $\Delta\tau_{0.5}$ in Fig. 2 are ≈ 2.21 and ≈ 1.96 for polystyrene beads of diameters 0.46 μm and 1.07 μm, respectively. These values are in satisfactory agreement with the value $\alpha=2$ obtained in the diffusion approach. Specifically, as was shown in Ref. 2, for example, for an optically thick layer of thickness L consisting of Brownian scattering particles and for isotropic point source and detector, the normalized autocorrelation function of the intensity fluctuations of the forward-scattered coherent radiation has the form $g_2(\tau)\sim 1+\exp[-2\sqrt{D_s k_0^2\tau}L/l^*]$. Since l^*

$\sim c^{-1}$, we obtain in the present case $\Delta\tau_{0.5}\sim c^{-2}$. The closeness to 2 of the values of α obtained can be interpreted as an indirect confirmation of the fact that a multiple-scattering regime of the probe radiation obtains in our experiments, despite the relatively low concentrations of polystyrene beads, and can be satisfactorily interpreted on the basis of the diffusion approach.

The experimental data (the data points ○ and ● in Fig. 2) confirm the conclusion, based on the hypothesis that the kernels of the integral transformations (2) and (4) have the same form, that the values of the characteristic correlation time for Brownian multiply scattering media are constant for the scattering-particle concentrations investigated. Therefore τ_{cd} can indeed be regarded, in a certain sense, as a universal optical parameter of multiply scattering media that does not depend on the concentration of elementary scatterers and is determined only by the ratio of the characteristic scales, obtained by averaging over an ensemble of scatterers, for the decorrelation and depolarization of the optical field and by the diffusion coefficient of the scattering particles.

It should be noted that a small systematic decrease of the characteristic correlation time with increasing c is observed for the 1.07 μm polystyrene beads. This could be due to the different behavior of the kernels of the integral transforms describing the depolarizing and decorrelating properties of the scattering media in the approach studied here. The correlation time τ_{cd} equals 1.04 ± 0.03 ms and 0.77 ± 0.11 ms for the 0.46 μm and 1.07 μm particles, respectively. Proceeding from the values obtained, we calculated the ratios ζ_L/l^* of the characteristic scale of the depolarization of linearly polarized radiation to the transport length. For the types of particles investigated here we used the diffusion coefficients obtained by interpolation from initial values of D_s presented in Ref. 8 for polystyrene beads with diameters of 0.137 μm, 0.300 μm, and 0.807 μm were used. The values employed for interpolation were obtained in the present work by treating them as adjustable parameters in fitting the results of the correlation experiment. The calculations gave the results $\zeta_L/l^*_{0.46\mu\mathrm{m}}\approx3.44$ and $\zeta_L/l^*_{1.07\mu\mathrm{m}}\approx8.73$. These values were compared with the values presented in Ref. 6, which are obtained as a result of statistical simulation and experimental investigations of the depolarization of semiconductor laser radiation by aqueous suspensions of polystyrene beads. The values of ξ_L/l were estimated for the two types of particles employed ($\xi_L/l\approx6$ for $2a=1.07$ μm and $\xi_L/l\approx13$ for $2a\approx0.46$ μm) from the dependence of the depolarization parameter ξ_L/l presented in the present work on the wave parameter k_0a (a is the radius of a scattering particle and l is the mean free path length for the scattering medium, introduced on the basis of the diffusion approach) using the wavelength of the laser radiation in water (0.385 μm). The parameter ξ_L, introduced to describe the depolarizing properties of multiply scattering plane-parallel layers, equals $(\zeta_L l/3)^{1/2}$ (Ref. 6). Substitution and calculation give $\zeta_L/l\approx1.0\times10^2$ for particles 0.46 μm in diameter and $\approx6.0\times10^2$ for particles 1.07 μm in diameter particles. Using for the ratio of the transport length to the mean free path the value $l^*/l\approx26$ calculated in Ref. 9 according to Mie theory for particles 0.46 μm in diameter and for a wavelength of 514 nm, we obtain from the data of Ref. 6 the estimate $\zeta_L/l^*_{0.46\mu\mathrm{m}}\approx3.80$, which is close to the value $\zeta_L/l^*_{0.46\mu\mathrm{m}}\approx3.44$ obtained in our experiments. The values of l^*/l were not determined for the 1.07 μm particles. Nonetheless, since this ratio tends to increase with wavelength, acceptable agreement of the two values should be expected in this case also.

In summary, the interrelation of the characteristic decorrelation and depolarization

scales of optical fields for multiply scattering Brownian media is expressed in the existence of a generalized parameter of the medium — a characteristic correlation time — that does not depend on the concentration of scattering particles. The proposed method of correlation–polarization analysis of scattered optical fields on the basis of measurement of this parameter can be recommended for use together with the conventional optical methods for investigating multiply scattering media in order to obtain additional information about their optical properties.

These investigations were supported in part by CRDF Grant RB1-230.

[a)]e-mail: optics@scnit.saratov.su

[1]V. L. Kuz'min and V. P. Romanov, Usp. Fiz. Nauk **166**, 247 (1996).
[2]F. C. MacKintoch and S. John, Phys. Rev. B **40**, 2383 (1989).
[3]S. John, G. Pang, and Y. Yang, J. Biomed. Opt. **1**, 180 (1996).
[4]G. Maret and P. E. Wolf, Z. Phys. B **65**, 409 (1987).
[5]F. C. MacCintosh, J. X. Zhu, D. J. Pine, and D. A. Weitz, Phys. Rev. B **40**, 9342 (1989).
[6]D. Bicout, C. Brosseau, A. S. Martinez, and J. M. Schmitt, Phys. Rev. B **49**, 1767 (1994).
[7]H. Z. Cummins and E. R. Pike (eds.), *Photon Correlation and Light Beating Spectroscopy*, Plenum Press, New York, 1974 [Russian translation, Mir, Moscow, 1978].
[8]D. A. Boas and A. G. Yodh, J. Opt. Soc. Am. A **14**, 192 (1996).
[9]P. D. Kaplan, M. H. Kao, A. G. Yodh, and D. J. Pine, Appl. Opt. **32**, 3828 (1993).

Translated by M. E. Alferieff

Is the Abrikosov model applicable for describing electronic vortices in plasmas?

A. V. Gordeev and S. V. Levchenko
Kurchatov Institute Russian Science Center, 123182 Moscow, Russia

(Submitted 26 February 1998)
Pis'ma Zh. Éksp. Teor. Fiz. **67**, No. 7, 461–466 (10 April 1998)

A new model of electronic vortices in plasma is studied. The model assumes that the profile of the Lagrangian invariant I, equal to the ratio $I=\Omega/n$ of the electronic vorticity to the electron density, is given. The proposed approach takes into account the magnetic Debye scale $r_B \simeq B/4\pi en$, which leads to breakdown of plasma quasineutrality. It is shown that the Abrikosov singular model cannot be used to describe electron vortices in plasmas because of the fundamental limitation on the electron vorticity on the axis of a vortex in a plasma. Analysis of the equations shows that in the model considered for the electronic vorticity, the total magnetic flux decreases when the size r_0 of the region in which $I\neq 0$ becomes less than c/ω_{pe} (ω_{pe} is the electron plasma frequency). For $\omega_{pe}r_0/c\ll 1$, an electronic vortex is formed in which the magnetic flux decreases as r_0^2 and the inertial component predominates in the electronic vorticity. The structure arising as $\omega_{pe}r_0/c\Rightarrow 0$ is a narrow ''hole'' in the electron density, which can be identified from the spectrum of electromagnetic waves in this region.
 [S0021-3640(98)00607-0]

PACS numbers: 52.20.−j

1. The model of electronic vortices that came into wide use after the publication of Abrikosov's paper[1] has been used for a long time in plasma physics. The fundamental nature of the vortex structure is due to the fact that in the absence of collisions the vorticity

$$\mathbf{\Omega}=\mathbf{B}-\frac{c}{e}[\nabla\times\mathbf{p}] \tag{1}$$

satisfies a conservation law[2,3]

$$\frac{\partial\mathbf{\Omega}}{\partial t}=[\nabla\times[\mathbf{v}\times\mathbf{\Omega}]]. \tag{2}$$

One can see that in this case the integral $\int\mathbf{\Omega}d^2\mathbf{r}$, where $\mathbf{r}$ is the vector in a plane perpendicular to the direction $\mathbf{\Omega}$ and $\mathbf{B}$, is conserved. However, the conservation law (2) asserts somewhat more: the possibility of local conservation and displacement of the vorticity in space are analogous to charge and mass.

Especially simple is the point-vortex model introduced in electrodynamics for type-II superconductors:[1]

$$\frac{c^2}{\omega_{pe}^2}\Delta B - B = -A\delta(\mathbf{r}), \tag{3}$$

which follows from Eq. (1) for $\Omega \sim \delta(\mathbf{r})$ [note: Δ is the Laplacian operator]. Here the constant A is determined by the properties of the medium. The Abrikosov vortex has become a classic object and has been confirmed in numerous experiments.[4,5]

The model (3) is often used to describe electronic vortices in plasma (see, for example, Ref. 6). The divergence of the magnetic field that occurs at the axis according to Eq. (3) is eliminated in superconductors because of the fact that in the vortex core the medium loses its superconducting properties as the axis is approached.[7] Significantly, for a single vortex Eq. (3) leads to a finite magnetic field flux. We shall assume that Eq. (3) holds for electronic vortices in a plasma. Then it also leads to a logarithmic divergence of the magnetic field on the axis if the electron density is assumed to equal the ion density. However, since the fields in a plasma are screened at the magnetic Debye length $r_B = \Omega/4\pi en$, the quasineutrality of the plasma breaks down at distances $r_0 < r_B$ near the axis of the vortex; this leads to a decrease in the electron density and, accordingly, in the electron currents. As will be seen from what follows, in plasma the total magnetic flux is determined by the size r_0 of the region where $\Omega \neq 0$ and approaches zero as $r_0 \Rightarrow 0$, which contradicts Eq. (3). For this reason, the Abrikosov model is incorrect in plasmas.

2. Simple and consistent equations for electronic vortices in plasma were obtained in Refs. 8–10. It was shown there that a correct model of a vortex in a plasma can be constructed by taking into account the small scale $r_B \simeq B/4\pi en$. The standard region of applicability for vortices

$$B^2 \ll 4\pi n_e m_e c^2 \tag{4}$$

corresponds to the case $r_B \ll c/\omega_{pe}$. It could seem that quasineutrality is not important because of the smallness of the magnetic Debye length. However, the magnetic Debye length near the axis may be much greater than the size r_0 of the region where $\Omega \neq 0$. Breakdown of quasineutrality in this region results in a sharp decrease of the electron density — the magnetic field decreases and its logarithmic divergence vanishes.

Therefore, in both superconductors and plasmas there exists a mechanism that eliminates the divergence of the magnetic field on the axis of a vortex. This mechanism relies upon the decrease in the number of current carriers. The difference lies in the fact that in a plasma there is no internal scale that is small compared with c/ω_{pe}. As r_0 decreases below c/ω_{pe}, the density and magnetic field on the axis decrease. As a result, the magnetic term in the vorticity is small compared with the inertial term. For this reason the structure of the vortex changes substantially.

It should be underscored that the general equations obtained in Refs. 8–10 are valid also for the opposite relation between r_B and c/ω_{pe}. Specifically, they are applicable for laser plasmas with very high magnetic fields.[11]

In Refs. 8–10 the equations for vortices were derived for a collisionless model of relativistic cold electrons. In this approximation the main equation for electron motion is

$$\frac{\partial \mathbf{p}}{\partial t}+\frac{1}{4\pi cn}\left[\frac{\partial \mathbf{E}}{\partial t}\times\mathbf{\Omega}\right]+\nabla\gamma mc^2+\frac{\Omega}{4\pi n}\nabla B=-e\mathbf{E}, \tag{5}$$

where Ω is the z component of the electronic vorticity for the case of a magnetic field B directed along the z axis. Equation (5) was derived under the assumption that electrons move in the (x,y) plane. Here $\gamma=(1-\mathbf{v}^2/c^2)^{-1/2}$, $\mathbf{p}=\gamma m\mathbf{v}$, and the electron velocity $\mathbf{v}$ equals

$$\mathbf{v}=-\frac{c}{4\pi en}[\nabla\times\mathbf{B}]+\frac{1}{4\pi en}\frac{\partial \mathbf{E}}{\partial t}. \tag{6}$$

The basic difference of the model of electronic vortices which is examined below from the standard model (3) is that Eq. (1) will be supplemented by the Poisson equation for the electron density

$$\nabla\mathbf{E}=4\pi e(N-n), \tag{7}$$

where N is the ion density. Thus the electron density n is no longer constant and is itself found from the equations.

In the stationary case the following equations can be obtained from Eqs. (1) and (5)–(7) for a cylindrically symmetric vortex:

$$\frac{1}{r}\frac{d}{dr}r\left(mc^2\frac{d\gamma}{dr}+\frac{\Omega}{4\pi n}\frac{dB}{dr}\right)=4\pi e^2(n-N), \tag{8}$$

$$\Omega=B-\frac{mc^2}{4\pi e^2}\frac{1}{r}\frac{d}{dr}r\left(\frac{\gamma}{n}\frac{dB}{dr}\right). \tag{9}$$

An important property of this system of equations is that it yields an explicit expression for the electron density n:

$$4\pi\gamma mc^2n+\Omega\left(G+\gamma^3F\frac{mc}{e}\right)=G^2+\gamma^4F^2\left(\frac{mc}{e}\right)^2+4\pi mc^2\gamma^3N, \tag{10}$$

where

$$G=B+\gamma F\frac{mc}{e},\quad -\frac{v}{r}=F>0,$$

satisfy the equations

$$\frac{dG}{dr}=\frac{\Omega-G}{r}-\frac{mc}{e}\gamma\frac{F}{r}-\frac{4\pi en}{c}rF, \tag{11}$$

$$\frac{dF}{dr}=\frac{e}{mc}\frac{\Omega-G}{\gamma^3r}-\frac{F}{r}. \tag{12}$$

Relation (10) is a consequence of the momentum conservation law. It implies that as Ω increases, the electron density n decreases in view of the aforementioned finiteness of the magnetic field. However, it is difficult to use this relation because the condition $n\geqslant 0$ imposes a limit on the quantity Ω. For this reason, it is convenient to introduce I

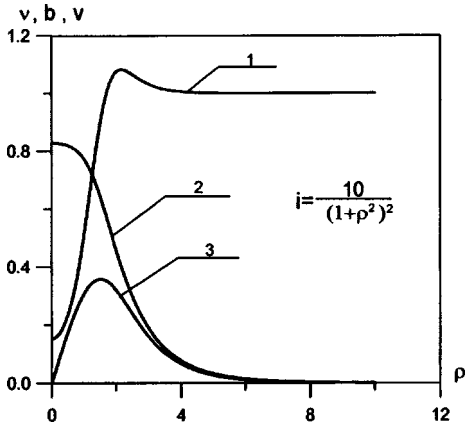

FIG. 1. Structure of an electronic vortex in plasma for a smooth profile of the Lagrangian invariant: *1* — electron density ν, *2* — magnetic field b, *3* — electron velocity v.

$=\Omega/n$, so as to obtain a positive definite expression for n for arbitrary I. The introduction of I has a deeper meaning: It is easy to show that I is a Lagrangian invariant, i.e., it satisfies the equation

$$\frac{\partial I}{\partial t}+\mathbf{v}\cdot\nabla I=0. \tag{13}$$

For this reason the profile of I is transported together with the electrons, thereby preserving the vortex structure.

Introducing the dimensionless coordinate $\rho=r\sqrt{4\pi e^2N/mc^2}$ and the dimensionless functions

$$\nu=\frac{n}{N},\quad g=\frac{G}{\sqrt{4\pi Nmc^2}},\quad f=\frac{F}{\sqrt{4\pi Ne^2/m}},\quad \text{and}\quad i=I\sqrt{N/4\pi mc^2},$$

the final system of equations for calculating an electronic vortex becomes[8–10]

$$\frac{dg}{d\rho}=\frac{\nu i-g}{\rho}-\frac{\gamma f}{\rho}-\nu\rho f, \tag{14}$$

$$\frac{df}{d\rho}=\frac{\nu i-g}{\rho\gamma^3}-\frac{f}{\rho}, \tag{15}$$

where the dimensionless electron density ν equals

$$\nu=\frac{\gamma^3+g^2+\gamma^4f^2}{\gamma+i(g+\gamma^3f)}. \tag{16}$$

3. The structure of an electronic vortex can be calculated on the basis of Eqs. (14)–(16) if the profile i is given. Figure 1 shows as an illustration the result of such a calculation for the profile $i(\rho)$ with a characteristic size $\rho\sim1$. A large decrease in the electron density due to breakdown of quasineutrality can be seen near the vortex axis.

To construct a vortex which is as close as possible to a point vortex analogous to the vortex (3), we shall now decrease the size of the region where I differs appreciably from zero. For simplicity, we choose the profile I in the form of a column with radius $r_0 < c/\omega_{pe}$, and we allow I to increase without bound in this column, decreasing the radius r_0. We shall prove that the on-axis vorticity will remain bounded.

It follows from Eq. (10) that as Ω increases, the electron density n decreases, so that for the maximum on-axis values of Ω the electron density in Eq. (10) can be neglected compared with the ion density. This gives the following relation for the quantities on the vortex axis:

$$\Omega_0\left(G_0+F_0\frac{mc}{e}\right)=G_0^2+F_0^2\left(\frac{mc}{e}\right)^2+4\pi Nmc^2. \tag{17}$$

Here we have set $\gamma=1$ everywhere, and an index 0 denotes the value on the vortex axis.

Furthermore, from the condition that F is constant near the axis and from Eq. (12) it follows that

$$\frac{e}{mc}(\Omega_0-G_0)=F_0. \tag{18}$$

The maximum on-axis value of Ω_0 can be found from Eqs. (17) and (18)

$$\Omega_0^2=8\pi Nmc^2+B_0^2. \tag{19}$$

Integrating Eq. (9), we obtain the following expression for the magnetic flux:

$$\int_0^\infty Br\,dr=\frac{\Omega_0 r_0^2}{2}+\frac{mc}{e}rv\Big|_{r=\infty}. \tag{20}$$

To calculate the electron velocity v at infinity we shall employ Eqs. (11) and (12) at large radii, where it can be assumed that $\gamma=1$ and $n=N$. The equation obtained for v in this limit makes it possible to express v in terms of Bessel functions

$$v=C_1K_1(\rho)+C_2I_1(\rho). \tag{21}$$

In view of the necessary boundary condition for the velocity $v|_{r=\infty}=0$, it follows hence that $v=C_1K_1(\rho)$. Therefore we can neglect the last term in Eq. (20) and, taking relation (19) into account, we find that the magnetic flux decreases as r_0^2 as $r_0\Rightarrow 0$.

Figure 2 displays computational results showing the change in the vortex structures as r_0 decreases and, correspondingly, the on-axis value of I increases. It follows from the analysis presented that, first, the structure of the vortices is determined substantially by an individual characteristic — the size r_0 — and, second, for small $r_0\omega_{pe}/c$ the magnetic flux in the vortex is small. According to the calculations, for $r_0\omega_{pe}/c\simeq 0.3$ the ratio of the magnetic to the inertial term is of the order of 0.1.

The values of the magnetic field and density on the vortex axis and the electron velocity at the boundary r_0 of the region are presented in Fig. 3 as functions of r_0.

4. Thus, in the present model, as I increases, in a narrow region $r_0<r_B=I/4\pi e$ near the axis quasineutrality breaks down, the electron density decreases by virtue of the relation (10), and a ''hole'' forms in the electron density. The magnetic field decreases, and a vortex structure in which the electron inertia makes the main contribution to the

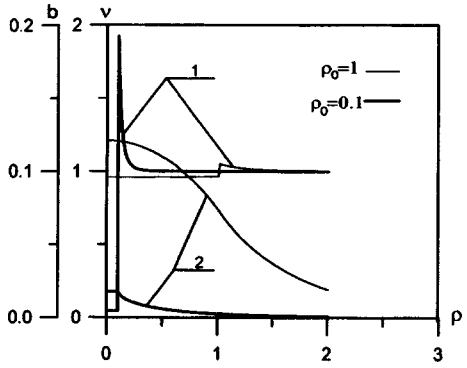

FIG. 2. Variation of the profile of the density (*1*) and magnetic field (*2*) in an electronic vortex with decreasing localization radius ρ_0 of the Lagrangian invariant.

vorticity is obtained. It is interesting that in this region the value of $(\nabla\times\mathbf{v})_z$ is finite, though the electron velocity is proportional to r_0 and is therefore vanishingly small. Despite the smallness of the magnetic flux, because of the existence of the Poisson equation the structure arising differs substantially from a vortex in an uncharged liquid.

The limiting structure of the vortex as $r_0\Rightarrow 0$ is virtually unobservable because of the very small size of the ''hole'' and the absence of a magnetic field. Apparently, the only way to observe such a formation is to analyze the electromagnetic waves in a medium with quite unusual properties: finite Ω_0 at zero electron density. To this end, we shall analyze small oscillations of a such a medium on the basis of Eqs. (5) and (6) and the induction equation

$$-\frac{1}{c}\frac{\partial\mathbf{B}}{\partial t}=[\nabla\times\mathbf{E}]. \tag{22}$$

The investigation of small oscillations in the region $I\neq 0$ leads, in the quasiclassical approximation, after longitudinal plasma oscillations are excluded, to the following dispersion relation for the frequency ω of electromagnetic waves:

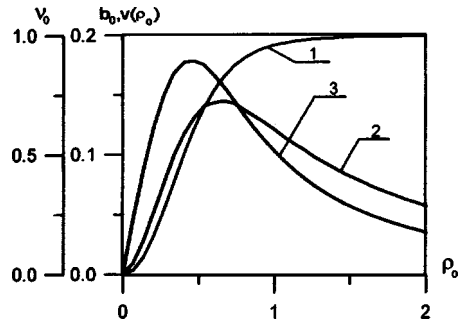

FIG. 3. Density ν_0 (*1*) and magnetic field b_0 (*2*) on the vortex axis and velocity $v(\rho_0)$ (*3*) at the outer boundary of the localization region of the Lagrangian invariant as a function of the size ρ_0 of the localization region.

$$\nu_0^2+\frac{\omega^2-k^2c^2}{\omega_{pe}^2}\left(\frac{\omega^2}{\omega_{pe}^2}-1\right)=\frac{\nu_0}{\omega_{pe}^2}(2\omega^2-k^2c^2), \tag{23}$$

where k is the azimuthal wave number, ν_0 is the ratio of the electron density in the region of the hole to the ion density, and $\omega_{pe}^2=4\pi e^2N/m$. One can see that as $\nu_0\Rightarrow 0$, in the absence of electrons, electromagnetic oscillations in the region of the hole acquire the obvious form $\omega^2=k^2c^2$, in contrast to the form $\omega^2=k^2c^2+\omega_{pe}^2$, as should be the case in the surrounding plasma.[12] We note that in our situation $k^2c^2\gg\omega_{pe}^2$, since $r_0^2\omega_{pe}^2/c^2\ll 1$.

5. It was shown that although there exists in plasmas a mechanism that suppresses the electron currents on the vortex axis and it is possible to eliminate the divergence of the magnetic field, because there is no characteristic length determining the vortex core the vortex electronic structures are determined by the localization radius r_0 of the vorticity and cannot be described by a single universal equation (3). Moreover, for $r_0\omega_{pe}/c\ll 1$ the total magnetic flux decreases, and the structure of the electronic vortex differs substantially from that following from Eq. (3).

Whereas a superconductor Eq. (3) leads to a universal value of the magnetic flux, for an electronic vortex in a plasma the total magnetic flux is determined by the quantity r_0 and is not universal. For this reason Eq. (3) is not applicable for electronic vortices in plasma. In plasmas Eq. (3) must be replaced by the system of equations (14)–(16) with a prescribed profile $i(\rho)$. Electronic vortices retain their individuality, and the characteristic size r_0 of such vortices can vary over wide limits.

This work was supported by Russian Fund for Fundamental Research Grant 97-02-16980.

[1] A. A. Abrikosov, Zh. Éksp. Teor. Fiz. **32**, 1442 (1957) [Sov. Phys. JETP **5**, 1174 (1957)].
[2] O. Buneman, Proc. R. Soc. London, Ser. A **215**, 346 (1952).
[3] S. I. Braginskiĭ, *Reviews of Plasma Physics*, Vol. 1 (edited by M. A. Lenotovich), Consultants Bureau, New York, 1963 [Russian original, Atomizdat, Moscow, 1963, Vol. 1, p. 183].
[4] D. Cribier, B. Jacrot, L. M. Rao, and B. Farnoux, Phys. Lett. **9**, 106 (1964).
[5] U. Essmann and H. Träuble, Phys. Lett. A **24**, 526 (1967); Phys. Status Solidi **20**, 95 (1967).
[6] A. S. Kingsep, K. V. Chukbar, and V. V. Yan'kov, *Topics in Plasma Theory* [in Russian], Énergoatomizdat, Moscow, 1987, Vol. 16, p. 209.
[7] A. A. Abrikosov, *Fundamentals of the Theory of Metals*, North-Holland, Amsterdam, 1988 [Russian original, Nauka, Moscow, 1987].
[8] A. V. Gordeev, Preprint N 5928/6, RRC ''Kurchatov Institute,'' Moscow, 1995.
[9] A. V. Gordeev, Fiz. Plazmy **23**, 108 (1997) [Plasma Phys. Rep. **23**, 92 (1997)].
[10] A. V. Gordeev and S. V. Levchenko, in *18th Symposium on Plasma Physics and Technology*, Prague, June 17–20, 1997, pp. 74-76.
[11] S. V. Bulanov, M. Lontano, T. Zh. Esirkepov *et al.*, Phys. Rev. Lett. **76**, 3562 (1996).
[12] V. D. Shafranov, *Reviews of Plasma Physics*, Vol. 3 (edited by M. A. Lenotovich), Consultants Bureau, New York, 1967 [Russian original, Atomizdat, Moscow, 1963, Vol. 3, p. 3].

Translated by M. E. Alferieff

X-ray spectra of multiply-charged hollow ions in the emission from a femtosecond laser plasma

A. M. Urnov
P. N. Lebedev Physics Institute, 117924 Moscow, Russia

J. Dubau
Paris Observatory, F-9211195 Midon, France

A. Ya. Faenov, T. A. Pikuz, and I. Yu. Skobelev
Center for Data on the Spectra of Multiply Charged Ions, All-Russia Scientific-Research Institute of Physicotechnical and Radioelectronic Measurements, 141570 Mendeleevo, Moscow Region, Russia

J. Abdallah, R. E. H. Clark, J. Cohen, R. P. Johnson, G. A. Kyrala, and M. D. Wilke
Los Alamos National Laboratory, Los Alamos, New Mexico 87545 USA

A. L. Osterheld
Livermore National Laboratory, Livermore, California 94551 USA

(Submitted 23 January 1998; resubmitted 10 March 1998)
Pis'ma Zh. Éksp. Teor. Fiz. **67**, No. 7, 467–472 (10 April 1998)

A new type of quasicontinuous emission spectrum from a femtosecond laser plasma near the Ly_α line of H-like ions is obtained and interpreted. It is shown that these spectra are emitted by multiply charged hollow ions, which are present in the plasma on account of its ultrahigh density, which, in turn, is due to the use of high-contrast laser pulses for producing the plasma. A new spectroscopic approach based on analysis of the composition of spectral complexes of hollow ions is discussed. © *1998 American Institute of Physics.*
[S0021-3640(98)00707-5]

PACS numbers: 52.50.Jm, 52.25.Nr

The x-ray emission spectra of nanosecond and subnanosecond laser plasmas have been investigated intensively for at least the last two decades. Specifically, the spectral characteristics of radiation near the resonance lines of H- and He-like multiply charged ions have now been studied in great detail. The spectra in this region have a typical structure (see Fig. 1a) characterized by the presence of satellite lines and their groups (dielectronic satellites, DSs), which are due to transitions from autoionizing states of the ions. This structure is described well by radiational-collisional kinetic models employing the theoretical values of the atomic characteristics (level energies, probabilities of elementary atomic processes). The diagnostic properties of such spectra in respect to the relative line intensities and spectral profiles are well known and widely used in plasma experiments (see, for example, the reviews in Refs. 1 and 2).

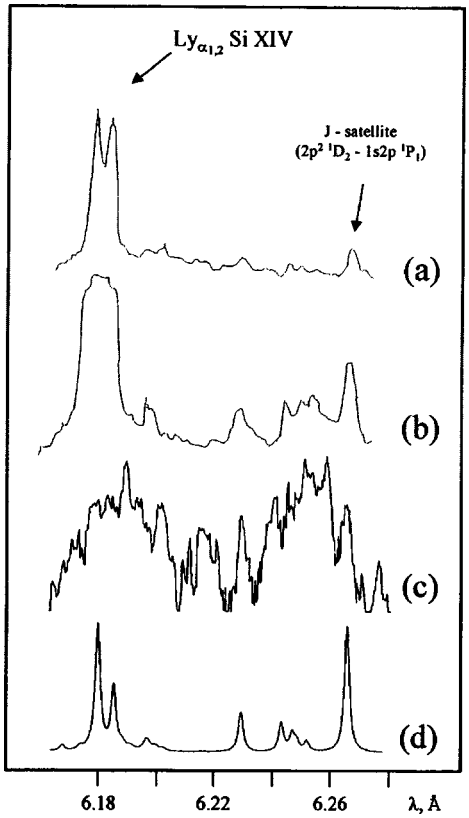

FIG. 1. Emission spectra of a silicon plasma heated with nanosecond[1] (a), subnanosecond[3] (b), and subpicosecond[4] (c) laser pulses near the Ly_α resonance line of the H-like ion Si XIV. The theoretical spectrum (d) corresponds to the corona model.

The x-ray emission of a plasma produced by picosecond and subpicosecond lasers has been the subject of various investigations in recent years. The spectral properties of this radiation are similar to those observed earlier in experiments with longer laser pulses. The measured spectra have a quite standard form (see Fig. 1b) which is reproduced well by a corona model, while the variations of the line intensities can be described by variations of the plasma parameters, such as the temperature, density, and the ionization composition. It is important to note that when short laser pulses interact with matter, the production of a preplasma due to the presence of a laser prepulse plays an important role. The present experiments were performed with a femtosecond laser characterized by an ultrahigh contrast (ratio of the pulse and prepulse intensities) of the order of 10^{11} (Ref. 4). The result of these experiments was detection of spectra of a new type, not previously observed in this spectral region (Fig. 1c).

The unconventional spectra that we observed differ from more familiar spectra by the presence of a complicated, quasicontinuous spectral structure in which the main lines are embedded. The theoretical spectra calculated in a quasistationary corona kinetic model of a plasma (see Fig. 1d), although similar to the typical experimental spectra

(Figs. 1a,b), are completely unsuitable for describing the new spectrum (Fig. 1c). The physical reason for such a sharp restructuring of the spectrum is naturally associated with the difference in plasma production mechanisms. When there is no preplasma, an ultrashort laser pulse interacts directly with the solid matter, resulting in the formation of plasma with a much higher electron density. At such densities many spectral lines that are hardly excited at all under corona conditions begin to dominate the emission spectra of the plasma.

In the present letter it is shown that the new type of spectra observed can be interpreted only by taking into account the radiation emitted by multiply charged hollow ions (i.e., ions with an empty K shell) in an ultradense plasma. Transitions of this type in neutral and quasineutral objects (hollow atoms) have been observed in experiments on the interaction of ion beams with a solid surface and have been actively studied during the last several years in connection with their atomic-clock properties (see, for example, Refs. 5–10). Similar structures for multiply charged ions were recently observed in the spectra from regions close to the target surface in plasmas produced by a pulse from the NIKE laser.[11]

The experimental investigations were performed on the TRIDENT laser installation at Los Alamos National Laboratory.[4] The laser pulse had a duration of 500 fs, energy 550 mJ, and maximum intensity of the order of $(0.5–1)\times 10^{19}$ W/cm^2. The power contrast between the main pulse and the natural nanosecond prepulse was at least $10^{10}–10^{11}$. Solid silicon targets were used.

The x-ray spectra of the plasma were observed with a spectrograph with a spherically curved mica crystal. Crystals with radii of curvature equal to 100, 150, and 186 mm were used. The crystal, plasma, and photographic film were arranged according to the FSSR-1D and FSSR-2D schemes.[2] This made it possible to record spectra with high spectral ($\lambda/\delta\lambda = 10\,000$) and spatial ($\delta x = 10\ \mu$m) resolutions simultaneously.

The spectral structures in the region 6.16–6.28 Å (near the resonance line of the Si XIV ion) can be due only to transitions from the excited levels of ions with no $1s$ electrons. Such transitions result in, for example, the emission of the Ly$_\alpha$ resonance line itself and its so-called He-like dielectronic satellites, i.e., lines whose upper levels are doubly excited states of a two-electron ion. To find additional spectral lines near the Ly$_\alpha$ line, we performed atomic calculations using the SUPERSTRUCTURE code.[12] The method of Refs. 13 and 14 was used to calculate the autoionization widths. The multiconfigurational wave functions for the bound states were calculated in the intermediate-coupling approximation taking into account the Breit–Pauli relativistic corrections. The autoionization matrix elements, including orbitals of the continuous spectrum, were calculated by the distorted-wave method.

Our calculations showed that many lines due to transitions in multielectron systems with $q \geqslant 3$ electrons (Li-like, Be-like, ... ions) and with an empty K shell, i.e., transitions in hollow ions, fall into the experimental range. The populations of the states of hollow ions with $q \geqslant 3$ in a corona plasma are negligibly small, and the emission spectra of such a plasma which are due to ions with $q < 3$ have the characteristic form shown in Figs. 1a and b. In the ultradense plasma with electron density N_e exceeding a critical value N^* (for a silicon plasma N^* is of the order of 10^{22} cm^{-3}) the level-populating mechanisms that are nonlinear in N_e lead to a large increase in the populations of the states of hollow

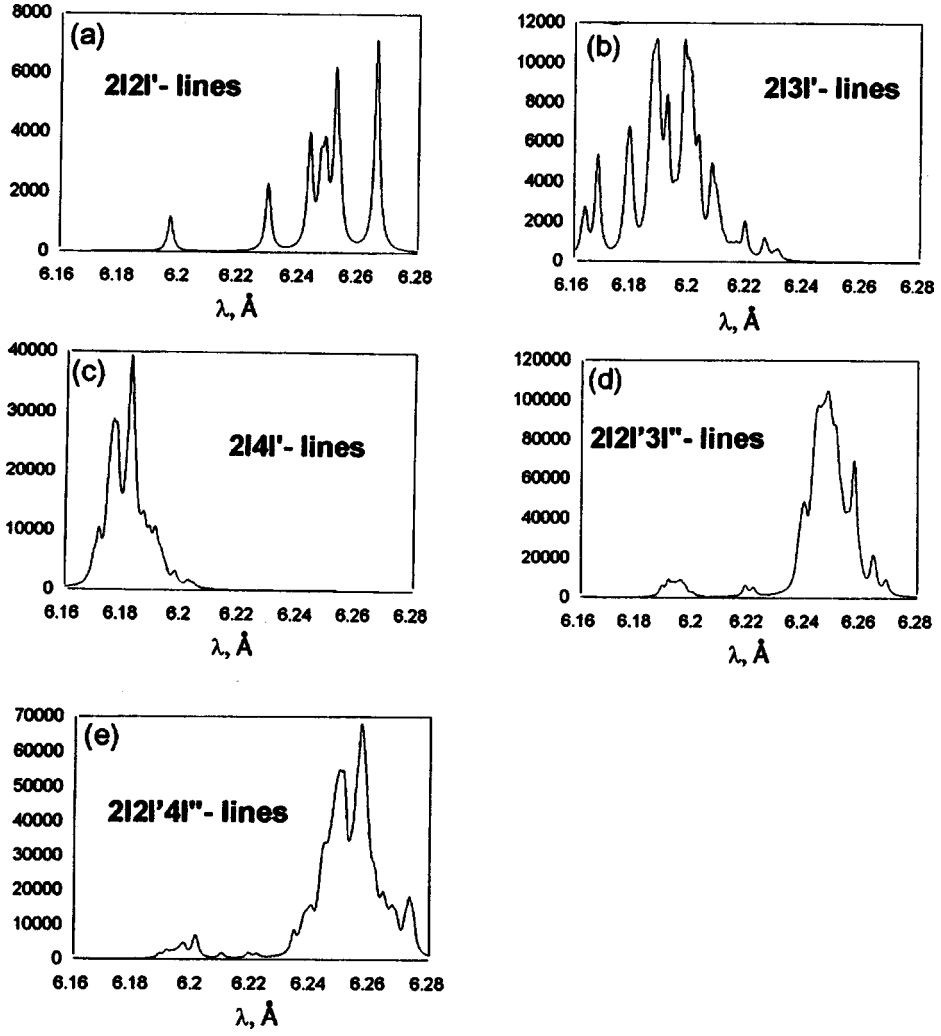

FIG. 2. Spectra emitted by different states of hollow ions, calculated for the case of a Boltzmann distribution of l-subshell populations.

ions, thereby increasing the amplitudes of the corresponding spectral lines. We note that the most important consequences of this effect are: a) collisional mixing of different l subshells in configurations with fixed principal quantum number n, and b) increase in the role of additional mechanisms for populating states with $q \geqslant 3$, such as, for example, dielectronic capture from excited states and ternary recombination.[15,16]

Figure 2 shows the computational results for spectra emitted by the states of hollow ions with $q=2$, 3 and characterized by different sets of principal numbers $[2, n]$ and $[2, n, n_1]$. To construct the total emission spectrum it necessary, obviously, to solve a corresponding system of kinetic equations. It should be noted that assuming a Boltzmann distribution over the l subshells substantially simplifies the kinetic simulation because the

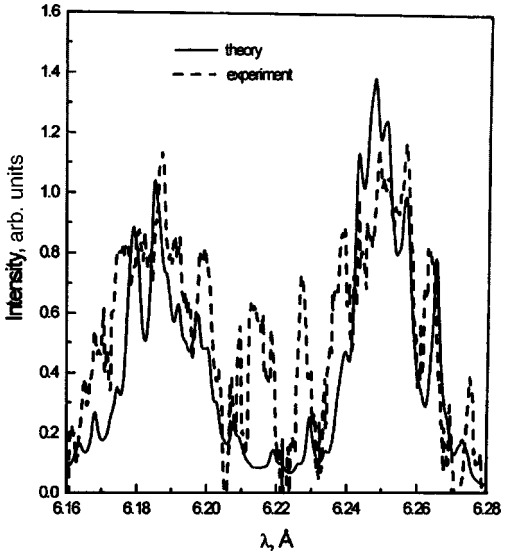

FIG. 3. Comparison of the emission spectra of a silicon femtosecond laser plasma with a calculation performed for a plasma in local thermodyamic equilibrium with $T_e=350$ eV and $N_e=6\times10^{23}$ cm^{-3}.

number of atomic levels studied decreases sharply. The kinetic system in this case must be solved not for individual atomic states but rather for entire ionic complexes characterized by different sets of principal quantum numbers. In an ultradense plasma the distribution of ions over ion complexes will be Saha–Boltzmann-like. The corresponding total spectrum is displayed in Fig. 3. We note that in calculating this spectrum the self-absorption of the Ly_α line was taken into account in the Biberman–Holstein approximation.

As one can see from Fig. 3, the synthesized spectrum on the whole agrees quite well with the experimental data. The differences (the presence of two unexplained maxima near 6.215 Å and 6.23 Å as well as the underestimation of the observed intensity in the entire spectral region) are due, according to preliminary calculations,[a)] to the neglect of hollow ionic complexes of the type $[2, n, n]$ with $n\geqslant3$ and $[2, n]$ with $n>4$ and configurations with $q\geqslant4$.

In the present work it was shown that the new type of quasicontinuous spectra observed in a femtosecond laser plasma produced by a high-contrast pulse is due to transitions in multiply charged hollow ions. Therefore a laser plasma is a natural source of hollow ions and offers new possibilities for analyzing their properties. The presence of ionic states with empty K shells in such a plasma is a consequence of its ultrahigh density, resulting in breakdown of corona conditions. A new type of spectral diagnostics based on the construction of the emission spectra of a plasma not from individual spectral lines but rather from entire spectral complexes characterized by different sets of principal quantum numbers $[n, n_1, n_2]$ was proposed. The model calculations performed assuming Saha–Boltzmann equilibrium demonstrate good quantitative agreement with the measured spectra and show that an adequate kinetic model of an ultradense plasma must be constructed with the states of hollow ions taken into account.

This work was supported in part by INTAS-RFBR Grant 95-0875, Russian Fund for Fundamental Research Grant 16111, and the US Department of Energy.

[a)]R. Doron, private communication (1998).

[1] V. A. Boiko, A. V. Vinogradov, S. A. Pikuz *et al.*, J. Sov. Laser Res. **6**, 85 (1985).
[2] I. Yu. Skobelev, A. Ya. Faenov, B. A. Bryunetkin *et al.*, Zh. Éksp. Teor. Fiz. **108**, 1263 (1995) [JETP **81**, 692 (1995).
[3] A. Ya. Faenov, I. Yu. Skobelev, S. A. Pikuz *et al.*, Phys. Rev. A **51**, 3529 (1995).
[4] A. Ya. Faenov, J. Abdallah, R. E. H. Clark *et al.*, Proc. SPIE-97 **3157**, 10 (1997).
[5] J.-P. Briand, L. de Billy, P. Charles *et al.*, Phys. Rev. Lett. **65**, 159 (1990).
[6] A. McPherson, B. D. Thompson, A. B. Borisov *et al.*, Nature **370**, 631 (1994).
[7] J.-C. Gauthier, J.-P. Geindre, P. Audebert *et al.*, Phys. Rev. E **52**, 2963 (1995).
[8] J.-P. Briand, G. Giardino, G. Borsoni *et al.*, Phys. Rev. A **54**, 4136 (1996).
[9] S. Ninomiya, Y. Yamazaki, F. Koike *et al.*, Phys. Rev. Lett. **78**, 4557 (1997).
[10] J.-P. Briand, D. Schneider, S. Bardin *et al.*, Phys. Rev. A **55**, 3947 (1997).
[11] Y. Aglitsky, J. Seely, C. Pawley *et al.*, Phys. Plasmas **3**, 9 (1996).
[12] W. Eissner, M. Jones, and H. Nussbaumer, Comput. Phys. Commun. **8**, 270 (1974).
[13] P. Faucher and J. Dubau, Phys. Rev. A **31**, 3672 (1985).
[14] M. K. Inal and J. Dubau, J. Phys. B **22**, 3329 (1989).
[15] F. B. Rosmej, A. Ya. Faenov, T. A. Pikuz *et al.*, JETP Lett. **65**, 708 (1997).
[16] F. B. Rosmej, A. Ya. Faenov, T. A. Pikuz *et al.*, J. Quant. Spectrosc. Radiat. Transf. **58**, 859 (1997).

Translated by M. E. Alferieff

On the influence of a square-root van Hove singularity on the critical temperature of high-T_c superconductors

É. A. Pashitskiĭ and V. I. Pentegov
Institute of Physics of the Ukrainian National Academy of Sciences, 252650 Kiev, Ukraine

E. Abraham
Department of Physics, Heriot-Watt University, Edinburgh, EH14 4AS, UK

(Submitted 6 February 1998)
Pis'ma Zh. Éksp. Teor. Fiz. **67**, No. 7, 473–477 (10 April 1998)

It is shown that the square-root van Hove singularity appearing in the density of states $\nu(E_F)\sim(E_F-E_0)^{-1/2}$ as a result of extended saddle-point singularities in the electron spectrum of high-T_c superconductors based on hole-type cuprate metal-oxide compounds gives a nonmonotonic dependence of the critical temperature T_c on the position of the Fermi level E_F relative to the bottom E_0 of the saddle. Because the divergence of $\nu(E_F)$ is canceled in the electron–electron interaction constant renormalized by strong-coupling effects, T_c approaches zero as $E_F\to E_0$, in contrast to the weak-coupling approximation, where in this limit T_c approaches a finite (close to maximum) value. The dependence obtained for T_c as a function of the doped hole density in the strong-coupling approximation agrees qualitatively with the experimental data for overdoped cuprate metal oxides. © *1998 American Institute of Physics.* [S0021-3640(98)00807-X]

PACS numbers: 74.25.Jb, 74.72.−h

1. Photoelectron spectroscopy experiments[1–5] with high angular and energy resolution show that the electronic spectra of layered crystals of cuprate metal oxide compounds (MOCs) with hole-type conductivity (YBaCuO, BiSrCaCuO, TlBaCaCuO) contain ''flat-band'' regions near the Fermi level which consist of extended saddle-point singularities (SPSs) with a square-root van Hove singularity (VHS) in the electronic density of states $\nu(E_F)\sim(E_F-E_0)^{-1/2}$. The Fermi energy $\mu_1\equiv(E_F-E_0)$ and the Fermi momentum $k_{F1}\approx\sqrt{2m_1^*\mu_1}$ in such quasi-one-dimensional parts of the spectrum with effective mass $m_1^*\gg m_0$ (where m_0 is the mass of a free electron) are anomalously small and for optimally doped crystals $\mu_1\cong 20$–30 meV and $k_{F1}\cong 0.15$–0.17 Å^{-1}, respectively, while the extent of the saddle-point singularity is $P_1\cong 0.5$ Å^{-1} (Refs. 4 and 5).

As was shown in Refs. 2 and 6 in the weak-coupling approximation (BCS model[7]), extended SPSs with square-root VHSs lead for $\mu_1\leqslant T_c$ to a nonexponential (power-law) dependence of T_c on the dimensionless effective electron–electron attraction constant λ: $T_c\approx\mu_1\lambda^2$, where $\lambda\approx\lambda_1\sqrt{E_1/\mu_1}$, i.e., the critical temperature approaches a constant limit $T_c\approx E_1\lambda_1^2$ as $\mu_1\to 0$. Therefore, according to Ref. 2, at energies E_1 of the order of the width of the band ($E_1>1$ eV), quite high values $T_c\geqslant 100$ K can be achieved at very low

values $\lambda_1 \sim 0.1$, irrespective of the mechanism of Cooper pairing of the charge carriers.

However, for large values of λ it is necessary to use the strong-coupling approximation,[8] in which the renormalization of the interaction constant $\tilde{\lambda} = \lambda/(1+\lambda)$ cancels the divergence $\lambda \sim \nu(\mu_1) \sim \mu_1^{-1/2}$ at the point $\mu_1 = 0$. Because of this, as is shown in the present work, $T_c \sim \mu_1$ as $\mu_1 \to 0$, i.e., T_c vanishes when the Fermi level touches the bottom of the extended SPSs, in contrast to the weak-coupling approximation,[2,6] where T_c approaches a finite (close to maximum) value as $\mu_1 \to 0$. The nonmonotonic dependence of T_c on the doped hole density n_p obtained when strong-coupling effects are taken into account agrees qualitatively with the experimental data for overdoped cuprate MOCs.[9,10]

2. We start from the assumption that the mechanism of high-T_c superconductivity (HTSC) in layered cuprate MOCs is Cooper pairing of fermions (electrons, holes) due to the exchange of virtual bosons (phonons, magnons, plasmons, excitons). As is well known,[7,8] in the strong-coupling approximation the superconducting state is described by a system of equations for the normal Σ_1 and anomalous Σ_2 self-energy parts. Assuming that the characteristic energy $\tilde{\Omega}$ of the bosons that carry the interaction is much higher than T_c, the linearized equation for the gap $\Delta(\mathbf{k},\omega)$ at the Fermi surface in the limit $T \to T_c$ can be represented in the following form, taking into account the quasi-two-dimensionality of the electron spectrum in layered MOC crystals and the anisotropic structure of the electron–electron interaction:

$$(1+\lambda(\theta))\Delta(\theta,0) = \frac{1}{2}\int_0^{2\pi}\frac{d\theta}{2\pi}\int_{-\tilde{\Omega}}^{\tilde{\Omega}}\frac{d\omega}{\omega}\Delta(\theta',\omega)\nu(\theta',\omega)W(\theta,\theta',\omega)\tanh\frac{\omega}{2T_c}, \tag{1}$$

where $\lambda(\theta) = -\partial\Sigma_1(\theta,\omega)/\partial\omega|_{\omega=0}$ is the dimensionless retarded-interaction constant, $\Delta(\theta,\omega) = \Sigma_2(\theta,\omega)/(1+\lambda(\theta))$ is the anisotropic gap in the quasiparticle spectrum, θ and θ' are the angles made by the electron momenta $\mathbf{k}$ and $\mathbf{k}'$ on the Fermi surface and the direction of one of the principal crystallographic axes (**a** or **b**) in the plane of the layers, and $W(\theta,\theta'\omega)$ and $\nu(\theta,\omega)$ are, respectively, the matrix element of the electron–electron interaction and the electronic density of states, which can be represented as Fourier series expansions in the angle θ and θ'. In what follows, we shall confine ourselves, for simplicity, to the first two terms in the expansion of $W(\theta,\theta',\omega)$, which correspond to the A_1 and B_1 representations of the $C_{4\nu}$ symmetry group of the CuO_2 cuprate plane,

$$W(\theta,\theta,\omega) = W_0(\omega) + W_2(\omega)\cos 2\theta\,\cos 2\theta' + W_4(\omega)\cos 4\theta\,\cos 4\theta', \tag{2}$$

and we represent the anisotropic density of states near a closed cylindrical hole-type Fermi surface (Fig. 1) in the form

$$\nu(\theta',\omega) = \nu_+(\omega) + \nu_-(\omega)\cos 4\theta'; \quad \nu_\pm(\omega) = \frac{1}{2}\left[\nu_1 \mathrm{Re}\sqrt{\frac{\mu_1}{\mu_1+\omega}} \pm \nu_2\right]. \tag{3}$$

Here $\nu_1(\mu_1) \sim \mu_1^{-1/2}$ is the density of states on the quasi-one-dimensional parts of the Fermi surface near extended SPSs with a square-root VHS, while ν_2 is the constant density of states on the quasi-two-dimensional parts of the Fermi surface in the direction of the diagonals of the Brillouin zone. In this case the anisotropic coupling constant $\lambda(\theta)$ has the form

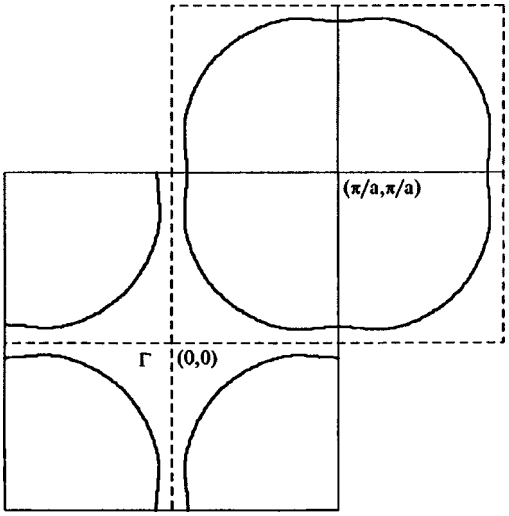

FIG. 1. Section of the Fermi surface of layered cuprate metal oxides of the type BSCCO. The closed cylindrical hole-type Fermi surface is centered at the corner $(\pi/a,\ \pi/a)$ of the Brillouin zone.

$$\lambda(\theta)=\lambda_0+\lambda_4\cos 4\theta;\quad \lambda_0=\nu_+(0)W_0(0);\quad \lambda_4=\frac{1}{2}\nu_-(0)W_4(0). \tag{4}$$

For sufficiently large positive values of $W_0(0)$ and $W_4(0)$ the s-wave symmetry of Cooper pairing with anisotropic gap parameter

$$\Delta_s(\theta,\omega)=\Delta_0(\omega)+\Delta_4(\omega)\cos 4\theta, \tag{5}$$

can predominate. Then the critical temperature T_c^s is determined by solving the following system of coupled integral equations (for simplicity, we neglect the ω dependence of Δ and W in the region $|\omega|<\tilde{\Omega}$):

$$(1+\lambda_0)\Delta_0+\frac{1}{2}\lambda_4\Delta_4=\frac{1}{2}W_0(0)\int_{-\tilde{\Omega}}^{\tilde{\Omega}}\frac{d\omega}{\omega}\left[\nu_+(\omega)\Delta_0+\frac{1}{2}\nu_-(\omega)\Delta_4\right]\tanh\frac{\omega}{2T_c^s}, \tag{6}$$

$$(1+\lambda_0)\Delta_4+\lambda_4\Delta_0=\frac{1}{4}W_4(0)\int_{-\tilde{\Omega}}^{\tilde{\Omega}}\frac{d\omega}{\omega}[\nu_+(\omega)\Delta_4+\nu_-(\omega)\Delta_0]\tanh\frac{\omega}{2T_c^s}. \tag{7}$$

At the same time, for a sufficiently large positive W_2 the $d_{x^2-y^2}$-wave symmetry of Cooper pairing with an anisotropic gap $\Delta_d(\theta)\sim\cos 2\theta$ and a critical temperature T_c^d determined by the equation

$$(1+\lambda_0)=\frac{1}{4}W_2(0)\int_{-\tilde{\Omega}}^{\tilde{\Omega}}\frac{d\omega}{\omega}\left[\nu_+(\omega)+\frac{1}{2}\nu_-(\omega)\right]\tanh\frac{\omega}{2T_c^d} \tag{8}$$

can predominate.

3. Since most experiments (see, for example, Refs. 11–14) attest to $d_{x^2-y^2}$-wave symmetry of the gap in high-T_c superconductors, we shall examine this particular case, which in our model corresponds to a large positive matrix element W_2 in Eq. (2). Then, with allowance for expressions (3), for $\mu_1<\tilde{\Omega}$ Eq. (8) becomes

$$1=\frac{W_2}{4(1+\lambda_0)}\left\{\frac{3}{2}\nu_1(\mu)\int_{\mu_1}^{\tilde{\Omega}}\frac{d\omega}{\omega}\sqrt{\frac{\mu_1}{\mu_1+\omega}}\tanh\frac{\omega}{2T_c^d}+\nu_2\ln\left(\frac{\tilde{\Omega}}{T_c^d}\right)\right\}. \tag{9}$$

The first term in braces in Eq. (9) describes the contribution of quasi-one-dimensional parts of the Fermi surface with a square-root VHS in the density of states, and the second term describes the contribution of the quasi-two-dimensional parts of the Fermi surface with a constant density of states.

For $T_c^d\ll\mu_1$ we obtain by approximate integration over ω in Eq. (9)

$$(T_c^d)^{3\alpha_1+\alpha_2}\approx(4\mu_1)^{3\alpha_1}\tilde{\Omega}^{\alpha_2}\exp\left\{-\frac{1+\lambda_0}{\lambda_2}\right\}, \tag{10}$$

where

$$\alpha_1(\mu_1)=\frac{\nu_1(\mu_1)}{\nu_1(\mu_1)+\nu_2};\quad \alpha_2(\mu_1)=\frac{\nu_2}{\nu_1(\mu_1)+\nu_2};\quad \lambda_2(\mu_1)=\frac{1}{2}(\nu_1(\mu_1)+\nu_2)W_2. \tag{11}$$

In the opposite case, i.e., $T_c^d\gg\mu_1$, in which $\nu_1\gg\nu_2$ and $\lambda_0\approx\frac{1}{2}\nu_1W_0\gg1$ as $\mu_1\to0$, it follows from Eq. (9) that as a result of the cancelation of ν_1 in the renormalized coupling constant one has

$$T_c^d\approx2\mu_1(3W_2/2W_0)^2, \tag{12}$$

so that $T_c^d\to0$ as $\mu_1\to0$. Using the equations (6) and (7), it can be shown that in the strong-coupling approximation a similar result ($T_c^s\sim\mu_1$ as $\mu_1\to0$) is also valid in the case of s-wave gap symmetry, in contrast to the result obtained in Refs. 2 and 6 in the weak-coupling approximation, where the value of T_c is finite and close to the maximum value with $\mu_1=0$.

Figure 2 shows the curves of T_c^d versus μ_1 obtained by solving Eq. (8) numerically for different values of the parameters $\tilde{\Omega}$ and $\lambda_1=\nu_1^*W$, where $\nu_1^*\equiv\nu_1(\mu_1^*)$ and $\mu_1^*\approx(0.02–0.03)$ eV, which corresponds to the position of the Fermi level in optimally doped cuprate MOC crystals.[3,4] The solid curves *1* and *2* were calculated for $\tilde{\Omega}=0.1$ eV and $\tilde{\Omega}=2$ eV with a fixed ratio $\nu_1^*/\nu_2=5$ and for values of the constants λ_1 and λ_0 that put the maximum of T_c^d as a function of μ_1 at the point $\mu_1^*=0.03$ eV and give the maximum value $T_c\approx110$ K observed experimentally for BSCCO. We note that for a fixed ratio of the constants λ_1 and $\lambda_0\equiv\lambda_0(\mu^*)$, these conditions, imposed on the position and magnitude of the maximum value of T_c, lead to a power-law dependence of λ_1 on $\tilde{\Omega}$ with a small exponent $\beta\approx-0.06$. A log–log plot of this dependence is shown in the inset of Fig. 2. As we can see, the value of the coupling constant λ_1 that gives quite high values of T_c is relatively small and is virtually independent of the characteristic interaction energy $\tilde{\Omega}$, which is determined by the specific mechanism of Cooper pairing.

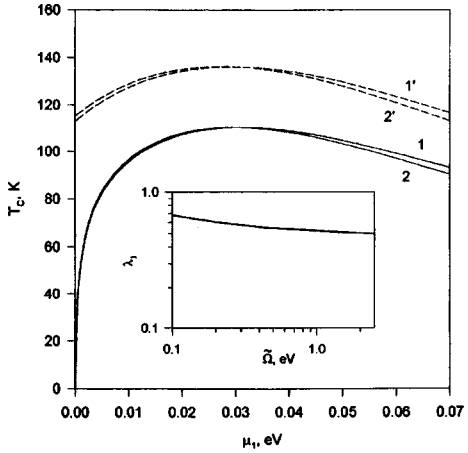

FIG. 2. T_c versus the Fermi energy $\mu_1 = E_F - E_0$ on extended SPSs, calculated in the strong-coupling (solid curves) and weak-coupling (dashed curves) approximations. Curves *1* and *1′* correspond to $\tilde{\Omega} = 0.1$ eV and $\lambda_1 = 0.68$, while curves *2* and *2′* correspond to $\tilde{\Omega} = 2$ eV and $\lambda_1 = 0.5$.

The dashed curves in Fig. 2 show T_c^d calculated for the same values of the parameters but neglecting the renormalization of the interaction constant by the factor $1 + \lambda_0$; this corresponds to the strong-coupling approximation.[2,6]

Figure 3 shows the concentration dependences of T_c^d corresponding to curves *1* and *1′* in Fig. 2 and obtained using Eq. (3) for the density of states. The experimental values given in Ref. 10 for the critical temperature as a function of the hole density n_p per Cu atom are presented for comparison. As one can see, good agreement is observed between the experimental data and the theoretical dependence $T_c(n_p)$ obtained in the strong-coupling approximation.

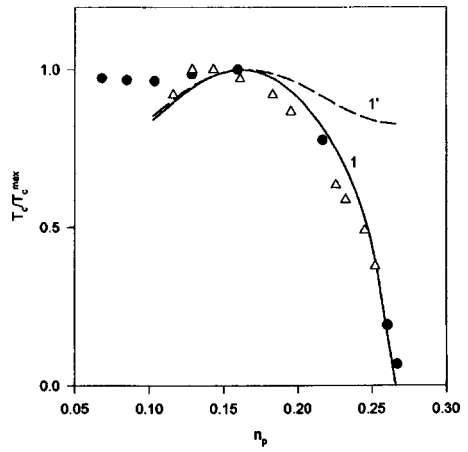

FIG. 3. T_c versus the hole density n_p per Cu atom. The theoretical curves correspond to curves *1* and *1′* in Fig. 2. The experimental data are from Ref. 10: ● — TlPbCaYSrCuO (1212), Δ — BiPbSrLaCuO (2201).

In summary, we have shown that the decrease of the critical temperature of a superconducting transition in overdoped cuprate MOCs with increasing hole density and the vanishing of T_c at some value of n_p are due to a square-root VHS in the electronic density of states on extended SPSs and do not depend on either the mechanism of Cooper pairing of the current carriers or the gap symmetry.

We thank A. V. Gurevich and A. V. Semenov for helpful discussions. This work was supported by Grant 2.4/561 from the Ukrainian State Fund for Fundamental Research and Grant GR/L25363 (Visiting Fellowship Research Grant, EPSRC, United Kingdom).

[1] D. S. Dessau, Z.-X. Shen, D. M. King *et al.*, Phys. Rev. Lett. **71**, 2781 (1993).
[2] A. A. Abrikosov, J. C. Campuzano, and V. Gofron, Physica C **214**, 73 (1993).
[3] D. M. King, Z.-X. Shen, and D. S. Dessau, Phys. Rev. Lett. **73**, 3298 (1994).
[4] V. Gofron, J. C. Campuzano, A. A. Abrikosov *et al.*, Phys. Rev. Lett. **73**, 3302 (1994).
[5] H. Ding, J. C. Campuzano, A. F. Bellman *et al.*, Phys. Rev. Lett. **74**, 2784 (1995); **75**, 1425 (1995).
[6] A. A. Abrikosov, Physica C **214**, 107 (1993); **222**, 191 (1994); **244**, 243 (1995).
[7] J. Schrieffer, *Theory of Superconductivity*, Benjamin, New York, 1964 [Russian translation, Nauka, Moscow, 1970].
[8] G. M. Éliashberg, Zh. Éksp. Teor. Fiz. **38**, 966 (1960) [Sov. Phys. JETP **10**, 696 (1960)]; Zh. Éksp. Teor. Fiz. **39**, 1437 (1960) [Sov. Phys. JETP **12**, 1000 (1961)].
[9] J. B. Torrance, A. Bezinge, A. I. Mazzal, and S. S. P. Parkin, Physica C **162-164**, 291 (1989).
[10] J. L. Tallon, R. G. Buckley, E. M. Haines *et al.*, Physica C **185-189**, 855 (1991).
[11] D. A. Wollman, D. J. Van Harlingen, W. C. Lee *et al.*, Phys. Rev. Lett. **71**, 2134 (1993); D. A. Wollman, D. J. Van Harlingen, J. Giapintzakis, and D. M. Ginsberg, Phys. Rev. Lett. **74**, 797 (1995).
[12] S. S. Tsuei, J. R. Kirtley, C. C. Chi *et al.*, Phys. Rev. Lett. **73**, 593 (1994).
[13] J. R. Kirtley, S. S. Tsuei, M. Rupp *et al.*, Phys. Rev. Lett. **76**, 1336 (1996).
[14] M. R. Norman, M. Randeria, H. Ding *et al.*, Phys. Rev. B **52**, 15107 (1995).

Translated by M. E. Alferieff

Anomalous proximity effect in *d*-wave superconductors

A. A. Golubov

Department of Applied Physics, University of Twente, The Netherlands; Institute of Solid State Physics, Russian Academy of Sciences, 142432 Chernogolovka, Russia

M. Yu. Kupriyanov

Department of Applied Physics, University of Twente, The Netherlands; Nuclear Physics Institute, Moscow State University, 119899 Moscow, Russia

(Submitted 12 January 1998; resubmitted 24 February 1998)
Pis'ma Zh. Éksp. Teor. Fiz. **67**, No. 7, 478–483 (10 April 1998)

The anomalous proximity effect between a *d*-wave superconductor and a thin disordered normal layer is studied theoretically in the framework of Eilenberger equations. It is shown that disorder of the quasiparticle reflection from this thin layer leads to the formation of an *s*-wave component localized near the boundary. The angular and spatial structure of the pair potential near the interface is studied. © *1998 American Institute of Physics.* [S0021-3640(98)00907-4]

PACS numbers: 74.50.+r

There is accumulating experimental evidence that the behavior of high-temperature superconductors (HTSs) can be understood in terms of the *d*-wave pairing scenario rather than the conventional *s*-wave picture. On the other hand, it is well known that the *d*-wave order parameter is strongly reduced by electron scattering on impurities and therefore can be formed only in clean materials. However, the condition of the clean limit is not fulfilled in the vicinity of grain boundaries or other HTS interfaces even if these materials are clean in the bulk. There are at least two reasons for that. The first is that quasiparticle reflection from realistic interfaces is diffuse rather than specular, thus providing isotropization in momentum space and suppression of the order parameter in the *d*-wave channel. The second reason is contamination of the material near interfaces as a result of the fabrication process or electromigration in large-scale application devices. Therefore the formation of a thin disordered layer near a HTS interface is highly probable. What kind of superconducting correlation one can expect in such a layer? The answer to this fundamental question is very important both for small- and large-scale applications of HTS materials.

Anomalies at the surface of a *d*-wave superconductor have been analyzed theoretically in models based on specular quasiparticle reflection from clean interfaces.[1–6] The zero- and finite-bias anomalies predicted in those papers were recently observed experimentally in Refs. 7 and 8. In this paper we focus on the problem of the anomalous proximity effect between a *d*-wave superconductor and a thin disordered layer. We will show that disorder of the quasiparticle reflection from such a layer leads to the formation of an *s*-wave component localized near the boundary, even if the coupling constant in the

s-wave pairing channel is zero. The magnitude of this component is studied as a function of interface orientation and temperature. We will argue that the s-wave state is gapless and the features in the density of states predicted in Refs. 1–6 are smeared out.

There are two approaches to the description of the influence of disorder of the quasiparticle reflection at interfaces on the properties of the interfacial regions. In the first approach it is assumed that an interface consists of facets with a random orientation of the normal to the interface with respect to the a axis of the HTS material.[5] In the second approach, both sides of the ideal interface are coated by an Ovchinnikov thin dirty layer.[4,9,10] In the latter case the degree of disorder (or interfacial roughness) was characterized by the ratio of the layer thickness d to the quasiparticle mean free path ℓ in the layer. Both models focus only on the study of Andreev surface bound states and do not take into account the effect of surface-induced changes of the symmetry of an order parameter near the boundaries.

To make the last effect more evident we consider the situation in which the crossover from the clean limit to the dirty limit takes place in a thin layer near the boundary. We will also assume that the lattice constant $a<\ell$ and that the thickness of the layer $d\ll\sqrt{\xi_0\ell}$, where ξ_0 is the coherence length of the bulk material.

To study the proximity effect at the interface we can use the quasiclassical Eilenberger equations,[11] which may be conveniently rewritten in terms of the functions $\Phi_+=(f(r,\theta)+f(r,\theta+\pi))/2$ and $\Phi_-=f(r,\theta)-f(r,\theta+\pi)$:

$$4\omega\Phi_+ + v\ \cos\ \theta\frac{d\Phi_-}{dx}=4\Delta g+\frac{2}{\tau}(g\langle\Phi_+\rangle-\Phi_+\langle g\rangle), \tag{1}$$

$$2v\ \cos\ \theta\frac{d\Phi_+}{dx}=-\left(2\omega+\frac{1}{\tau}\langle g\rangle\right)\Phi_-, \tag{2}$$

$$2v\ \cos\ \theta\frac{dg}{dx}=\left(2\Delta+\frac{1}{\tau}\langle\Phi_+\rangle\right)\Phi_-, \tag{3}$$

$$\Delta\ \ln\frac{T}{T_c}+2\pi T\sum_{\omega>0}\left(\frac{\Delta}{\omega}-\langle\lambda(\theta,\theta')\Phi_+\rangle\right)=0. \tag{4}$$

Here $\omega=\pi T(2n+1)$ are the Matsubara frequencies, v is the Fermi velocity, x is a coordinate in the direction of the interface normal, θ is the angle between the interface normal and the quasiparticle trajectory, $\tau=\ell/v$, and $\langle\ldots\rangle=(1/2\pi)\int_0^{2\pi}(\ldots)d\theta$. On the assumption that the coupling constant $\lambda(\theta,\theta')$ in a d-wave channel has the form[12] $\lambda_d(\theta,\theta')=2\lambda\ \cos(2\theta)\cos(2\theta')$ and $\lambda_s=0$, the self-consistency equation (4) yields for the pair potential $\Delta=\sqrt{2}\Delta(x)\cos(2(\theta-\alpha))$. We also assume that the Fermi surface has a cylindrical shape.

Equations (1)–(4) must be supplemented by the appropriate boundary conditions. Far from the interface the functions Φ_+ must coincide with the bulk solution

$$\Phi_+=\frac{\sqrt{2}\Delta_\infty\ \cos(2(\theta-\alpha))}{\sqrt{\omega^2+2\Delta_\infty^2\ \cos^2(2(\theta-\alpha))}}. \tag{5}$$

Two boundary conditions for the function Φ_+ and its derivative $d\Phi_+/dx$ are required at the interface between the clean and disordered regions of a d-wave superconductor ($x=0$). These conditions can be derived by integration of the Eilenberger equations (1) and (2) in a small region near the interface. In accordance with Ref. 13, the first condition is the continuity of Φ_- at the interface and can be written in the form

$$\frac{\ell \cos\theta}{\langle g(-0)\rangle}\frac{d\Phi_+(-0)}{dx}=\frac{v\cos\theta}{2\omega}\frac{d\Phi_+(+0)}{dx}. \tag{6}$$

This condition is a statement of conservation of current across the interface.

The second boundary condition depends on the backscattering properties of the interface. To account for such a backscattering we introduce a strongly disordered thin layer located near the interface at $-\delta\leqslant x\leqslant 0$, which is characterized by the mean free path ℓ_δ, where $a\ll\ell_\delta,\delta\ll d,\ell$. Assuming that all the interfaces are transparent and integrating Eqs. (1) and (2) over the interval $-\delta\leqslant x\leqslant 0$ in the limit $\delta\to 0$, we arrive at the second boundary condition

$$D\ell\frac{d\Phi_+(-0)}{dx}=\Phi_+(+0)-\Phi_+(-0), \tag{7}$$

where $D=2\delta/\ell_\delta$. For $D=0$ Eq. (7) is a direct consequence of the continuity of the Eilenberger functions along quasiclassical trajectories, which is valid for a transparent SN boundary.[13] As D increases, the probability of quasiparticle penetration into the N layer ($\Phi_+(-0)\approx D^{-1}\Phi_+(+0)$) decreases as D^{-1}. This means that the most of them are diffusely reflected back to the bulk d-wave region at length scales smaller than ℓ.

In the following we will consider the case of strong disorder, $\ell\ll d$. Then it follows from Refs. 13 and 14 that for a totally reflecting free interface ($x=-d$) the boundary condition is

$$\frac{d}{dx}\Phi_+=0. \tag{8}$$

In the limit $\ell\ll\xi_0$ it follows from (1)–(4) that $\Delta=0$ in the disordered layer. Then Eqs. (1)–(4) in the region $-d\leqslant x\ll-\ell$ are reduced to the dirty limit form,[15] which formally coincides with that for a normal metal with $T_{cn}=0$. Since in this regime the scale of variation of $\langle\Phi_+\rangle$ and $\langle g\rangle$ is of the order of the dirty limit coherence length $\sqrt{\xi_0\ell}$, the functions $\langle\Phi_+\rangle$ and $\langle g\rangle$ in the disordered layer are independent of x when $d\ll\sqrt{\xi_0\ell}$. Then the Eilenberger equations in the region $-d\leqslant x\leqslant 0$ are substantially simplified and have the solution

$$\Phi_+=\langle\Phi_+\rangle+A\frac{\cosh(k(x+d))}{\cosh(kd)},\quad \Phi_-=-2A\frac{\sinh(k(x+d))}{\cosh(kd)},\quad k=\frac{1}{\ell|\cos\theta|}, \tag{9}$$

$$g=\langle g\rangle-\frac{\langle\Phi_+\rangle}{\langle g\rangle}A\frac{\cosh(k(x+d))}{\cosh(kd)},\quad \langle\Phi_+\rangle^2+\langle g\rangle^2=1. \tag{10}$$

Making use of the boundary conditions (6), (7) at $x=0$ and (9), (10), one can further reduce the problem to the solution of the Eilenberger equations (1)–(4) in the clean d-wave superconductor ($x\geqslant 0$)

$$\kappa^2 \frac{d^2\Phi_+}{dx^2} - \Phi_+ = -\sqrt{2}\,\frac{\Delta(x)}{\omega}\cos(2(\theta-\alpha))g, \quad \kappa = \frac{v|\cos\theta|}{2\omega}, \tag{11}$$

$$\frac{dg}{dx} = -\sqrt{2}\,\frac{\Delta(x)}{\omega}\cos(2(\theta-\alpha))\frac{d\Phi_+}{dx} \tag{12}$$

with the condition (5) in the bulk ($x \gg \xi_0$) and the boundary condition

$$\left\{\kappa\langle g(0)\rangle + D\frac{v}{\omega}\right\}\frac{d}{dx}\Phi_+(0) = (\Phi_+(0) - \langle\Phi_+(0)\rangle), \quad \langle g(0)\rangle = \sqrt{1-\langle\Phi_+(0)\rangle^2} \tag{13}$$

at $x=0$.

In the following we will limit ourselves to the situation when the disordered layer has the strongest effect, namely when $\ell \ll d$ and $D=0$. In this case the boundary condition (13) has a closed form. The isotropic Usadel function $\langle\Phi_+(0)\rangle$ has to be determined self-consistently as the result of an iteration procedure.

In the limit $\kappa \ll 1$ the pair potential $\Delta(x)$ is a smooth function of x at distances of the order of κ. Then the boundary value problem (11)–(13) is substantially simplified and has the asymptotic solution

$$\Phi_+ = \Psi(x) + \eta\sqrt{\frac{G(x)}{G(0)}}\exp\left\{-\int_0^x \frac{dy}{\kappa G(y)}\right\},$$

$$\eta = G(0)\,\frac{\langle\Phi_+(0)\rangle - \Psi(0) + \langle g(0)\rangle\kappa\Psi'(0)}{G(0) + \langle g(0)\rangle[1-\kappa(\Psi(0)/\Delta)']}, \tag{14}$$

$$G(x) = \frac{\omega}{\sqrt{\omega^2 + 2\Delta^2(x)\cos^2(2(\theta-\alpha))}}, \quad \Psi(x) = \frac{\sqrt{2}\cos(2(\theta-\alpha))\Delta(x)}{\sqrt{\omega^2 + 2\Delta^2(x)\cos^2(2(\theta-\alpha))}}. \tag{15}$$

Here a prime denotes the derivative with respect to the coordinate x. If follows from Eqs. (14) and (15) it follows that at $x=0$ the anomalous Green's function $\Phi_+(0)$ is a sum of three terms with different angular symmetry. Two of them are simply the isotropic part and the term with the d-wave symmetry. The last one is proportional to the product $\Delta'(0)|\cos\theta|\cos(2(\theta-\alpha))$ and can be considered to be a source for the formation of a nonzero component in the s-wave channel. Thus the gradient of the pair potential at the interface results in spatial variation of the function $\Phi_+(x)$ with a characteristic length that depends on the direction in momentum space. This difference in $\kappa(\theta)$ leads to a larger deformation of the d-wave angular dependence of $\Phi_+(x)$ the closer x is to the interface. As a result, a nonzero angle-averaged value $\langle\Phi_+(x)\rangle$ appears which is localized near the interface.

In the general case of arbitrary values of κ the problem was solved numerically. The isotropic function $\langle\Phi_+(0)\rangle$ and the space-dependent pair potential $\Delta(x)$ were calculated by an iteration procedure from the boundary condition (13) and the self-consistency equation (4). The results of numerical calculations shown in Figs. 1, 2, and 3 confirm the simple arguments presented above.

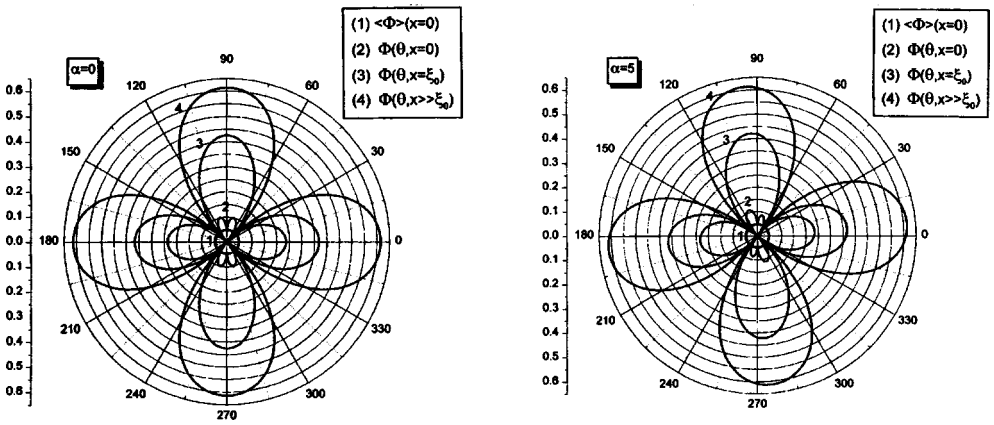

FIG. 1. Angular dependence of $\Phi_+(x)$ at different distances from the interface at $T=0.7T_c$.

Figure 1 shows the angular dependence of $\Phi_+(x)$ far from the boundary ($x \gg \xi_0$) and at $x=\xi_0$, 0 for two different orientations α of the a axis with respect to the normal to the interface. In both cases far from the interface the angular distribution is typical for a d-wave superconductor. At $x=\xi_0$ the positive lobe is suppressed more strongly than the negative one, since $\kappa(\theta)$ is smaller in this direction than in the direction of the negative lobe. Hence at $x \approx \xi_0$ the negative lobes of $\Phi_+(x)$ practically reach the local value $\Psi(x)$, while the positive lobes have not yet done so. This difference leads to a negative sign of the s component $\langle \Phi_+(x) \rangle$ (see Fig. 2). In the vicinity of the interface ($x \leqslant 0.3\xi_0$) the situation is just the opposite. According to Eq. (14), on account of the angular dependence $\kappa(\theta) \propto |\cos\theta|$ the negative lobes are suppressed more strongly than the positive lobes, and the function $\langle \Phi_+(x) \rangle$ changes sign to positive and reaches its maximum at $x=0$. It is important to note that exactly at $\theta=\pi/2$ it follows from (14) that $\Phi_+(0,\pi/2)=\Psi(0,\pi/2)$, while $\lim_{\theta \to \pm \pi/2} \Phi_+(0,\theta)=\Psi(0,\pi/2)+\eta$. This discontinuity is a manifestation of the simple fact that quasiparticles which propagate exactly parallel to the interface have information about the disordered region only via the local value of

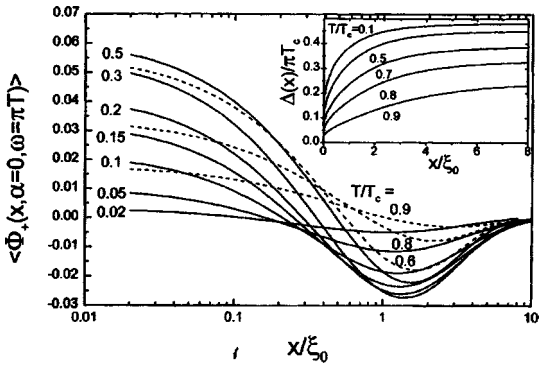

FIG. 2. Spatial dependence of the surface-induced s-wave component $\langle \Phi_+(x) \rangle$ at various temperatures. Inset: Behavior of the pair potential $\Delta(x)$ near the interface.

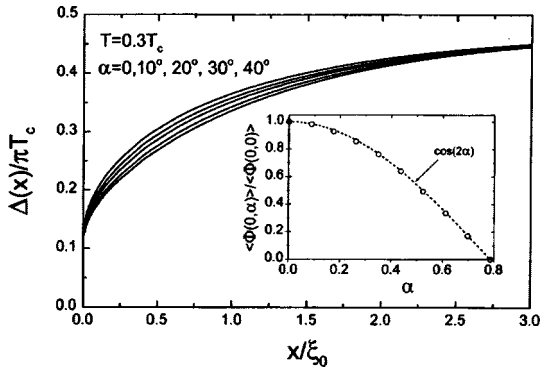

FIG. 3. Behavior of the pair potential near the interface for different misorientation angles α. Inset: Dependence of $\langle\Phi_+(0)\rangle$ on α.

$\Delta(0)$, while for all other directions a direct interaction between the two regions takes place. However, this discontinuity at $\theta=\pi/2$ does not contribute to the result of the angular averaging of Φ_+ in (13).

Figure 3 shows the spatial variations of $\Delta(x)$ for different values of the angle α. As is seen from (14), (15), the function $\Phi_+(0,\theta)$ near an interface has a contribution proportional to $|\cos\theta|\cos(2(\theta-\alpha))$. This immediately leads to the result that the amplitude of the s component induced in the disordered layer scales with misorientation angle α as $\langle\Phi_+(0,\alpha=0)\rangle\cos 2\alpha$. At $\alpha=\pi/4$ the superconducting correlations are not induced in the disordered layer, i.e., $\langle\Phi_+(0)\rangle=0$. Further increase of α leads to a sign change of the s component. As is seen from Fig. 3, these qualitative considerations are in good agreement with the results of exact numerical calculations. In particular, for the d_{xy} case ($\alpha=\pi/4$) we have $\langle\Phi_+(0)\rangle=0$. At the same time, it is important to note that the pair potential $\Delta(0,\alpha=\pi/4)$ is nonzero, in contrast to the case of a specular reflecting boundary. The reason is that in the present case of diffuse scattering from the interface there is no symmetry requirement that the function $\Phi_+(0,\alpha=\pi/4)$ must vanish.

In the whole temperature range the amplitude of the of the s-wave component $\langle\Phi_+\rangle$ induced in the disordered layer (see Fig. 2) is an order of magnitude smaller than the amplitude of the order parameter in the bulk superconductor. That means that $\langle g(0)\rangle$ is practically temperature independent and is close to unity. Thus, taking into account that $\langle g(0)\rangle$ is independent of the Matsubara frequencies and that $\xi\Phi'_+(0)\approx\Phi_+(0)$, from the boundary condition (13) we immediately have that at low temperatures $\langle\Phi_+(0)\rangle\propto\omega$ if $\omega\leqslant\Delta$ and that it falls off as $\langle\Phi_+(0)\rangle\propto\omega^{-2}$ as soon as ω exceeds the value of Δ. Since the density of states $N(\varepsilon)=\mathrm{Re}\langle g(0,\varepsilon=i\omega)\rangle$, where $\langle g\rangle=\sqrt{1-\langle\Phi_+\rangle^2}$, the property $\langle\Phi_+\rangle\propto\omega$ at small ω results in a gapless density of states in the disordered layer. The density of states has only small anomalies at energies $\varepsilon\approx\Delta$. The behavior of the density of states will be discussed in more detail elsewhere.

In conclusion, we have studied theoretically the proximity effect between a d-wave superconductor and a thin disordered normal layer. It is shown that disorder of the quasiparticle reflection from this layer leads to the formation of an s-wave component

localized near the interface. This model might be relevant for description of rough HTS interfaces.

We would like to thank H. Rogalla, G. Gerritsma, and Yu. Nazarov for helpful discussions. This work is supported in part by INTAS Grant 93-790ext and by the Program for Russian–Dutch Research Cooperation (NWO).

[1] Y. Tanaka and S. Kashiwaya, Phys. Rev. Lett. **74**, 3451 (1995).
[2] Y. Tanaka and S. Kashiwaya, J. Phys. Chem. Solids **56**, 1761 (1995); Phys. Rev. B **53**, 11957 (1996).
[3] S. Kashiwaya, Y. Tanaka, M. Koyanagi, and K. Kajimura, Phys. Rev. B **53**, 2667 (1996).
[4] Yu. S. Barash, A. A. Svidzinsky, and H. Burkhardt, Phys. Rev. B **55**, 15282 (1997).
[5] M. Fogelström, D. Rainer, and J. A. Sauls, Phys. Rev. Lett. **79**, 281 (1997).
[6] D. Rainer, H. Burkhardt, M. Fogelström, and J. A. Sauls, http://xxx.lanl.gov/abs/cond-mat/9712234.
[7] L. Alff, H. Takashima, S. Kashiwaya *et al.*, Phys. Rev. B **55**, R14757 (1997).
[8] M. Covington, M. Aprili, L. H. Greene *et al.*, Phys. Rev. Lett. **79**, 277 (1997).
[9] F. J. Culetto, G. Kieselmann, and D. Rainer, in *Proceedings of the 17th Intern. Conf. on Low Temperature Physics* (edited by U. Eckern, A. Schmid, W. Weber, and H. Wühl), North Holland, Amsterdam, 1984, p. 1027.
[10] Yu. N. Ovchinnikov, Zh. Éksp. Teor. Fiz. **56**, 1590 (1969) [Sov. Phys. JETP **29**, 853 (1969)].
[11] G. Eilenberger, Z. Physik **214**, 195 (1968).
[12] E. Schachinger, J. P. Carbotte, and F. Marsiglio, Phys. Rev. B **56**, 2738 (1997).
[13] A. V. Zaitsev, Zh. Éksp. Teor. Fiz. **86**, 1742 (1984) [Sov. Phys. JETP **59**, 1015 (1984)].
[14] M. Yu. Kupriyanov and V. F. Lukichev, Zh. Éksp. Teor. Fiz. **94**, 139 (1988) [Sov. Phys. JETP 1 (1988)].
[15] K. D. Usadel, Phys. Rev. Lett. **25**, 507 (1970).

Published in English in the original Russian journal. Edited by Steve Torstveit.

On the experimental possibilities of observing single spins in a STM

M. A. Kozhushner,[a] B. R. Shub, and R. R. Muryasov
N. N. Semenov Institute of Chemical Physics, Russian Academy of Sciences, 117977 Moscow, Russia

(Submitted 26 February 1998)
Pis'ma Zh. Éksp. Teor. Fiz. **67**, No. 7, 484–488 (10 April 1998)

A method is proposed for observing the spins of individual particles by combining ESR and STM methods using a ferromagnetic needle or paramagnetic tip. © *1998 American Institute of Physics.* [S0021-3640(98)01007-X]

PACS numbers: 07.79.Cz, 07.57.Pt

1. INTRODUCTION

The use of scanning tunneling microscopy for detection of single paramagnetic centers (PMCs) has been an object of attention of both experimenters and theorists for a number of years.[1–7] This interest is linked with the general problem of surface nanoscopy — the application of nanoscopy for qualitative and quantitative chemical analysis of surfaces. The attribution of definite ''spots'' in a STM pattern to some atoms or molecules on a surface is still mainly heuristic. In Ref. 1 a peak was observed in the spectral distribution of current fluctuations at the Larmor precession frequency ω_0 in a static field H_0, $\omega_0=\gamma_s H$, where γ_s is the gyromagnetic ratio for the PMC. In the experiments of Ref. 2, besides a static field H_0 there was also an ac field $H_1 \perp H_0$ of frequency ω acting on surface spins. It was observed that when the field passed through resonance, the Fourier component of the current at frequency ω changed. The high shot-noise level at frequencies $\geqslant \omega_0$ makes it difficult to measure the effect. The theoretical models explaining the experiments of Refs. 1 and 2 were continued in Refs. 3–6. In Ref. 4 the correlation of the spin-dependent scattering of tunneling electrons by PMCs, leading to current modulations,[1] was studied. In Refs. 3, 5, and 6 single-particle mechanisms of current modulation were proposed, based on allowance for the off-diagonal elements of the spin density matrix in the scattering by PMCs. We note that spin rotation can be detected with the aid of a current only if the polarization of the tunneling electrons is appreciable.

In Ref. 7 it was shown that the tunneling current in a STM can be modulated by spin transitions in a biradical on the surface. This is hardly a general case, since biradicals are rarely encountered on surfaces.

2. PHYSICAL ORIGIN OF THE EFFECT

We shall study PMCs on the surface of a nonmagnetic material and, as in Ref. 2, consider the classical experimental arrangement for ESR. The stationary tunneling current through a surface region containing PMCs can depend on the average polarization δ_s

of the PMC spin. The characteristic current measuring time τ in a STM is 10^{-4}–10^{-5} s, which is much longer than all relaxation times of the PMC spin, during which a stationary spin polarization is established. In the presence of a $\sim 10^{-9}$ A current $10^4 - 10^5$ electrons pass near a PMC over a time τ. Therefore it can be asserted that to a high degree of accuracy the observed current depends on the stationary spin populations.

Let us examine the physical reasons for the possible dependence of the current on the direction of the spin of PMCs on a surface. The tunneling barrier $U(\mathbf{r})$ varies at the location of the PMC. The magnitude and form of the change δU_s in the tunneling barrier depends on the spin state of the system ''electron + PMC'' — triplet or singlet. According to Ref. 8, the amplitude of the tunneling transition is proportional to the subbarrier Green's function $G(\mathbf{r},\mathbf{r}',E)$ of the tunneling electron that connects the region on the surface ($\mathbf{r}$) and a region of the needle ($\mathbf{r}'$):

$$G(\mathbf{r},\mathbf{r}',E) \sim \exp\left\{ \int_{\mathbf{r}}^{\mathbf{r}'} \sqrt{2[|E| + U(\mathbf{r}'') + \delta U_s(\mathbf{r}'')]}\, d\mathbf{r}'' \right\}. \tag{1}$$

Here atomic units are used, E is the energy of the tunneling electron, and the integral is taken along the ''tunneling trajectory.''[8] The amplitude of the spin-elastic (no change in the spin direction of the particles) tunneling transition of an electron can be written in the form

$$A = A_0(1 + a), \tag{2}$$

where A_0 is the transition amplitude in the absence of PMCs, while a is the relative magnitude of the spin-dependent part of the amplitude due to PMCs on the surface. It appears only when the needle is located above a PMC, i.e., when the ''tunneling trajectory'' passes near a PMC. The quantity a is negative for positive δU and positive for negative δU. Correspondingly, we should observe a decrease or increase in the electron tunneling probability. We note that an adsorbed particle can change the tunneling current not only by changing the tunneling barrier. The interaction of the adsorbed particle with conduction electrons changes the density of states near the Fermi surface,[9] which also changes the tunneling current. However, for nonmagnetic materials this change does not depend on the spin direction of the PMCs.

Let us denote the relative transition amplitudes of an electron with spin parallel or antiparallel to the PMC as a_t and a_s, respectively. Besides the spin-elastic, a spin-exchange tunneling transition is possible in the case of antiparallel spins of the electron and PMC. We shall denote the relative amplitude of such a process by b. It is easy to see that to observe changes induced in the tunneling current by a change in the spin polarization of PMCs, either the tunneling electrons must be polarized or the tip in the STM must be spin-sensitive, i.e., the ''terminal'' atom on the tip must be paramagnetic in order for the tunneling amplitude to depend also on the spin of the tip (just as in optics, in order to observe rotation of the polarizer either polarized light must be passed through the polarizer or the transmitted light must be analyzed with a second polarizer). We shall examine both possibilities.

The equilibrium polarization of PMCs in a magnetic field H_0 is

$$\delta_s = \frac{n_+ - n_-}{n_+ + n_-} = \tanh\left(\frac{\omega_0}{2T}\right), \tag{3}$$

where n_+ and n_- are the populations of the spin states parallel and antiparallel to the field, and T is the temperature. Even in a ~ 1 T field δ_s becomes appreciable only at liquid-helium temperatures, while at room temperature $\delta_s \sim 10^{-3}$. The equilibrium polarization of the conduction electrons of nonmagnetic metals in an energy layer equal to V — the voltage in the STM — is much smaller, $\delta_s \approx \omega_0 / V$. For characteristic voltages $V \sim (0.1-1)$ V we have $\delta \sim 10^{-4}$–10^{-5}. For this reason, the polarization of the tunneling electrons in such metals can be neglected. But in ferromagnets, such as Fe, Co, Ni, and their alloys, the polarization of the d electrons is close to 1. Taking into account the nonmagnetic s electrons, the polarization of electrons with energies close to E_f and δ_f is of the order of tenths. The polarization of electrons tunneling from a ferromagnet will be of the same order of magnitude.

Let us examine the current in an STM with a ferromagnetic needle. Using Eq. (2), it is not difficult to separate in the expression for the total tunneling current J_0 a part J_1 that depends on the polarization δ_s of the PMC. We obtain

$$\frac{J_1}{J_0} = \delta_f \delta_s \frac{\delta J_s}{J_0} \frac{\alpha - 1}{\alpha + 1}. \tag{4}$$

Here $\delta J_s / J_0$ is the relative change occurring in the tunneling current in the presence of PMCs on the surface. Ordinarily, $\delta J_s / J_0 \sim 10^{-1}$–1. We have introduced the ratio α of the tunneling amplitudes:

$$\alpha = a_s / a_t. \tag{5}$$

In the derivation of Eq. (4) we neglected the inelastic amplitude b, since ordinarily it is less than a. For the case when a paramagnetic center is present on the needle we obtain instead of Eq. (4)

$$\frac{J_1}{J_0} = \frac{\delta_s \cdot \delta_t}{2} \frac{\delta J_s}{J_0} \frac{\delta J_t}{J_0} \frac{\alpha - 1}{\alpha + 1} \frac{\beta - 1}{\beta + 1}. \tag{6}$$

Here δ_t is the polarization of the spin on the needle, $\beta = a_s^t / a_t^t$ is the amplitude ratio for PMCs on the needle, and $\delta J_t / J_0$ is the relative change occurring in the current due to a PMC on the needle.

To measure the effect (4), (6) it is necessary to change the polarization δ_s. An alternating field $H_1(t)$ perpendicular to $H_0(t)$ and with frequency ω close to ω_0 can appreciably decrease δ_s (it can saturate the ESR line of the PMC). If the field H_0 is modulated so that it would, with modulation frequency ω_m, pass through resonance ($\omega_0 = \omega$), then the polarization δ_s will vary with the modulation frequency. A necessary condition for observing this modulation in the current J_1 is

$$\omega_m < \tau^{-1}. \tag{7}$$

3. OBSERVATION POSSIBILITIES

The amplitude of the modulational variation of the current in the STM is proportional to the difference $\overline{\delta_s} - \widetilde{\delta_s}$ between the steady-state value of δ_s, denoted $\overline{\delta_s}$, and δ_s in the saturation regime, denoted $\widetilde{\delta_s}$. The inequality $(\overline{\delta_s} - \widetilde{\delta_s}) / \overline{\delta_s} \ll 1$ is reached when[10]

$$\tau_1 \gamma_s H_1 \gg 1, \tag{8}$$

where τ_1 is the spin relaxation time.

The time τ_1 for PMCs on the surface of a metal at room temperature is very short, since the spin–lattice relaxation is due to spin-exchange scattering of conduction electrons by PMCs, $\tau_1 < 10^{-10}$ s, so that it is impossible to decrease δ_s substantially. For this, H_1 must be of the order of 1000 Oe. Only at liquid-helium temperatures can τ_1 become sufficiently long for the condition (8) to be satisfied and to be able to make δ_s close to zero. Under these conditions the equilibrium values of δ_s and δ_t in ~ 1 T fields can be $\sim 10^{-1}$. Then the amplitude J_1/J_0 of the modulational variation can be $\sim 10^{-2}$ and can be observed experimentally.

In our view, a ferromagnetic needle and PMCs on a semiconductor surface are much more promising for observing ESR in a STM. The charge carrier density in lightly doped semiconductors can be $\sim(10^{14}$–$10^{15})$ cm^{-3}. For such electron densities different mechanisms of spin–lattice relaxation are based on the spin–phonon interaction, and even at room temperatures $\tau_1 \geqslant 10^{-7}$ s. In these cases a spin-exchange tunneling transition with amplitude b can make an appreciable contribution to the spin kinetics of PMCs. It is not difficult to obtain for the reciprocal of the time of such a transition

$$\tau_{1s}^{-1} \approx b^2 \cdot \delta J_s . \tag{9}$$

For the usual currents $\sim 10^{-9}$ A in STMs and reasonable values $b^2 \sim 10^{-2}$–10^{-3} we obtain $\tau_{1s} \leqslant 10^{-8}$–$10^{-7}$ s. Taking into account the times τ_1 and τ_{1s}, we obtain the following kinetic equation for δ_s:

$$\frac{d\delta_s}{dt} = -\frac{1}{\tau_1}(\delta_s - \delta_s^0) - \frac{1}{t_{1s}}(\delta_s - \delta_f), \tag{10}$$

where δ_s^0 is the equilibrium value of δ_s, and δ_f is the spin polarization of electrons tunneling from the ferromagnetic needle. Then the stationary polarization $\overline{\delta_s}$ appearing in Eq. (4) equals

$$\overline{\delta_s} = (\tau_1^{-1} + \tau_{1s}^{-1})(\delta_f \tau_{1s}^{-1} + \delta_s^0 \tau_1^{-1}). \tag{11}$$

If

$$\tau_{1s}/\tau_1 \ll 1, \tag{12}$$

then $\overline{\delta_s} \approx \delta_f$. We now call attention to the fact that, in contrast to δ_s^0, δ_f does not depend on the magnetic field H_0. This effect, consisting of a substantial increase (by several orders of magnitude) in the stationary polarization over the equilibrium polarization δ_s^0, is due to the character of the spin-exchange relaxation and is analogous to the Overhauser effect[11] — an increase in the stationary nuclear polarization.

If the conditions (8) and (12) are satisfied, the amplitude of the modulation variation of the current (4) on passage of the field H_0 through resonance is

$$\frac{J_1}{J_0} \approx \delta_f^2 \frac{\delta J_s}{J_0} \frac{\alpha_s - 1}{\alpha_s + 1} \tag{13}$$

and can be substantial, of the order of several percent.

We note the following: 1) The modulation signal (13) is virtually temperature-independent so long as the relation (12) holds and $T < T_C$, where T_C is the Curie tem-

perature of the ferromagnetic material of the needle; 2) the signal does not depend on the field H_0, which can be taken as the magnetic field H_0 produced by the needle; and, 3) the signal will be large only for a single polarity of the current in the STM, when electrons tunnel from the needle into the surface, i.e., a negative potential must be applied to the needle. When the polarity of the current changes, the amplitude of the modulation signal decreases sharply, since then $\overline{\delta_s} = \delta_s^0$.

If the metal surface is coated with a thin film of a crystalline insulator, then it is also possible to study PMCs on such a film. For this, the potential difference in the STM must be such that the tunneling electrons reach the conduction band of the insulator. Then they can traverse a distance of the order of λ, the mean free path, without being captured or scattered, and they can give a so-called ballistic current in the STM. If the thickness of the insulator film is less than λ, then we can use Eqs. (4) and (6) to study PMCs on its surface.

We are deeply grateful to F. I. Dalidchik and G. K. Ivanov for fruitful discussions.

This work was supported by the Russian Fund for Fundamental Research (Grants 96-03-34052 and 96-03-34442).

[a)]e-mail: kozhush@center.chph.ras.ru

[1] Y. Manassen, R. J. Hamers, J. E. Demoth *et al.*, Phys. Rev. Lett. **62**, 2531 (1989).
[2] A. W. McKinnon, W. E. Welland, T. Rayment *et al.*, in *Abstracts of the International Conference on STM*, Interlaken, Switzerland, 1991.
[3] D. Shachal, Y. Manassen, Phys. Rev. B **46**, 4795 (1992).
[4] S. N. Molotkov, Surf. Sci. **294**, 264 (1992).
[5] S. N. Molotkov, Surf. Sci. **302**, 235 (1994).
[6] S. N. Molotkov, JETP Lett. **59**, 190 (1994).
[7] F. I. Dalidchik, A. A. Lundin, and B. R. Shub, Khim. Fiz., (in press).
[8] G. K. Ivanov and M. A. Kozhushner, Chem. Phys. **170**, 303 (1993).
[9] D. Lang, Comments Condens. Matter Phys. **14**, 253 (1989).
[10] S. A. Al'tshuler and B. M. Kozyrev, *Electron Spin Resonance* [in Russian], Fizmatgiz, Moscow, 1961.
[11] A. Overhauser, Phys. Rev. **92**, 411 (1953).

Translated by M. E. Alferieff

Phase-sensitive reentrance into the normal state of mesoscopic SNS structures

V. T. Petrashov

Department of Physics, Royal Holloway, University of London, Egham, Surrey TW20 0EX, UK; Institute of Problems in the Technology of Microelectronics and Ultrapure Materials, Russian Academy of Sciences, 142432 Chernogolovka, Moscow Region, Russia

R. Sh. Shaĭkhaĭdarov

Institute of Problems in the Technology of Microelectronics and Ultrapure Materials, Russian Academy of Sciences, 142432 Chernogolovka, Moscow Region, Russia; Department of Physics, Chalmers University of Technology and University of Gothenburg, S-412 96 Gothenburg, Sweden

P. Delsing and T. Claeson

Department of Physics, Chalmers University of Technology and University of Gothenburg, S-412 96 Gothenburg, Sweden

(Submitted 3 March 1998)
Pis'ma Zh. Éksp. Teor. Fiz. **67**, No. 7, 489–494 (10 April 1998)

Normal (N) metallic (Ag) mesoscopic conductors with two superconducting (S) faces (Al), arranged mirror-symmetrically relative to the streamlines of the current, periodically switch into the normal state as the superconducting phase difference $\Delta\varphi$ between the NS boundaries approaches the values $\Delta\varphi=(2n+1)\pi$, $n=0,1,2,\ldots$, irrespective of temperature and applied voltage. For $\Delta\varphi=2n\pi$ and low applied voltages the conductance passes through a maximum and approaches the normal value as temperature decreases (reentrance). As the voltage subsequently increases, the conductance increases and passes through a maximum. As the phase difference moves away from the values $\Delta\varphi=2n\pi$, the maxima shift in the direction of low temperatures and voltages. The latter result shows unequivocally that in our metal structures it is necessary to take into account the next-order corrections to the ''weak'' proximity effect approximation. © *1998 American Institute of Physics.* [S0021-3640(98)01107-4]

PACS numbers: 74.80.Fp, 74.50.+r

Electron transport in normal (N) disordered mesoscopic structures with contacts to superconductors (S) exhibits a number of unusual features.[1–5] As the temperature decreases below the critical value, the conductance of structures with one superconducting contact increases, reaching a maximum value at a finite temperature corresponding to the Thouless energy and returns to its value in the normal state as temperature decreases further (reentrance). A similar maximum is observed as a function of the applied voltage.[5] The conductance of structures with several N/S contacts oscillates with a ''gi-

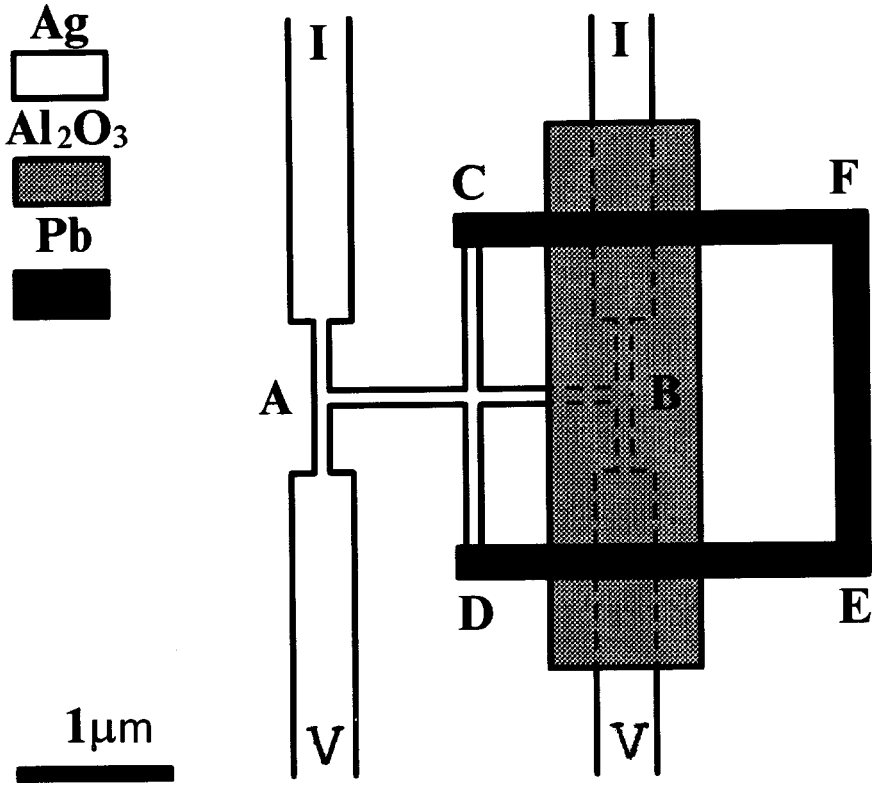

FIG. 1. Sample geometry: I,I,V,V — current and potential contacts for measuring the resistance of the section AB. $CDEF$ — superconducting loop, producing a phase difference between the points C and D. The marker length corresponds to 1 μm.

ant'' amplitude, much greater than that predicted at the early stage of development of the theory,[6] as a function of the difference $\Delta\varphi$ of the superconducting phases between the N/S boundaries.[1,2] Both the reentrance phenomenon and the ''giant'' oscillation amplitude have been successfully explained on the basis of a quasiclassical theory,[7–11] and it was found that reentrance can be understood on the basis of a very simple model of a ''weak'' proximity effect,[8,10,11] in the approximation of low transmittance of the N/S boundaries, without using more accurate models.[7,12]

In the present work we studied the effect of the phase difference on the reentrance phenomena. The structures had two N/S contacts, arranged mirror-symmetrically relative to the measuring currents. The structures shown in Fig. 1 were studied. These structures were proposed in Refs. 1 and 2. It was observed that the transport properties of such structures are virtually identical to those of normal structures when the difference of the superconducting phases between the NS boundaries had the values $\Delta\varphi=(2n+1)\pi$, $n=0,1,2,\ldots$, irrespective of temperature and applied voltage. For $\Delta\varphi=2n\pi$ and at low applied voltages the conductance passes through a maximum and approaches the normal value as temperature decreases, similarly to the manner in which this occurs in structures with one contact. The dependence of the conductance on the applied voltage at low

temperatures also has a maximum. The results of measurements with the indicated fixed phases agree well with the predictions of the quasiclassical theory in the limits of both a ''weak'' proximity effect,[8,10,11] in the approximation of weak transmittance of N/S boundaries, and a ''strong'' proximity effect, when the transmittance of the boundaries high.[7,12] This indeterminacy is due to inadequate accuracy of the direct experimental determination of the transmittance of the boundaries. However, more profound conclusions about the mechanism of the influence of the superconductors can be drawn by studying the line shape of the oscillations and the dependence of the positions of the maxima of the conductance on the phase in the intervals $2n\pi<\Delta\varphi<(2n+1)\pi$. It was found that when the phase difference deviates from the values $\Delta\varphi=2n\pi$ the maxima of the conductance shift in the direction of low temperatures and voltages. The latter result indicates unequivocally that in our metal structures it is necessary to take into account the next-order corrections to the ''weak'' proximity effect approximation even when the deviation of the conductance from the normal value is relatively small (of the order of 10%), since in this approximation the positions of the maxima are completely independent of temperature and voltage.

Figure 1 shows schematically one of the experimental samples. This picture was drawn from a photograph made with an electron microscope. The ends *C* and *D* of the vertical part of the cross are in good contact with lead superconducting loops. To prevent electrical contact between the normal current leads and the superconducting loops, a thin dielectric interlayer (Al_2O_3, Fig. 1) was placed between them. The samples were fabricated by three-layer lift-off electron-beam lithography with the layers aligned to within an accuracy of the order of 50 nm. The first layer consisted of silver, the second layer was a dielectric, and the third layer consisted of lead. The Ag, Al_2O_3, and Pb films were 50 nm, 20 nm, and 60 nm thick, respectively. The differential resistance dV/dI, the current–voltage characteristics, and the magnetic field dependences of the resistance of the section *AB* (see Fig. 1) were measured by a four-point method. Special filters were used to eliminate high-frequency noise.[13,14]

Figure 2 shows oscillations of the resistance of the section *AB*, the normal part of the structure. The phase difference was produced by a magnetic field applied perpendicular to the substrate. The period of the oscillations with respect to the magnetic field was equal to 4 G and corresponded to a quantum $hc/2e$ of magnetic flux through the area enclosed by the superconducting loops and the normal segment *AB*. The curves have a number of interesting features. For the phase differences $\Delta\varphi=(2n+1)\pi$ the resistance is independent of temperature and equals its value in the absence of the superconductors. As temperature decreases, the oscillations become nonsinusoidal, peaks appear near the points $\Delta\varphi=(2n+1)\pi$, and the resistance near the phase differences $\Delta\varphi=2n\pi$ depends nonmonotonically on temperature and forms a plateau. Hysteresis of the oscillations,[15] which can arise as a result of shielding of the magnetic field, was not observed.

Figure 3 shows the temperature dependence of the correction to the resistance. One can see that the position of the minimum depends strongly on the phase difference: As the phase difference increases, the minimum shifts in the direction of lower temperatures and is not observed in the experimental temperature interval for phase differences above approximately $\Delta\varphi=3\pi/4$ (Fig. 3).

The current–voltage characteristics of the section *AB* of the normal structures were also found to be very sensitive to the phase difference between the points *C* and *D*. Just

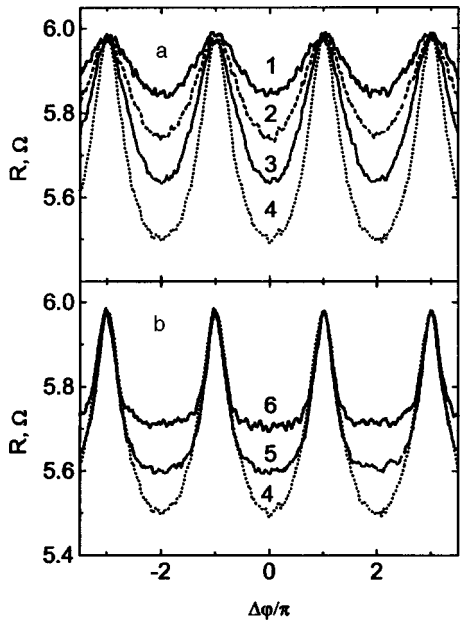

FIG. 2. Oscillations of the resistance of the section *AB* (see Fig. 1) as a function of the phase difference between *C* and *D* at different temperatures: a) above T_{max}; curve *1* — 900 mK, *2* — 500 mK, *3* — 300 mK, *4* — 120 mK; b) below T_{max}; *4* — 120 mK, *5* — 70 mK, *6* — 30 mK. T_{max} is the temperature at which the amplitude of the oscillations is maximum.

as in the case of the temperature dependences for the phase difference $\Delta\varphi=(2n+1)\pi$, the resistance remained practically constant and equalled its value in the absence of the superconductors, while near the phase difference $\Delta\varphi=2n\pi$ at temperatures below the minimum the correction to the resistance was found to be a nonmonotonic function of the applied voltage (Fig. 4). Just as in the case of the temperature dependence, the position of

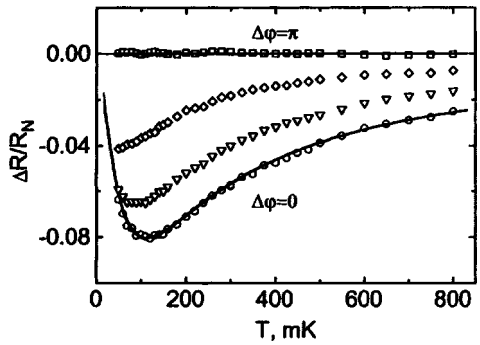

FIG. 3. Temperature dependence of the correction to the resistance for phase differences $\Delta\varphi=0$ (○), $\Delta\varphi=\pi/2$ (▽), $\Delta\varphi=3\pi/4$ (◇), $\Delta\varphi=\pi$ (□). The solid line shows the temperature dependences calculated using Eqs. (1)–(4) for phase differences $\Delta\varphi=0$ and π.

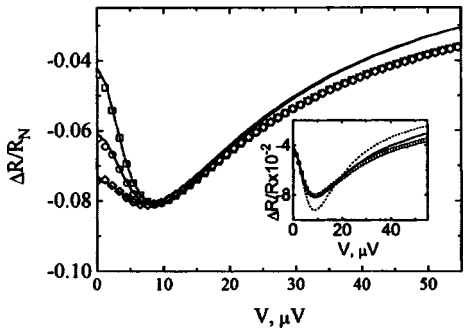

FIG. 4. Relative correction to the resistance versus the voltage on the section AB with phase difference $\Delta\varphi = 0$ and different temperatures: ○,□, ◇ correspond to measurements at 30 mK, 50 mK, and 70 mK, respectively. The solid lines show the curves obtained using Eqs. (1) and (5) for the corresponding temperatures. Inset: The experimental data for 30 mK (□) and curves calculated using Eq. (1) with different distribution functions — solid line, Eq. (5); dotted line, Eq. (2) — are shown for comparison.

the minimum was found to depend on the phase difference: As the phase difference increases, the minimum shifts in the direction of lower voltages.

The principal microscopic mechanism of the observed oscillations are Andreev reflections of the quasiparticles.[16] This process couples the condensate wave functions and their phases in the N and S regions. The nonmonotonic dependences of the resistance near the phase differences $\Delta\varphi = 2n\pi$ are due to the reentrance of the conductance of the conductors into the normal state. The physical picture of the reentrance phenomena is simplest in the limit of a ''weak'' proximity effect[8–11] with a small transmittance of the N/S boundaries, when the amplitude of the induced condensate functions in the normal conductors is small, while the changes in the wave functions and distribution functions in the S regions can be neglected. In this limit the contribution of the condensate wave functions to the conductance can be represented as a sum of two contributions due to the penetration of Cooper pairs and decrease of the density of states in the N region. They have different signs: Cooper-pair penetration, similarly to the Maki–Thompson mechanism,[17] increases conductance, while a decrease in the density of states decreases it. Reentrance into the normal state is due to the characteristic energy dependence of these contributions.[10,11] At low temperatures they compensate each other, and as a result the superconductors have no influence at all. As energy increases, decompensation appears and then vanishes at high energies.

The quasiclassical theory developed in Refs. 8–11 and 18 in the weak proximity effect approximation makes it possible to explain the result quantitatively for the phase differences $\Delta\varphi = 0$ and $\Delta\varphi = \pi$. The solid lines in Fig. 3 show the theoretical curves calculated using the following formulas:[18]

$$\frac{\Delta R}{R_N} = \frac{1}{V}\int_{-\infty}^{\infty} d\epsilon F(\epsilon, V, T)\langle m\rangle, \tag{1}$$

where

$$F(\epsilon, V, T) = \frac{1}{2}\left[\tanh\left(\frac{\epsilon + V}{2T}\right) - \tanh\left(\frac{\epsilon - V}{2T}\right)\right], \tag{2}$$

$$\langle m_- \rangle = \frac{1}{16}(1+\cos\,\varphi) r \left\{ \mathrm{Re}\left(\frac{F_0^2}{(\Theta\,\cosh\,\Theta_t)^2} \frac{\sinh 2\Theta - 2\Theta}{\Theta} \right) - \frac{|F_0|^2}{|\Theta\,\cosh\,\Theta_t|^2} \left[\frac{\sinh(2\Theta')}{\Theta'} - \frac{\sin(2\Theta'')}{\Theta''} \right] \right\}, \tag{3}$$

$$F_0^2 = \frac{\Delta^2}{\Delta^2 - (\epsilon + i\Gamma)}; \quad \Theta = Lk; \quad \Theta_t = (L+L_1)k;$$

$$k = \sqrt{(2i\epsilon + \gamma)/hD}; \quad \Theta = \Theta' + i\Theta''. \tag{4}$$

Here $F(\epsilon,V,T)$ is the distribution function (V and T are, respectively, half the voltage across the section AB and the temperature); φ is the phase difference between C and D; $r=(r_N/r_b)2$, where r_b is the resistance of the N/S boundary and r_N is the resistance of the normal part of the structure; Δ is the superconducting gap; Γ is the depairing rate in the superconductor; $\gamma = hD/L_\varphi^2$ is the depairing rate in the normal metal; L_φ is the phase interruption length; D is the diffusion coefficient; and, L and L_1 are, respectively, half the lengths of the segments AB and CD (see Fig. 1).

As one can see from Fig. 3, the agreement between theory and experiment is satisfactory. The values of the quantities employed in making the fit — $D=72$–85 cm^2/s, $L_\varphi = 1.5$–2 μm, $r=0.48$–0.77, $L=1$ μm, $L_1=1$ μm, $\Gamma=0.1\Delta$, and $\Delta=1.36$ meV — are reasonable, considering the fact that the accuracy of the experimental determination of a number of quantities to which the curves are especially sensitive, for example, the resistance r of the barriers, is low.

Fitting of expression (1) to the voltage dependence of the resistance of the normal structure presents a number of difficulties and requires additional assumptions. Direct substitution of the parameters obtained from the temperature dependence yields a value of the voltage for which the resistance is minimum. It is much greater than the experimentally observed value ($V_{\mathrm{theor}} = 5.5 V_{\mathrm{exp}}$). This could be due to the fact that the derivation of Eq. (1) assumed an equilibrium distribution function near the current leads. In other words, the energy of the quasiparticles in the reservoir is determined by the temperature T and the potential difference V between the reservoirs. In reality, the electron energy relaxation length can reach tens of microns at low temperatures.[19] Therefore, electrons with energy greater than eV could have been present in our samples, the thermalization process in the reservoirs themselves could be impeded, making it necessary to introduce an effective temperature that depends on the voltage and the spatial coordinates. In our experimental temperature interval, if electron–phonon collisions are neglected, the distribution function (2) can be written, according to the model of Ref. 20, in the form

$$F_1(\epsilon,V,T) = \frac{1}{2}\left[\tanh\left(\frac{\epsilon+V}{2T_1} \right) - \tanh\left(\frac{\epsilon-V}{2T_1} \right) \right], \tag{5}$$

where $T_1 = (T^2 + V_1^2/\Lambda)^{1/2}$ is the electron temperature near the contacts, $\Lambda = \pi^2/3e^2$ is the Lorentz number, T is the temperature in the reservoirs, and $V_1 = aV$ is the effective potential difference, which, as we have said, can be greater than the measured value V; and a is a constant, serving as an adjustable parameter ($a>1$).

The solid lines in Fig. 4 show the curves calculated using Eqs. (1) and (5). The only adjustable parameter was the coefficient $a \approx 3.7$; all other parameters were determined by fitting to the temperature dependence.

The quasiclassical formulas (1)–(5), which describe completely satisfactorily the behavior of structures with fixed phase differences $\Delta\varphi = n\pi, n = 0,1,2, \ldots$, are found to be inapplicable at intermediate phases. This is indicated by the qualitative changes which we observed in the temperature and voltage dependences of the conductance as a function of the phase difference as well as the substantial deviations in the line shape of the oscillations from a sinusoid in the entire experimental temperature interval (Figs. 2 and 3). According to Eqs. (1)–(5), all dependences should be described by a universal function with a similarity factor $1 + \cos\varphi$. The deviations of the line shape of the oscillations can in principle arise, as was shown in Ref. 15, as a result of partial screening with a finite induced critical current in the normal segment CD. However, this explanation is inapplicable, since in virtually the entire experimental temperature interval the distance $L_{CD} > \xi_T = (\hbar D/2\pi k_B T)^{1/2}$, and the critical current was negligibly small.

In summary, the quasiclassical theory in the approximation of a weak proximity effect[8–11] and low transmittance of the N/S boundaries, which made it possible to explain quantitatively the reentrance phenomenon in mesoscopic S/N structures with one superconducting contact,[5] explains quite satisfactorily the transport properties of symmetric S/N/S structures with fixed phase differences between the S/N contacts, $\Delta\varphi = n\pi$, $n = 1,2, 3, \ldots$. However, measurements with intermediate phases $\Delta\varphi$ indicate the need for more realistic models and can serve as a helpful method for studying the mechanism of mesoscopic proximity effects.

We thank Yu. Nazarov and A. F. Volkov for a discussion of the results. The work was supported by the Russian Academy of Sciences (Grants 104D/57, 97-0217031, and 97-1059) and the Swedish Academy of Sciences, The Wallenberg Foundation, and the British EPSRC (Grant Ref: GR/L94611).

[1] V. T. Petrashov, V. N. Antonov, P. Delsing, and T. Claeson, JETP Lett. **60**, 606 (1994).
[2] V. T. Petrashov, V. N. Antonov, P. Delsing, and T. Claeson, Phys. Rev. Lett. **74**, 5268 (1995).
[3] P. G. N. Pothier, S. Gueron, D. Esteve, and M. H. Devoret, Phys. Rev. Lett. **73**, 2488 (1994).
[4] A. Dimoulas, J. P. Heida, B. V. Wees *et al.*, Phys. Rev. Lett. **74**, 602 (1995).
[5] P. Charlat, H. Courtois, Ph. Gandit *et al.*, Phys. Rev. Lett. **77**, 4950 (1996).
[6] B. Z. Spivak and D. E. Khmelnitskiĭ, JETP Lett. **35**, 412 (1982).
[7] Yuli V. Nazarov and T. H. Stoof, Phys. Rev. Lett. **76**, 823 (1996); T. H. Stoof and Yuli V. Nazarov, Phys. Rev. B **53**, 14497 (1996).
[8] A. Volkov, N. Allsopp, and C. J. Lambert, J. Phys.: Condens. Matter **8**, L45-L50 (1996).
[9] A. V. Zaĭtsev, JETP Lett. **61**, 771 (1995).
[10] A. F. Volkov and V. P. Pavlovsky, in *Proceedings of the Moriond International Symposium on Correlated Fermions and Transport in Mesoscopic Systems*, Les Arcs, France, 1996.
[11] A. F. Volkov and H. Takayanagi, Phys. Rev. B **56**, 11184 (1997).
[12] A. F. Volkov and A. V. Zaitsev, Phys. Rev. B **53**, 9267 (1996).
[13] A. B. Zorin, Rev. Sci. Instrum. **66**, 4296 (1994).
[14] D. B. Haviland, S. H. M. Persson, P. Delsing, and C. D. Chen, J. Vac. Sci. Technol. A **14**(3), 1839 (1996).
[15] V. T. Petrashov, R. Ṣh. Shaikhaidarov and I. A. Sosnin, JETP Lett. **64**, 839 (1996).
[16] A. F. Andreev, Zh. Éksp. Teor. Fiz. **49**, 655 (1965) [Sov. Phys. JETP **22**, 455 (1965)].
[17] R. S. Thompson, Phys. Rev. B **1**, 327 (1970).

[18] V. T. Petrashov, R. Sh. Shaikhaidarov, I. A. Sosnin *et al.*, submitted to Phys. Rev. B.
[19] P. Santhanam, S. Wind, and D. E. Prober, Phys. Rev. Lett. **53**, 1179 (1984).
[20] K. E. Nagaev, Phys. Rev. B **52**, 4740 (1995).

Translated by M. E. Alferieff

Evolution of large-scale correlations in a strongly nonequilibrium Bose condensation process

Yu. Kagan and B. V. Svistunov
Kurchatov Institute Russian Science Center, 123182 Moscow, Russia

(Submitted 5 March 1998)
Pis'ma Zh. Éksp. Teor. Fiz. **67**, No. 7, 495–501 (10 April 1998)

The evolution of off-diagonal correlation functions (for the example of a single-particle density matrix) in the process of Bose condensation of an initially nonequilibrium interacting gas is discussed. Special attention is given to the character of the decay of the density matrix at distances much greater than the size of the quasicondensate region. Specifically, it is shown that the exponential decay of the density matrix necessarily presupposes the presence of a chaotic vortex structure — a tangle of vortex lines — in the system. When topological order is established but there is no off-diagonal long-range order, the density matrix decays with distance according to a power law. © *1998 American Institute of Physics.* [S0021-3640(98)01207-9]

PACS numbers: 03.75.Fi

One of the most interesting aspects of the kinetics of Bose condensation is the character of the formation of quantum correlations and the long-range order in an initially strongly nonequilibrium, chaotic gas system. A characteristic feature of such a gas system is total absence of a condensate phase. Let us assume that an isolated gas system with a fixed number of particles N or density n and characteristic particle energy ε_* much lower than the equilibrium Bose-condensation temperature $T_c(n)$ has formed as a result of rapid cooling. In this case, evolution actually reduces to the formation of a particle flux in energy space, transporting into the region $\varepsilon \approx 0$ particles that form a Bose condensate at equilibrium. If $\varepsilon_* \gg nU_0$ ($U_0 = 4\pi\hbar^2 a/m$, where a is the scattering length), then a description based on a Boltzmann kinetic equation is adequate at the first stage of evolution (see Refs. 1–4 for a more detailed discussion). It is easy to see that even at this stage the system passes through a state with occupation numbers $n_k \gg 1$, and this inequality only intensifies in the course of evolution (if $\varepsilon_* \ll T_c(n)$, then this inequality holds from the outset for all modes with $\varepsilon_k \leqslant \varepsilon_*$).

In Ref. 5 it was shown that for large occupation numbers the temporal evolution of the system can be described by a statistical matrix which is diagonal in the coherent-states representation

$$W(t) = \int \mathcal{D}\alpha Q(\alpha) |\Phi(t,\alpha)\rangle\langle\Phi(t,\alpha)|. \tag{1}$$

Here the coherent states $|\Phi(t,\alpha)\rangle$ are eigenfunctions of the field operator

$$\hat{\psi}|\Phi(t,\alpha)\rangle = \psi(t,\alpha)|\Phi(t,\alpha)\rangle, \tag{2}$$

with eigenvalues ψ satisfying the nonlinear Schrödinger equation

$$i\frac{\partial\psi}{\partial t}=-\frac{\Delta}{2m}\psi+V\psi+U_0|\psi|^2\psi \tag{3}$$

(Here and below, $\hbar=1$ and V is the external potential; Δ is the Laplacian operator).

In expression (1) averaging over the initial distribution of coherent states is performed. Initially, the single-particle modes are independent, and the index $\alpha\equiv\{\alpha_{\mathbf{k}}\}$ characterizes the set of complex parameters $\alpha_{\mathbf{k}}=\rho_{\mathbf{k}}\exp i\varphi_{\mathbf{k}}$ of the standard coherent states.[6] Accordingly, in Eq. (1)

$$\mathcal{D}\alpha\equiv\prod_{\mathbf{k}} d(\rho_{\mathbf{k}}^2)\frac{d\varphi_{\mathbf{k}}}{\pi}. \tag{4}$$

The phases of the harmonics in the initial state are completely uncorrelated, and $Q(\alpha)$ is a smooth function

$$Q(\alpha)=\prod_{\mathbf{k}} Q_{\mathbf{k}}(\rho_{\mathbf{k}}^2). \tag{5}$$

For fixed α the solution of Eq. (3) (in the homogeneous case) should correspond to the initial condition

$$\psi(0,\alpha)=\sum_{\mathbf{k}} \alpha_{\mathbf{k}}e^{i\mathbf{k}\cdot\mathbf{r}}=\sum_{\mathbf{k}} \rho_{\mathbf{k}}e^{i\varphi_{\mathbf{k}}+i\mathbf{k}\cdot\mathbf{r}}. \tag{6}$$

The objective of the present work is to analyze the evolution of the correlation properties in the process of formation of long-range order. For this, we shall examine the temporal evolution of the single-particle density matrix.

According to Eq. (1), the density matrix averaged over an individual coherent state in a homogeneous space can be represented in the form (Ω is the volume of the system)

$$\begin{aligned}K_\alpha(\mathbf{r},t)&=\frac{1}{\Omega}\int d\mathbf{r}'\langle\Phi(t,\alpha)|\hat{\psi}^\dagger(\mathbf{r}+\mathbf{r}')\hat{\psi}(\mathbf{r}')|\Phi(t,\alpha)\rangle\\&=\frac{1}{\Omega}\int d\mathbf{r}'\,\psi^*(\mathbf{r}+\mathbf{r}',t,\alpha)\psi(\mathbf{r}',t,\alpha).\end{aligned} \tag{7}$$

The function $\psi(\mathbf{r},t,\alpha)$ in Eq. (7) is a solution of Eq. (3). The complete density matrix $K(\mathbf{r},t)$ presupposes an averaging of Eq. (7) with the statistical matrix (1).

Expressions (7), (3), and (1) imply that to analyze the correlation properties it is sufficient to find the solution of Eq. (3) for different values of α. This is an extremely important result, since the Boltzmann transport equation ceases to be valid after the particles that ultimately form a condensate have arrived in the energy interval $\varepsilon_k<nU_0$ (coherent region). To describe the evolution we must employ an equation for the classical field (3). Actually, even the solution obtained for one representative value of α gives a comparatively complete picture of the evolution of the system.

When most of the future condensate particles have arrived in the coherent region, their kinetic energy drops below the potential energy of their mutual interaction. The individual modes are no longer independent, and at this stage large-scale quantum cor-

relation effects appear. It is significant that Eq. (3) is valid in the kinetic region $\varepsilon > nU_0$. In this sense it gives a unified description, valid in both the coherent and kinetic regions. This implies the existence of a continuous flux from the kinetic into the coherent region, without any characteristic features at the boundary between these regions.

At the initial stage of evolution, fluctuations of both the phase and modulus (or density) of the complex field ψ are large in the coherent region, but even when the particle density lies in the narrow energy interval $\varepsilon_0(t) \ll nU_0$ or $k_0(t) \ll k_c$ ($k_c = 1/r_c = \sqrt{2mnU_0}$ is the reciprocal of the correlation radius) the modulus fluctuations are suppressed (see Ref. 2). The correlation properties are actually determined by the phase fluctuations. At the same time, the excess energy which must be transferred to the above-condensate subsystem when the equilibrium condensation is reached is small to the extent that the density fluctuations are weak:

$$\left\langle \left(\frac{\delta n}{n} \right)^2 \right\rangle \approx \left(\frac{k_0(t)}{k_c} \right)^2 \ll 1 \ . \tag{8}$$

This signifies, specifically, that starting at this stage of evolution the properties of the above-condensate subsystem actually do not change, and the subsystem is effectively already in equilibrium. The character of the shortening of the interval $k_0(t)$ is now limited by energy transfer from nonequilibrium fluctuations and topological defects to this subsystem.

The existence of a finite interval $k_0(t)$ in which the Fourier components of the classical field ψ are concentrated determines the spatial scale of the regions $r_0(t) \approx k_0^{-1}(t) \gg r_c$ in which the relative fluctuations are weak. For $r < r_0(t)$ the phase difference between the functions ψ appearing in the correlation function (7) practically vanish and $K_\alpha \approx n_0$ (n_0 is the density, essentially identical to the equilibrium density of a condensate established at the end of evolution; for $\varepsilon_* \ll T_c$ the value of n_0 is close to the total density n). Averaging with the statistical matrix (1) preserves this result. Thus the density matrix for $r < r_0(t)$ behaves as it would in the presence of a true Bose condensate. One can arrive at the same conclusion by studying more complicated correlation functions. For example, it was shown in Ref. 2 that under these conditions the three-particle density correlation function (responsible for the three-particle recombination rate) is a factor of six lower than the value in the kinetic region. But this result was predicted earlier[8] for systems with a true equilibrium condensate. (This effect was recently discovered experimentally.[9])

Thus, a unique quasicondensate state, exhibiting properties of a true condensate for all characteristics that depend on correlations at distances $r < r_0(t)$, is established. At the same time, regions $r \gg r_0(t)$ are still uncorrelated, which signifies the absence of long-range order, and they should accordingly be characterized by a decrease of the density matrix with increasing r.

The breakdown of phase correlations at large distances occurs for two reasons.[7] The first one is the inevitable appearance of a chaotic vortex structure (vortex tangle) during the evolution of the nonequilibrium system. A simple description of such a structure presupposes the introduction of a spatial scale l, determining the average distance between the vortex lines (see, for example, Ref. 10). The interaction with the above-condensate particles results in a decrease of the total length of the vortex lines in a tangle

and, correspondingly, an increase in $l(t)$ (see Ref. 7 for a more detailed discussion). The other reason is the presence of anomalous long-wavelength fluctuations of the phase or an anomalous distribution of nonequilibrium long-wavelength phonons, which is associated with these phase fluctuations, in the relaxing system. (In Ref. 2 it was shown that for $k \ll k_c$ collective excitations possess a Bogolyubov spectrum even in the absence of a condensate.) Relaxation of these phonons is also associated with an interaction with the above-condensate particles.

In contradistinction to the preceding stages of evolution, the establishment of long-range order is now due to time scales that depend on the size of the system. Let us consider the asymptotic behavior of the density matrix for $r \gg r_0(t) \gg r_c$. Let the ''wave function'' ψ be of the form

$$\psi = \sqrt{n_0} e^{i\chi} \tag{9}$$

and let us expand the phase difference in the exponential in Eq. (7) in a Fourier series

$$\chi(\mathbf{r}',t,\alpha) - \chi(\mathbf{r}'+\mathbf{r},t,\alpha) = \sum_{k<k_0(t)}{}' \; [\chi_{\mathbf{k}} e^{i\mathbf{k}\cdot\mathbf{r}'}(1-e^{i\mathbf{k}\cdot\mathbf{r}}) + \text{c.c.}]. \tag{10}$$

The prime on the summation sign signifies summation over half the phase space. Assuming the Fourier components to be independent, we rewrite the exponential as a product of exponentials for separate $\mathbf{k}$ and expand the latter in a series, retaining quadratic terms ($\chi_{\mathbf{k}} \sim \Omega^{-1/2}$). After integrating over $\mathbf{r}'$ in Eq. (7) we obtain

$$\prod_{k<k_0(t)}{}' \; (1 - 2|\chi_{\mathbf{k}}|^2(1-\cos\,\mathbf{k}\cdot\mathbf{r})). \tag{11}$$

Returning to the exponential form, we find finally

$$K_\alpha(\mathbf{r},t) = n_0 e^{-S(\mathbf{r},t)}, \quad S(\mathbf{r},t) = \sum_{k<k_0(t)} |\chi_{\mathbf{k}}|^2(1-\cos\,\mathbf{k}\cdot\mathbf{r}). \tag{12}$$

It is easy to show directly that the function $S(\mathbf{r},t)$ can be rewritten in the form

$$S(\mathbf{r},t) = \frac{1}{2}\overline{[\chi(\mathbf{r}'+\mathbf{r},t,\alpha) - \chi(\mathbf{r}',t,\alpha)]^2}, \tag{13}$$

where the averaging is performed over the initial reference point $\mathbf{r}'$.

Let us first consider the case when the relaxation of the vortex structure, characterized by the time $\tau_V(l)$, is slower than the decay of the nonequilibrium phonons with $k \approx l^{-1}$, i.e., the corresponding time $\tau_\varphi(k=l^{-1}) < \tau_V(l)$. Since photons with $k > l^{-1}$ decay more rapidly ($\tau_\varphi^{-1} \sim k^\nu$, $\nu = 2, 1$; see Ref. 7 for a more detailed discussion), a virtually quasiequilibrium state is established in regions of size $\sim l(t)$. Therefore the characteristic scale size of the quasicondensate regions in this case is $r_0(t) \sim l(t)$.

The phase difference in Eq. (13) can be written in the form

$$(\delta\chi)_{\mathbf{r}} = \int_{\mathbf{r}'}^{\mathbf{r}+\mathbf{r}'} d\mathbf{r}_1 \nabla_{\mathbf{r}_1}\chi. \tag{14}$$

For $r \gg l(t)$ the contour of integration intersects a large number $N \sim r/l(t) \gg 1$ of phase-uncorrelated quasicondensate regions. The random spatial distribution of the vortex lines

in a tangle and of the sign of the circulations on them has the effect that the phase gradients at distances larger than l are uncorrelated. Keeping this in mind, we have

$$\overline{(\delta\chi)_{\mathbf{r}}^2} \approx r l \overline{(\nabla\chi)_0^2}. \tag{15}$$

Here the local correlation function $\overline{(\nabla\chi)_0^2} \sim l^{-2}$. As a result

$$S(\mathbf{r},t) = \xi \frac{r}{l(t)}, \tag{16}$$

where ξ is a numerical coefficient of order 1. Therefore the density matrix (12) and (13) decays exponentially at distances $r \gg l(t)$. In studying the relaxation of the vortex structure, we found earlier[7] for $l(t)$ the relation (to logarithmic accuracy)

$$l(t) \sim \sqrt{\Gamma_0 \alpha^{1/3}} \sqrt{t}. \tag{17}$$

Here $\Gamma_0 = 2\pi/m$ is the circulation quantum; $\alpha = (n_0 U_0/T)^{3/2}$ is a dimensionless friction coefficient, obtained assuming that the temperature of the above-condensate particles $T \gg n_0 U_0$. It follows from Eqs. (16) and (17) that the size of the quasicondensate regions where $K(\mathbf{r},t) \approx n_0$ increases with time as $\sqrt{t}$.

When $l(t)$ reaches the size of the system L as a result of complete relaxation of the vortex structure, S ceases to depend on r. The function $K_\alpha(\mathbf{r},t)$ and together with it the complete density matrix assume a constant **r**-independent value. As a result, simultaneously with the topological order there arises off-diagonal long-range order, and a true Bose condensate is formed.

Let us examine the opposite limiting case, where the vortex structure relaxes more quickly than the nonequilibrium fluctuations of the regular phase. Assume that at some moment the vortex structures vanishes and topological order is established. However, complete long-range order (or, equivalently, a true condensate) is absent. The size of the quasicondensate regions and its evolution in time are now dictated by the relaxation of the fluctuations of the regular phase (i.e., nonequilibrium long-wavelength phonons). Although phase correlation once again breaks down at distances $r > r_0(t)$, we cannot make use of the foregoing considerations concerning the behavior of the correlation function of the phase gradients. These considerations are valid only in the presence of a vortex tangle (see below).

For $k_0(t) \ll k_c$ the kinetic energy concentrated in a quasicondensate can be estimated as

$$E_{\text{kin}} = \frac{n_0}{2m} \int d\mathbf{r} (\nabla\chi)^2 = \frac{n_0 \Omega}{m} \sum_{\mathbf{k}} k^2 |\chi_{\mathbf{k}}|^2. \tag{18}$$

At the same time, we have from the initial Hamiltonian

$$E_{\text{kin}} = \sum_{\mathbf{k}} \frac{k^2}{2m} \langle n_{\mathbf{k}} \rangle \sim \frac{k_0^2(t)}{m} n_0 \Omega. \tag{19}$$

Since

$$\sum_{k < k_0(t)} k^2 |\chi_{\mathbf{k}}|^2 \sim \Omega k_0^5(t) |\chi_{k_0}|^2, \tag{20}$$

and comparing both expressions for $E_{\rm kin}$ we have

$$|\chi_{k_0}|^2 \sim 1/\Omega k_0^3(t). \tag{21}$$

This relation is valid for arbitrary $k_0(t)$ in the process of evolution. At the same time, the fluctuations relax from the ''head,'' since the decay of the nonequilibrium acoustic modes satisfies the law $\tau_\varphi^{-1} \sim k^\nu$, $\nu = 2, 1$ (see Ref. 7). Therefore it can be asserted that there is not enough time for the distribution with smaller values of k to be restructured and therefore the result (21) implies that for all $k < k_0(t)$

$$|\chi_{\mathbf{k}}|^2 = \gamma/\Omega k^3. \tag{22}$$

Substituting expression (22) into Eq. (13), we find

$$S(\mathbf{r},t) \approx 4\pi\gamma \ln(k_0(t)r) \quad (k_0(t)r \gg 1). \tag{23}$$

Comparing Eqs. (23) and (16), we find that the advanced appearance of topological order strongly changes the asymptotic behavior of the density matrix. Off-diagonal order appears when $r_0(t)$ reaches the size of the system L. The corresponding establishment time $\tau_\varphi \sim L^2$ in the hydrodynamic regime or $\tau_\varphi \sim L$, if the above-condensate particles are in a Knudsen regime (see Ref. 7).

For $\tau_\varphi \gg \tau_{\rm V}$, until topological order appears, the behavior of the density matrix is more complicated. In this case the relaxation of the phonons lags the relaxation of the vortices and the size of the quasicondensate regions $r_0(t) \ll l(t)$ is determined by fluctuations of the regular phase. In the interval $r_0(t) < r < l(t)$ the density matrix decays with distance with an exponent determined by expression (23). For $r > l(t)$ the decay law changes markedly in accordance with the dependence (16).

In conclusion, we shall present two general remarks. In the derivation of Eqs. (12) and (13) we assumed that the Fourier components of the phase difference in Eq. (7) are independent. If the behavior of the density matrix is determined by fluctuations of the regular phase (after relaxation of the vortex structure), then the expansion (10) is actually an expansion in the long-wavelength phonon modes. The independence of these modes automatically leads to Eqs. (11) and (12). In the presence of a vortex structure the behavior of the density matrix for $r \gg l(t)$ is determined by the accumulated phase difference (14). Since at distances of the order $l(t)$ the phase increment $\Delta\chi$ changes in an uncorrelated manner in sign and magnitude, while integration over the initial reference point in Eq. (7) gives complete averaging, we have a typical Markovian picture. For $r/l(t) \gg 1$ this leads to a Gaussian distribution for the probability of the appearance of a definite value of the phase difference $(\delta\chi)_{\mathbf{r}}$, which leads directly to the result (13). This agreement reflects the fact that the long-wavelength fluctuations with wave numbers k corresponding to the condition $kl(t) \ll 1$ and responsible for the behavior of the density matrix for $r \gg l(t)$ are statistically independent under the conditions studied.

The other remark is linked with some general considerations which make it possible to understand the reason for the different asymptotic behavior of the nonequilibrium density matrix in the presence or absence of a vortex structure. For an individual component of the classical field appearing in Eq. (7), going around a closed contour gives

$$\oint \nabla\chi \cdot d\mathbf{l} = 2\pi M. \tag{24}$$

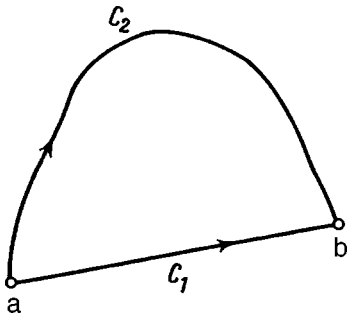

FIG. 1.

Here M is an integer. (We assume that the contour does not intersect any vortex lines.) Let us consider the contour shown in Fig. 1, and let $r_{ab} \gg r_0(t)$. If it is assumed that all quasicondensate regions are independent and that the sign of $\nabla\chi \cdot d\mathbf{l}$ in these regions is arbitrary (as a consequence of the arbitrariness of the direction of $\nabla\chi$), the phase difference is

$$\chi_b - \chi_a = \int_{C_1} \nabla\chi \cdot d\mathbf{l} \approx \sqrt{r_{ab} r_0(t)}\,|(\nabla\chi)_0| \tag{25}$$

(see Eq. (15)). But if we take a different contour, C_2, of length L_{ab}, then

$$\chi_b - \chi_a = \int_{C_2} \nabla\chi \cdot d\mathbf{l} \approx \sqrt{L_{ab} r_0(t)}\,|(\nabla\chi)_0|. \tag{26}$$

For $L_{ab} \gg r_{ab}$, in going around a closed contour we clearly obtain $2\pi M$ with $M \neq 0$. This signifies the presence of vortex lines intersecting the area enclosed by the contour. If there are no vortex lines, then the assumption that $\nabla\chi$ has an arbitrary direction in individual quasicondensate regions is incorrect. This signifies that the vanishing of a vortex structure leaves the nonequilibrium system with finite disorder. This is why the asymptotic behavior of the density matrix changes from (16) to (23).

[1] B. V. Svistunov, J. Mosc. Phys. Soc. **1**, 373 (1991).
[2] Yu. Kagan, B. V. Svistunov, and G. V. Shlyapnikov, Zh. Éksp. Teor. Fiz. **101**, 528 (1992) [Sov. Phys. JETP **75**, 387 (1992)].
[3] Yu. Kagan, in *Kinetics of Bose-Einstein Condensate Formation in an Interacting Bose Gas, Bose-Einstein Condensation*, edited by A. Griffin, D. W. Snoke, and S. Stringari, Cambridge University Press, New York, 1995, p. 202.
[4] D. V. Semikoz and I. I. Tkachev, Phys. Rev. Lett. **74**, 3093 (1995); Phys. Rev. D **55**, 489 (1997).
[5] Yu. Kagan and B. V. Svistunov, Phys. Rev. Lett. **79**, 3331 (1997).
[6] R. J. Glauber, Phys. Rev. **131**, 2766 (1963).
[7] Yu. Kagan and B. V. Svistunov, Zh. Éksp. Theor. Fiz. **105**, 353 (1994) [Sov. Phys. JETP **78**, 187 (1994)].
[8] Yu. Kagan, B. V. Svistunov, and G. V. Shlyapnikov, JETP Lett. **42**, 209 (1985); Zh. Éksp. Teor. Fiz. **93**, 552 (1987) [Sov. Phys. JETP **66**, 314 (1987)].
[9] E. A. Burt, R. W. Christ, C. J. Myatt *et al.*, Phys. Rev. Lett. **79**, 337 (1997).
[10] K. W. Schwarz, Phys. Rev. B **18**, 245 (1978).

Translated by M. E. Alferieff

Vortex mass in BCS systems: Kopnin and Baym–Chandler contributions

G. E. Volovik

Low Temperature Laboratory, Helsinki University of Technology, P. O. Box 2200, FIN-02015 HUT, Finland; Landau Institute for Theoretical Physics, Russian Academy of Sciences, 117334 Moscow, Russia

(Submitted 6 March 1998)
Pis'ma Zh. Éksp. Teor. Fiz. **67**, No. 7, 502–506 (10 April 1998)

The Kopnin mass and the Baym–Chandler mass of a vortex have the same origin. Both represent the mass of the normal component trapped by the vortex. The Kopnin mass of a vortex is formed by quasiparticles localized in the vicinity of the vortex. In the superclean limit it is calculated as a linear response, in exactly the same way as the density of the normal component is calculated in a homogeneous superfluid. The Baym–Chandler mass is the hydrodynamic (associated) mass trapped by a vortex. It is analogous to the normal component formed by inhomogeneities, such as pores and impurities. Both contributions are calculated for a generic model of a continuous vortex core. © *1998 American Institute of Physics.* [S0021-3640(98)01307-3]

PACS numbers: 74.20.Fg

It is well known that in BCS superfluids and superconductors the most important contribution to the vortex mass originates from the vortex core. The core mass in these systems is proportional to the area of the core $A \sim \xi^2$, where ξ is the coherence length (see Ref. 1 for the vortex mass in superconductors and Ref. 2 for the vortex mass in superfluid ^{3}He-B). This core mass is substantially larger than the logarithmically divergent contribution, which comes from the compressibility. In spite of the logarithmic divergence, the latter contains the speed of sound in the denominator and thus is smaller by a factor of $(a/\xi)^2 \ll 1$, where a is the interatomic distance. The compressibility mass of the vortex dominates in Bose superfluids, where the core size is small, $\xi \sim a$.

According to Kopnin theory the core mass comes from the fermions trapped in the vortex core.[1–4] Recently the problem of another vortex mass of hydrodynamic origin was raised in Ref. 5. It is the so-called backflow mass discussed by Baym and Chandler,[6] which also can be proportional to the core area. Here we compare these two contributions in the superclean regime and at low $T \ll T_c$ using the continuous-core model.

The continuous-core vortex is one of the best models and helps solve many problems in vortex core physics. Instead of considering the singular core, one can smoothen the $1/r$ singularity of the superfluid velocity by introducing point gap nodes in the core region. As a result the superfluid/superconducting state in the vortex core of any system acquires the properties of the A phase of superfluid ^{3}He, with its continuous vorticity and point gap nodes.[7,8] Using the continuous-core model one can show, for example, that the Kopnin (spectral flow) force comes directly from the Adler–Bell–Jackiw chiral anomaly

equation,[9] and this shows the real origin of this anomalous force. In this model one can easily separate different contributions to the vortex mass. Actually this is not only the model: The spontaneous smoothing of the velocity singularity occurs in the core of both types of vortices observed in ^{3}He-B (Ref. 8); in heavy fermionic and high-T_c superconductors such smoothening can occur due to admixture of different pairing states in the vortex core.

It appears that both the Kopnin mass and the Baym–Chandler mass are related to the normal component. In general the normal component of a superfluid comes from two sources: (i) the local contribution, which comes from the system of quasiparticles, and (ii) the associated mass related to the backflow. The latter is dominant in porous materials, where some part of superfluid component is hydrodynamically trapped by the pores and thus is removed from the overall superfluid motion. The normal component, which gives rise to the vortex mass, contains precisely the same two contributions. (i) The local contribution comes from the quasiparticles localized in the vortex core and thus moving with the core. This is the origin of the Kopnin mass according to Ref. 4. (ii) The associated mass contribution arises because the profile of the local density of the normal component in the vicinity of the vortex core disturbs the superflow around the vortex when the vortex moves. This creates a backflow, and thus some part of the superfluid component is trapped by the moving vortex, resulting in the Baym–Chandler mass of the vortex.

Let us consider this for the example of the simplest continuous-core vortex (Fig. 1). It has the following distribution of the unit vector $\hat{\mathbf{l}}(\mathbf{r})$, which shows the direction of the point gap nodes in the smooth core:

$$\hat{\mathbf{l}}(\mathbf{r}) = \hat{\mathbf{z}} \cos\ \eta(r) + \hat{\mathbf{r}} \sin\ \eta(r), \tag{1}$$

where z, r, ϕ are cylindrical coordinates. For superfluid ^{3}He-A the $\hat{\mathbf{l}}$ vector in the smooth core changes from $\hat{\mathbf{l}}(0) = -\hat{\mathbf{z}}$ to $\hat{\mathbf{l}}(\infty) = \hat{\mathbf{z}}$, which represents a doubly quantized continuous vortex. For the smoothed singly quantized vortices in ^{3}He-B and superconductors one has two $\hat{\mathbf{l}}$ vectors with $\hat{\mathbf{l}}_1(0) = \hat{\mathbf{l}}_2(0) = -\hat{\mathbf{z}}$ and $\hat{\mathbf{l}}_1(\infty) = -\hat{\mathbf{l}}_2(\infty) = \hat{\mathbf{r}}$ (Ref. 8). The region of radius R in which the texture of the $\hat{\mathbf{l}}$ vectors is concentrated is called the smooth (or soft) core of the vortex.

Kopnin mass. Let us recall the phenomenological derivation of the Kopnin mass of the vortex at low T and in the superclean regime.[4] If the vortex moves with velocity $\mathbf{v}_L$ with respect to the superfluid component, the fermionic energy spectrum in the vortex frame is Doppler shifted: $E = E_0(\nu) - \mathbf{k}\cdot\mathbf{v}_L$, where ν stands for the fermionic degrees of freedom in the stationary vortex. The summation over fermionic degrees of freedom leads to an extra linear momentum of the vortex $\propto \mathbf{v}_L$:

$$\mathbf{P} = \sum_{\nu} \mathbf{k}\theta(-E) = \sum_{\nu} \mathbf{k}(\mathbf{k}\cdot\mathbf{v}_L)\,\delta(E_0) = M_{\mathrm{Kopnin}}\mathbf{v}_L\,. \tag{2}$$

Note that this vortex mass is determined in essentially the same way as the normal component density in the bulk system. The Kopnin vortex mass is nonzero if the density of fermionic states is finite in the vortex core. The density of states (DOS) is determined by the interlevel spacing ω_0 in the core: $N(0) \propto 1/\omega_0$, which gives the following estimate for the Kopnin vortex mass: $M_{\mathrm{Kopnin}} \sim k_F^3/\omega_0$ (the exact expression is M_{Kopnin}

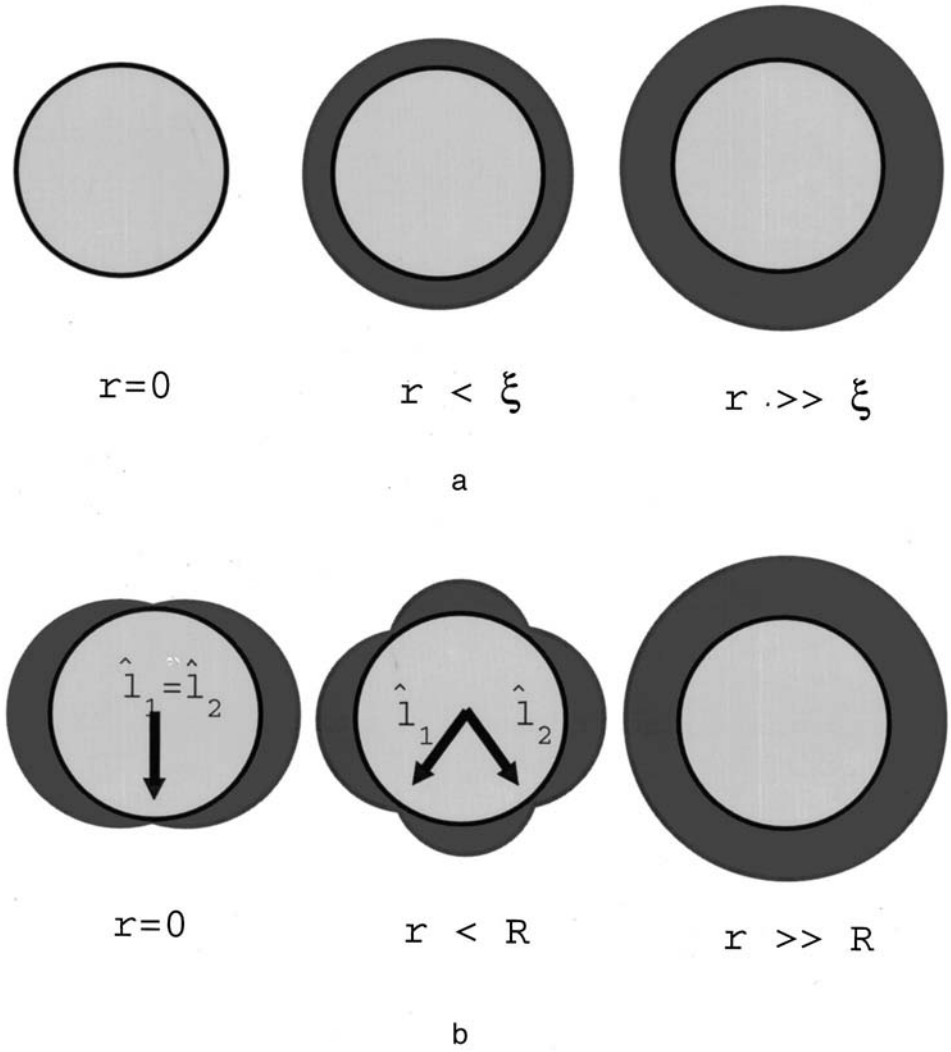

FIG. 1. Singular vortex versus soft-core vortex: a — in the singular vortex the gap continuously decreases and becomes zero on the vortex axis (at $r=0$); b — for some vortices it is energetically favorable to escape the nullification of the order parameter at $r=0$. Instead, within the smooth core, $r<R$, point gap nodes appear in the spectrum of fermions.[7] The unit vectors $\hat{\mathbf{l}}_1$ and $\hat{\mathbf{l}}_2$ show the directions to the nodes at different r. Close to the gap nodes the spectrum of fermions is similar to that in ^{3}He-A.

$=\int_{-k_F}^{k_F}(dk_z/4\pi)(k_\perp^2/\omega_0(k_z)))$. For the soft-core vortex the interlevel spacing is $\omega_0 \sim \hbar^2/(m\xi R)$, which gives a Kopnin mass $M_{\rm Kopnin}\sim\rho\xi R$ (Ref. 10), where ρ is the mass density of the liquid.

For our purposes it is instructive to consider the normal component associated with the vortex as a local quantity determined at each point in the vortex core. Such a treatment is valid for a smooth core with a radius $R\gg\xi$, where the local classical description

of the fermionic spectrum can be applied. The main contribution comes from the point gap nodes, for which the classical spectrum has the form $E_0 = \sqrt{v_F^2(k-k_F)^2+\Delta_0^2(\hat{\mathbf{k}}\times\hat{\mathbf{l}})^2}$, where Δ_0 is the gap amplitude. In the presence of the gradient of the $\hat{\mathbf{l}}$ field, which acts on the quasiparticles as an effective magnetic field, this gapless spectrum leads to a nonzero local DOS and finally to the following local density of the normal component at $T=0$ (see Eq. (5.24) in the review[11]):

$$(\rho_n)_{ij}(\mathbf{r})=\rho_n\hat{l}_i\hat{l}_j, \quad \rho_n=\frac{k_F^4}{2\pi^2\Delta_0}|(\hat{\mathbf{l}}\cdot\vec{\nabla})\hat{\mathbf{l}}|=\frac{k_F^4\sin\eta}{2\pi^2\Delta_0}|\partial_r\eta|. \tag{3}$$

The integral of this normal density tensor over the cross section of the soft core gives the same Kopnin mass of the vortex but in the local density representation,[4]

$$M_{\text{Kopnin}}=\frac{1}{2}\int d^2r\,\rho_n(r)\sin^2\eta(r)\sim\rho\xi R. \tag{4}$$

Here we have used the fact that $v_F/\Delta_0\sim\xi$. Note that the area law for the vortex mass is valid only for vortices with $R\sim\xi$, but in general one has the linear law $M_{\text{Kopnin}}\sim\rho\xi R$ (Ref. 10).

The associated (or induced) mass appears when, say, an external body moves in the superfluid. This mass depends on the geometry of the body. For a moving cylinder of radius R it is the mass of the liquid displaced by the cylinder,

$$M_{\text{associated}}=\pi R^2\rho, \tag{5}$$

which is to be added to the actual mass of the cylinder to obtain the total inertial mass of the body. In superfluids this part of the superfluid component moves with the external body and thus can be associated with the normal component. A similar mass is responsible for the normal component in porous materials and in aerogels, where some part of superfluid is hydrodynamically trapped by the pores. It is removed from the overall superfluid motion and thus becomes part of the normal component.

In the case when the vortex is trapped by a wire of radius $R\gg\xi$, such that the vortex core is represented by the wire, Eq. (5) gives the vortex mass due to the backflow around the moving core. This is the simplest realization of the backflow mass of the vortex discussed by Baym and Chandler.[6] For such a vortex with a wire core the Baym–Chandler mass is the dominant mass of the vortex. The Kopnin mass, which can result from the normal excitations trapped near the surface of the wire, is substantially less.

Let us now consider the Baym–Chandler mass for the free vortex at $T=0$, again using the continuous-core model. In the wire-core vortex this mass arises due to the backflow caused by the inhomogeneity of ρ_s: $\rho_s(r>R)=\rho$ and $\rho_s(r<R)=0$. A similar but less severe inhomogeneity of $\rho_s=\rho-\rho_n$ occurs in the continuous-core vortex on account of the nonzero local normal density in Eq. (3). Due to the profile of the local superfluid density the external flow is disturbed near the core according to continuity equation

$$\boldsymbol{\nabla}\cdot(\rho_s\mathbf{v}_s)=0. \tag{6}$$

If the smooth core is large, $R\gg\xi$, the deviation of the superfluid component in the smooth core from its asymptotic value outside the core is small: $\delta\rho_s=\rho-\rho_s\sim(\xi/R)\rho\ll\rho$ and

can be considered as perturbation. Thus if the asymptotic value of the velocity of the superfluid component with respect of the core is $\mathbf{v}_{s0}=-\mathbf{v}_L$, the disturbance $\delta\mathbf{v}_s=\boldsymbol{\nabla}\Phi$ of the superflow in the smooth core is given by:

$$\rho\boldsymbol{\nabla}^2\Phi=v_{s0}^i\nabla^j(\rho_n)_{ij}\,. \tag{7}$$

The kinetic energy of the backflow gives the Baym–Chandler mass of the vortex

$$M_{\rm BC}=\frac{\rho}{v_{s0}^2}\int d^2r(\boldsymbol{\nabla}\Phi)^2. \tag{8}$$

In the simple approximation in which the normal component in Eq. (3) is considered as isotropic, one obtains

$$M_{\rm BC}=\frac{1}{2\rho}\int d^2r\rho_n^2(r)\sim\rho\xi^2. \tag{9}$$

The Baym–Chandler mass does not depend on the core radius R, since the large area R^2 of integration in Eq. (9) is compensated by the small value of the normal component in the rarefied core, $\rho_n\sim\rho(\xi/R)$. That is why if the smooth core is large, $R\gg\xi$, this mass is parametrically smaller than the Kopnin mass in Eq. (4).

In conclusion, both contributions to the mass of the vortex result from the mass of the normal component trapped by the vortex. The difference between Kopnin mass and Baym–Chandler backflow mass lies only in the origin of the normal component trapped by the vortex. The relative importance of the two masses depends on the vortex core structure: 1) For a free continuous vortex with a large core size $R\gg\xi$, the Kopnin mass dominates: $M_{\rm Kopnin}\sim\rho R\xi\gg M_{\rm BC}\sim\rho\xi^2$. 2) For a vortex trapped by a wire of radius $R\gg\xi$, the Baym–Chandler mass is proportional to the core area, $M_{\rm BC}\sim\rho R^2$, and is parametrically larger than the Kopnin mass. 3) For a free vortex core with the core radius $R\sim\xi$ the situation is not clear, since the continuous-core approximation no longer works. But extrapolation of the result in Eq. (9) to $R\sim\xi$ suggests that the Baym–Chandler mass can be comparable with the Kopnin mass.

I thank G. Blatter and N. B. Kopnin for numerous discussions. This work was supported by the Russian Fund for Fundamental Research, Grant 96-02-16072, by the Russian Academy of Sciences program ''Statistical Physics,'' and by Intas Grant 96-0610.

[1] N. B. Kopnin, JETP Lett. **27**, 390 (1978).
[2] N. B. Kopnin and M. M. Salomaa, Phys. Rev. B **44**, 9667 (1991).
[3] A. van Otterlo, M. V. Feigel'man, V. B. Geshkenbein, and G. Blatter, Phys. Rev. Lett. **75**, 3736 (1995).
[4] G. E. Volovik, JETP Lett. **65**, 217 (1997).
[5] E. B. Sonin, V. H. Geshkenbein, A. van Otterlo, and G. Blatter, Phys. Rev. B **57,** 575 (1998).
[6] G. Baym and E. Chandler, J. Low Temp. Phys. **50**, 57 (1983).
[7] G. E. Volovik and V. P. Mineev, Zh. Éksp. Teor. Fiz. **83**, 1025 (1982) [Sov. Phys. JETP **56**, 579 (1982)].
[8] M. M. Salomaa and G. E. Volovik, Rev. Mod. Phys. **59**, 533 (1987).
[9] T. D. C. Bevan, A. J. Manninen, J. B. Cook *et al.* Nature **386**, 689 (1997).
[10] N. B. Kopnin, Physica B **210**, 267 (1995).
[11] G. E. Volovik, in *Helium Three* (edited by W. P. Halperin and L. P. Pitaevskii), Elsevier Science Publishers, 1990, p. 27.

Published in English in the original Russian journal. Edited by Steve Torstveit.

Terahertz emission from square wells in a longitudinal electric field

L. E. Vorob'ev, D. V. Donetskiĭ, D. A. Firsov,[a)] and E. B. Bondarenko
St. Petersburg State Technical University, 195251 St. Petersburg, Russia

G. G. Zegrya
A. F. Ioffe Physicotechnical Institute, Russian Academy of Sciences, 194021 St. Petersburg, Russia

E. Towe
Thornton Hall, University of Virginia, Charlottesville, VA 22903-2442, USA

(Submitted 11 March 1998)
Pis'ma Zh. Éksp. Teor. Fiz. **67**, No. 7, 507–511 (10 April 1998)

Terahertz emission accompanying heating of two-dimensional electrons by a strong electric field applied along size-quantized GaAs/AlGaAs layers is observed and investigated. The emission is due to indirect optical transitions of hot electrons in the bottom size-quantization band. The experimentally obtained emission spectra are compared with the spectra calculated taking into account scattering of electrons by optical phonons, impurities, and interfacial roughness and electron–electron scattering. Satisfactory agreement is obtained. The temperature of the hot electrons is determined from a comparison of the spectra. © *1998 American Institute of Physics.*
[S0021-3640(98)01407-8]

PACS numbers: 78.66.Fd, 73.20.Dx

1. INTRODUCTION

Intraband (occurring within a conduction band or valence band) transitions of electrons and holes in quantum wells have been under extensive investigation in the last ten years.[1] This is due in part to the development of fast IR-range detectors and modulators.[1] The development of quantum cascade[2] and fountain[3] lasers provided a new impetus to this direction in the physics of low-dimensional systems. Most works on optical intraband phenomena are devoted to the study of absorption and emission of IR radiation in the process of direct transitions of electrons or holes between size-quantization subbands. Specifically, the emission of far-IR radiation due to interlevel direct transitions of hot electrons[4] and holes[5–7] in quantum wells has been investigated. However, as far as we know, emission due to intrasubband transitions of hot charge carriers in quantum wells has not been investigated. At the same time, this phenomenon also accompanies the emission of light in direct transitions and serves as a source of information about charge carriers.

In the present work we observed and investigated experimentally and theoretically a

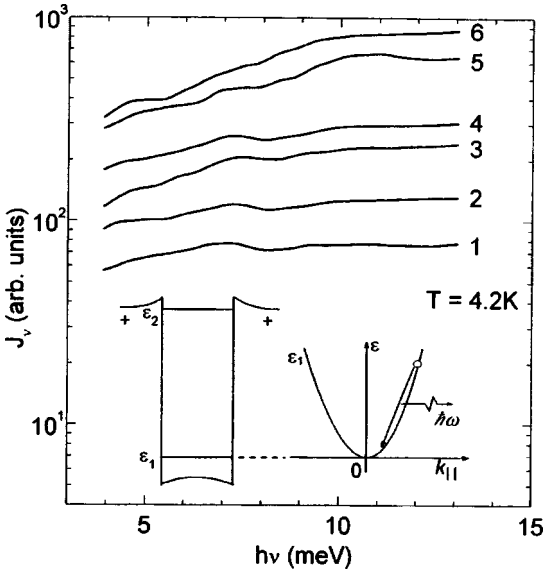

FIG. 1. Experimentally obtained spontaneous emission spectra from structures with GaAs/$Al_{0.22}Ga_{0.78}As$ quantum wells for different external longitudinal electric field intensities E, V/cm; *1* — 71, *2* — 214, *3* — 286, *4* — 414, *5* — 1429, *6* — 2000. Inset: Energy levels in a quantum well and scheme of optical transitions.

new phenomenon — terahertz emission due to indirect intrasubband transitions of hot electrons in a system of quantum wells in a longitudinal electric field. Despite the fact that in the present work intrasubband emission has been studied in specific GaAs/AlGaAs structures with quantum wells (GaAs/AlGaAs MQW) in the presence of electron heating by an electric field, this radiation is of a general character and can be observed in different systems and devices with quantum wells for all cases where the energy of the nonequilibrium electrons or holes is greater than the average energy of the equilibrium charge carriers. Such a situation can occur, for example, in the presence of injection or tunneling in heterostructures, in nanostructures, accompanying excitation of charge carriers by light, and so on.

Analysis of the emission spectra makes it possible, as will be shown below, to determine the temperature T_e of hot electrons. This method of determining the temperature of hot charge carriers is universal and has advantages over the well-known method of finding T_e by analyzing the short-wavelength wing of the photoluminescence spectrum (see, for example, Ref. 8) and over the method of finding of T_e from studying transport phenomena.

2. CALCULATION OF THE EMISSION SPECTRA

Let us consider a simple, selectively doped (doped barrier) square quantum well with one or several, for example, two, size-quantization levels ϵ_1 and ϵ_2 (see inset in Fig. 1). If the splitting $\Delta\epsilon = \epsilon_2 - \epsilon_1$ between the size-quantization subbands in a quantum well is sufficiently large, absorption and emission of light with photon energy $\hbar\nu \ll \Delta\epsilon$ and polarization in the plane of the quantum-size layers (the polarization vector $\mathbf{e}_\omega \perp Z$, where Z is the direction of growth of the structure) can occur only by means of indirect tran-

sitions of electrons within the ground subband $\epsilon_1(k_\parallel)$. Momentum conservation obtains as a result of electron scattering processes, the main ones being scattering by optical phonons, impurities, and interfacial roughness and electron–electron scattering. We note that absorption of light polarized perpendicular to the layers ($\mathbf{e}_\omega \parallel Z$) can occur only via intermediate states in the second size-quantization subband $\epsilon_2(k_\parallel)$. However, as calculations show, since $\hbar\nu \ll \Delta\epsilon$, the contribution of these transitions to absorption is small, and we shall neglect it in the present letter.

The spectral density of spontaneously emitted photons is described by the formula

$$\frac{dN}{d\omega} = \rho_\omega W^{em} = \rho_\omega \sum_{\mathbf{k}} \sum_{k'} w(\mathbf{k},\mathbf{k}') f_k (1 - f_{k'}), \tag{1}$$

where the wave vectors $\mathbf{k}$ and $\mathbf{k}'$ describe the initial and final states of an electron in a photon absorption event, $\rho_\omega = 2n^3\omega^2/\pi c^3$ is the photon density of states, n is the refractive index, c is the speed of light, and $w(\mathbf{k},\mathbf{k}')$ is the probability of photon emission during indirect transitions and is determined in second-order perturbation theory as

$$w(\mathbf{k},\mathbf{k}') = \frac{2\pi}{\hbar} \left| \sum_i \frac{H^\omega H^s}{\epsilon_0 - \epsilon_i} \right|^2 \delta(\epsilon_f - \epsilon_0). \tag{2}$$

Here ϵ_0, ϵ_1, and ϵ_f are the energy of the initial, intermediate, and final states of the system; H^ω is the matrix element of the electron–photon interaction energy; and, H^s is the matrix element of the interaction energy during scattering of an electron. The expressions for H^ω and H^s for electron–photon scattering are presented in Ref. 9. The matrix element of the interaction of an electron with an ionized impurity was obtained in Ref. 10. Scattering of an electron by interfacial roughness was studied, for example, in Ref. 11. In the present work we employ a simplified variant of the approach used in Ref. 11. The computational parameter was the density of scattering islands on the GaAs and AlGaAs interface. This density was determined by comparing the theoretically computed and experimentally determined values of the electron mobility.

It was shown in this work that electron–electron scattering can also lead to absorption and emission of long-wavelength radiation, but the necessary condition for this is that the nonparabolicity of the energy spectrum of an electron in a quantum well must be taken into account. Analytical expressions for the transition probability were obtained for the limiting cases of nondegenerate and highly degenerate electron gas. For the case of a nondegenerate electron gas the electron–electron Coulomb interaction leads to the following expression for the probability of spontaneous emission of a photon:

$$W^{em} = \frac{2^{10}\pi^3}{n^2} \frac{n_s^2 \lambda_g^4}{L_W} \frac{e^2}{\hbar} \frac{(k_B T_e)^2}{(\hbar\omega)^2} \frac{\epsilon_b}{\hbar\omega} \exp\left(- \frac{\hbar\omega}{k_B T_e} \right). \tag{3}$$

Here n_s is the surface density of electrons in the quantum well, $\lambda_g = \hbar/\sqrt{2m_c\epsilon_g}$, ϵ_g is the band gap, L_W is the width of the well, T_e is the electron temperature, $\epsilon_B = m_e e^4/2\hbar^2 k_0^2$ is the Bohr energy for electrons in the crystal, m_e is the effective mass, and k_0 is the static dielectric constant.

To calculate the spectral density we employed, following Ref. 1, the Fermi distribution with electron temperature T_e and took into account the electron scattering mechanisms presented above.

To make compare the computed and experimentally obtained spontaneous emission spectra correctly, in the calculations we also took into account the self-absorption of radiation. To this end, together with calculations of emission, we calculated the intraband absorption coefficient $\alpha(\omega)$. As a result of self-absorption, radiation leaves the sample from a depth not greater than the reciprocal $1/\alpha(\omega)$ of the absorption coefficient. Therefore the spectral dependence of the absorption coefficient introduces substantial corrections to the spectral density of the radiation calculated according to Eq. (1).

3. SAMPLES AND EXPERIMENTAL PROCEDURE

The $GaAs/Al_{0.22}Ga_{0.78}As$ heterostructures investigated contained 150 undoped quantum wells with width $L_W = 6$ nm, separated by doped barriers with width $L_B = 14$ nm. The width of a spacer was equal to 4 nm. They were grown by MBE on semi-insulating GaAs substrates. The electron mobility at $T = 77$ K was equal to $\mu = 3300$ cm^2/V·s. The surface electron density was $n_s = 3 \times 10^{11}$ cm^{-2}. Ohmic contacts were deposited on the ends of the structure, and a pulsed electric field ($\Delta t = 200$ ns) heating the electrons was applied to these contacts. The experiment was performed at temperature $T = 4.2$ K. The electric current flowed in the structure parallel to the quantum-size layers. Long-wavelength radiation was observed from the end of the structure with the aid of a wide-band Ge⟨Ga⟩ photodetector. The emission spectra were measured with a magnetic-field-tunable *n*-InSb filter (the method used for investigating the spectrum is described in greater detail in Ref. 12).

4. EXPERIMENTAL AND COMPUTATIONAL RESULTS

Figure 1 shows the spontaneous emission spectra from the above-described structures for different values of the longitudinal electric field. The structure in the curves is not a reflection of some feature of the phenomenon but is due to experimental error. As

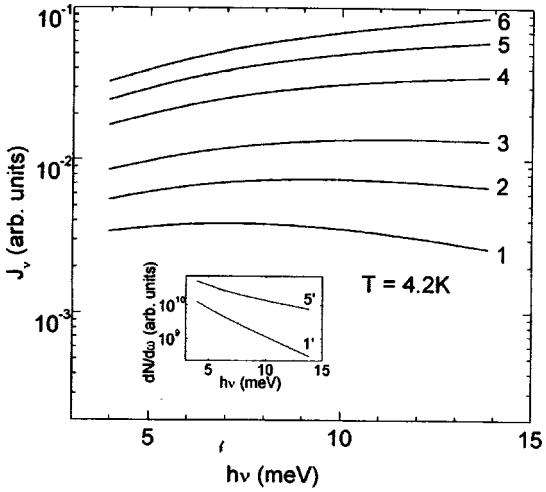

FIG. 2. Computed spontaneous emission spectra from structures taking into account self-absorption of radiation for different electron gas temperatures T_e, K: *1* — 50, *2* — 70, *3* — 100, *4* — 200, *5* — 300, *6* — 400. Inset: Spectral density of radiation at $T_e = 50$ K (*1′*) and 300 K (*5′*), neglecting self-absorption.

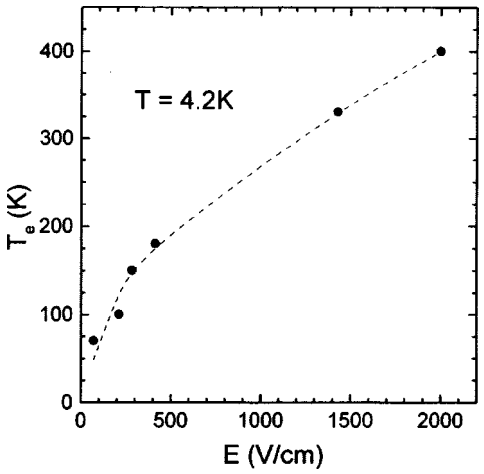

FIG. 3. Curve of the electron temperature obtained by comparing experimental data and the calculations.

the electric field intensity increases, the electron gas heats up, which increases the slope of the curves for the emission spectra. The computational results are presented in Fig. 2. It should be noted that in different regions of the spectrum and for different values of the electron temperature the ratio of the contributions of different scattering mechanisms to the spontaneous emission process changes. For example, in sufficiently high electric fields $E>100$ V/cm transitions of electrons involving scattering by optical phonons and impurities make the greatest contribution to the spontaneous emission of radiation, while the contribution of electron–electron scattering and scattering by interfacial roughness is much smaller. Self-absorption strongly affects the emission spectra from the sample (compare the data presented in Fig. 2 and the inset in this figure). Comparing the experimentally obtained and the computed emission spectra made it possible to determine the dependence of the electron temperature on the electric field (see Fig. 3). The dependence obtained agrees with the results of Ref. 13, where emission of a similar type but from a single heterojunction and much lower electric fields was investigated, as well as with the data of Ref. 14, where the electron temperature was found from the short-wavelength wing of the interband emission spectra ($h\nu>\epsilon_g$) from GaAs/AlGaAs quantum wells under intense optical excitation.

This work was supported in part by Grant 96-02-17404 from the Russian Fund for Fundamental Research, Grant 00615i96 from INTAS-RFBR, and Grant 96-1029 from the Ministry of Science and Technology under the program ''Physics of Solid-State Nanostructures,'' and also by the Federal Target Program ''Integration'' under Project No. 75.

[a)]e-mail: dmfir@phsc2.stu.neva.ru

[1] E. Rosencher and B. Levine (eds.), *Intersubband Transitions in Quantum Wells*, NATO ASI Series, Ser. B, Physics, Vol. 288, Plenum Press, New York, 1992.
[2] J. Faist, F. Capasso, D. L. Sivco *et al.*, Science **264**, 553 (1994).
[3] O. Gauthier-Lafaye, S. Sauvage, P. Boucaud *et al.*, Appl. Phys. Lett. **70**, 3197 (1997); in *Proceedings of the International Symposium ''Nanostructures: Physics and Technology''*, St. Petersburg, 1997, p. 567.

[4] E. Gornick, R. Schawarz, D. C. Tsui *et al.*, Solid State Commun. **38**, 541 (1981).
[5] L. E. Vorob'ev, L. E. Golub, and D. V. Donetskiĭ, JETP Lett. **63**, 977 (1996).
[6] V. Ya. Aleshkin, A. A. Andronov *et al.*, JETP Lett. **64**, 520 (1996).
[7] V. Ya. Aleshkin, A. A. Andronov *et al.*, Phys. Status Solidi B **204**, 173 (1997); *ibid.* **204**, 563 (1997).
[8] C. V. Shank and B. P. Zakharchenya (eds.), *Spectroscopy of Nonequilibrium Electrons and Phonons*, *Series on Modern Problems in Condensed Matter Sciences* (V. M. Agranovich and A. A. Maradudin, General Editors), Vol. 35, North-Holland, New York, 1992.
[9] V. L. Gurevich, D. A. Parshin, and K. É. Shtengel', Fiz. Tverd. Tela (Leningrad) **30,** 1466 (1988) [Sov. Phys. Solid State **30**, 845 (1988)].
[10] F. V. Gashimzade and E. V. Tairov, Phys. Status Solidi B **160**, K177 (1990).
[11] H. Sakaki, T. Noda, K. Hirakawa *et al.*, Appl. Phys. Lett. **51**, 1934 (1987).
[12] L. E. Vorob'ev, D. V. Donetskiĭ, and A. Kastal'skiĭ, Fiz. Tekh. Poluprovodn. **29,** 1771 (1995) [Semiconductors **29**, 924 (1995)].
[13] K. Hirakawa, M. Grayson, D. C. Tsui *et al.*, Phys. Rev. B **47**, 16651 (1993).
[14] E. Ozturk, N. C. Constantinou, A. Straw *et al.*, Semicond. Sci. Technol. **9**, 782 (1994).

Translated by M. E. Alferieff

Mechanism of silicon epitaxy on porous silicon layers

P. L. Novikov, L. N. Aleksandrov, A. V. Dvurechenskiĭ, and V. A. Zinov'ev

Institute of Semiconductor Physics, Siberian Branch of the Russian Academy of Sciences, 630090 Novosibirsk, Russia

(Submitted 26 December 1997; resubmitted 12 March 1998)
Pis'ma Zh. Éksp. Teor. Fiz. **67**, No. 7, 512–517 (10 April 1998)

The mechanism of silicon epitaxy on porous Si(111) layers is investigated by the Monte Carlo method. The Gilmer model of adatom diffusion extended to the case of arbitrary surface morphology is used. Vacancies and pendants of atoms are allowed in the generalized model, the activation energy of a diffusion hop depends on the state of the neighboring positions in the first and second coordination spheres, and neighbors located outside the growing elementary layer are also taken into account. It is shown that in this model epitaxy occurs by the formation of metastable nucleation centers at the edges of pores, followed by growth of the nucleation centers along the perimeter and the formation of a thin, continuous pendant layer. Three-dimensional images of surface layers at different stages of epitaxy were obtained. The dependence of the kinetics of the epitaxy process on the amount of deposited silicon is determined for different substrate porosities. © *1998 American Institute of Physics.* [S0021-3640(98)01507-2]

PACS numbers: 81.15.Hi

In recent years appreciable attention has been devoted to epitaxy on porous silicon. The preservation of long-range order and the low defect density on flat boundaries of porous layers make it possible to use these layers as a substrate for epitaxial growth of silicon. In a number of experimental works[1–3] it has been shown that it is possible to obtain continuous single-crystal films over a porous silicon layer. However, the mechanism by which pores near the initial surface of the porous layer become overgrown remains unclear. Most works on the simulation of growth on a flat solid surface are based on the Weeks–Gilmer model of diffusion inside a layer.[4] In this model two types of kinetic processes are studied: flow of atoms to a surface from a molecular beam, and thermally activated diffusion hops of atoms. The activation energy depends on the number of neighbors in the first and second coordination spheres. In the model, the following restrictions are important. In the first place, vacancies and pendant atoms are forbidden. In the second place, the neighbors in the second coordination sphere that are located outside the growing elementary layer are neglected. These restrictions make it impossible in principle to use this model to describe growth on a porous substrate. The first restriction rules out motion of atoms along vertical pore walls and the second one makes it impossible to take account of the specific nature of atom diffusion between layers. In the

present letter the model of Ref. 4 is extended so as to take account of interlayer diffusion, and the initial stage of Si epitaxy on porous Si(111) layers is studied on the basis of the model developed.

The generalized diffusion model is constructed on the basis of the initial premises of the Weeks–Gilmer model and includes two new assumptions. First, vacancies and pendants of atoms are permitted. Second, the summation of the second-nearest neighbors, which determine the activation energy of diffusion, extends over 12 positions in the second coordination sphere. Evaporation of atoms is not studied. All numerical parameters of the generalized model are corrected so that the growth process on a smooth Si(111) surface would occur identically to the process in the Gilmer diffusion model.

The computational algorithm is constructed on a $N_X \times N_Y \times N_Z = 160 \times 160 \times 20$ three-dimensional grid whose nodes correspond to regular positions of atoms in the crystal structure of silicon. The state of the cells that are filled with atoms is characterized by the numbers N_1 and N_2 of neighbors in the first and second coordination spheres ($0 \leqslant N_1 \leqslant 4$, $0 \leqslant N_2 \leqslant 12$), respectively. Each atom executes a diffusion hop with probability $p(N_1, N_2, T)$. The first position of a diffusion hop is chosen randomly among the unoccupied cells in the first and second coordination spheres. Transitions which result in an atom not having any neighbors in the first coordination sphere are forbidden. The probability of a diffusion hop (with the condition that the end-point position is free) equals

$$p(N_1, N_2, T) = p_0 \cdot \exp(-E/kT), \quad E = E_1 N_1 + E_2 N_2,$$

where k is Boltzmann's constant, T is the temperature, and $p_0 = \exp((E_1 + 3E_2)/kT)$ is a factor chosen so that the probability of a diffusion hop on the free (111) surface equals 1. To decrease the amount of computation, a threshold probability p_s, which limits the number of ''candidates'' for a diffusion hop (active array) to atoms for which $p(N_1, N_2, T) > p_s$, is introduced. Scanning over the elements in an active array is performed during an iteration. The time interval corresponding to one iteration is estimated as $\tau = \chi \cdot p_0 / \nu$, where $\nu = 2.5 \times 10^{13}$ s^{-1} is the frequency of atomic oscillations and $\chi = 6/16$ is a coefficient that takes account of the ratio between the numbers of possible final positions for Si(111) in the intralayer and generalized diffusion models.

The parameter E_2 characterizes the kinetics of incorporation/detachment of atoms on the faces of the elementary layers. These processes were investigated by the simulation method of Ref. 5, where for $E_2 = 0.2$ eV good agreement with experiment was obtained. Since in our model an adatom on a smooth surface has one neighbor in the first and three in second coordination spheres, the activation energy of surface diffusion can be expressed as $E_A = E_1 + 3E_2$. At the same time, the value $E_A = 1.3 \pm 0.2$ eV was obtained experimentally in a number of works. We employed the value $E_A = 1.34$ eV,[5] which corresponds to $E_1 = 0.74$ eV.

The probability that an atom from a molecular beam reaches the surface over time τ is

$$p_F = 2F\tau N_X N_Y,$$

where F is the molecular flux density (bilayer/s).

The growth processes on a smooth Si(111) surface in the Gilmer model and in the generalized model presented above proceed identically.

A $160\times160\times14$ layer, through which cylindrical openings penetrate, was taken as the substrate. The cylinders were distributed randomly over the surface and oriented along the normal to it. The number and radius of the cylinders are parameters of the simulation.

Two competing processes occur during epitaxy on a porous substrate: island growth and overgrowth of pores on the free surface. The specific nature of the first process is due to the presence of effective sinks in the form of pores, and that of the second is due to interlayer diffusion.

Figure 1 shows a fragment of a layer at different stages of epitaxy. A graduated scale of tones from dark to light with increasing height relative to the initial surface is used to show the surface relief. Islands of the next layer are indicated by the light color. These islands grow by incorporation of adatoms at the boundaries. The adatoms reaching the surface of small islands from a molecular beam diffuse rapidly to the boundary and pass into a lower-lying layer and are incorporated. Under the conditions of the computer simulation ($T=1000$ K, $F=1.15$ bilayers/s) the formation of pendant configurations and ''frozen-in'' vacancies at the boundaries of the islands, though not forbidden, is unlikely. The transverse sections shown on the end faces (pores — dark tone, silicon — light tone) make it possible to follow the evolution of the structure of the pores over depth. One can see that the main changes in the pores occur in the upper monolayers. This justifies the choice of a thin surface layer of the substrate as the object for simulation.

The process by which pores become overgrown is random. However, statistical analysis of the bond configurations formed between the structure and the atoms diffusing along the pore walls reveals some general laws. At first, an unstable nucleation center forms at the edge of a pore — an atom secured by two bonds on the lateral surface of a pore (Fig. 2a). The nucleation center forms a third bond with the structure and becomes stable after a new atom attaches to it. Thus, as atoms are added, a pendant layer one to two diatomic layers thick forms along the perimeter of a pore and gradually closes it. It can be shown that desorption processes do not destroy an unstable nucleation center before a new atom attaches to it. Assuming that the activation energy of desorption depends on the number of first and second neighbors as $E_{DS}=E_{1DS}N_1+E_{2DS}N_2$ and comparing its value for a smooth Si(111) surface 2.1 eV (Ref. 6) with the activation energy of surface diffusion 1.34 eV (2.1/1.34 = 1.57), we obtain the following estimate for the parameters E_{1DS} and E_{2DS}:

$$E_{1DS}\approx E_1\cdot 1.57=1.16\text{ eV},\quad E_{2DS}\approx E_2\cdot 1.57=0.31\text{ eV}.$$

Then the probability that an atom in a pendant layer desorbs can be estimated from the ratio to the probability of a diffusion hop:

$$p_{DS}(N_1,N_2,T)/p(N_1,N_2,T)\approx\exp((E_1-E_{1DS})\cdot N_1+(E_2-E_{2DS})\cdot N_2)/kT).$$

For the configuration $N_1=1$, $N_2=2$, corresponding to the least strongly bound atom in the pendant layer, for $T=1100$ K we have $p_{DS}/p\approx1.2\times10^{-3}$. Since this is an upper limit, the contribution of desorption to the process leading to the formation of a pendant layer can be neglected at temperatures $T\leqslant1100$ K.

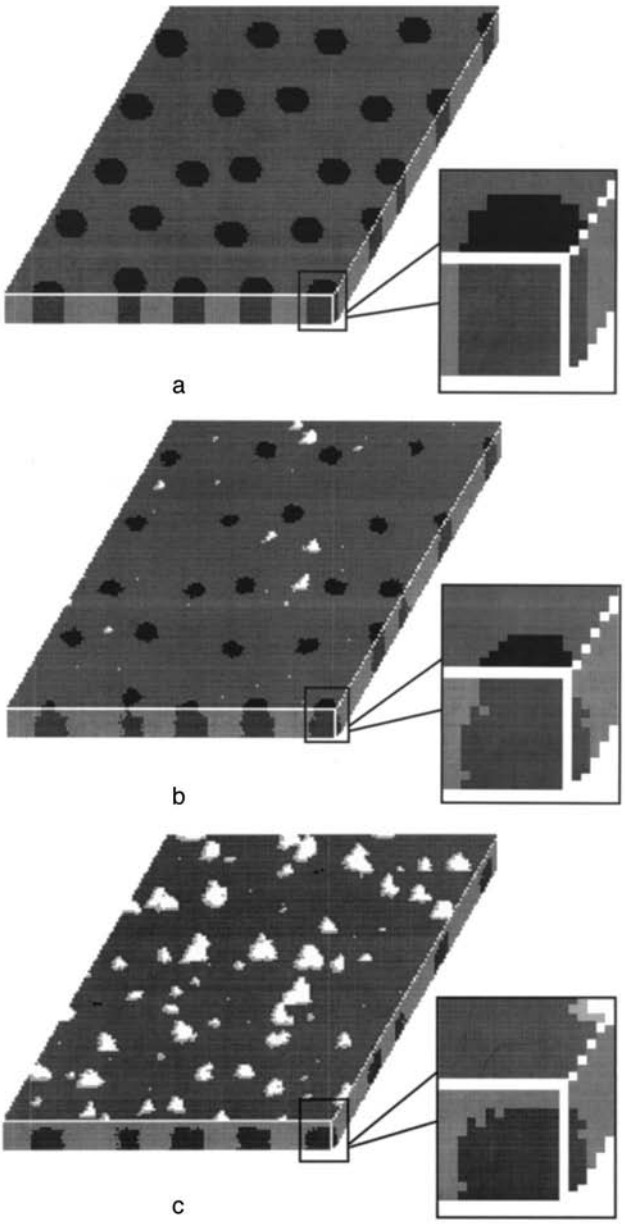

FIG. 1. Fragment of a porous Si(111) layer at different stages of Si epitaxy: a) Before epitaxy starts, b) after a 0.25 bilayer is deposited, c) after 0.5 bilayers are deposited ($T=1000$ K, $F=1.15$ bilayers/s).

As long as the diameter of a still-open pore is sufficiently large ($\geqslant 10$ interatomic distances), the growth front of the pendant layer is divided among six distinguished directions, reflecting the symmetry of the Si(111) structure. This explains the tendency for the shape of a pore edge to transform from round to hexagonal. As the pore grows in

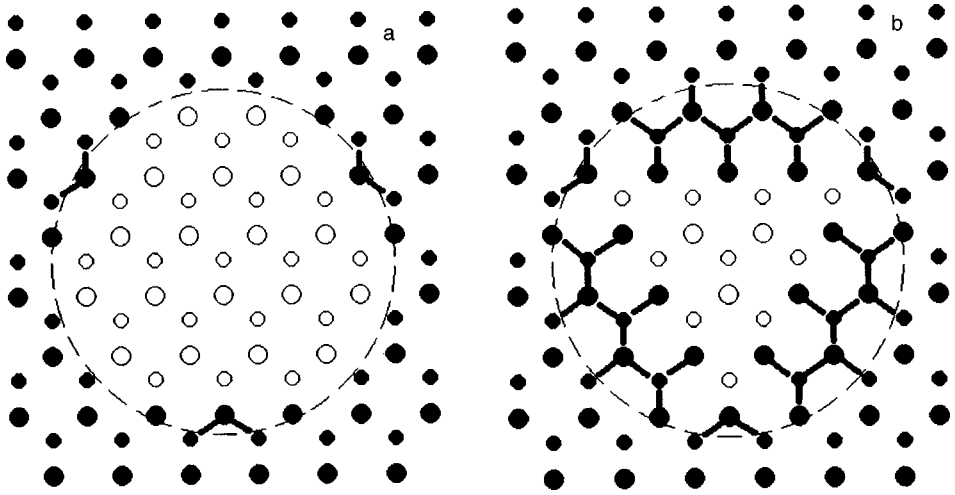

FIG. 2. Formation of a pendant bilayer. The regular positions in the planes of a Si(111) double layer are denoted by large and small circles. Occupied positions are marked in black. Bonds with the nearest neighbors are shown for atoms in the pendant layer: a) unstable nuclei, b) pendant layer formed by attachment of new atoms to stable nucleation centers.

size, random fluctuations intensify the nonequivalence of the distinguished directions and the form of the pore edge changes from hexagonal to triangular (Fig. 2b).

As a characteristic of the surface morphology of the porous Si(111) layer, the density S (Ref. 5), defined as the fraction of atoms on the vertical sections, was calculated. Figure 3 shows the density of steps as a function of the amount of deposited material for different porosities P. At the initial stage the curves have a descending section for $P \geqslant 0.15$. This corresponds to a decrease of the roughness of the growing surface as a result of overgrowth of the pores. At this stage the pores are effective sinks for adatoms, island nucleation is suppressed, and most atoms from the deposition beam drift into the pores. This result agrees with RHEED data[3] obtained during Si epitaxy on porous Si(111). The roughness continues to decrease up to a certain time, after which it starts to increase. The increase in S is due to nucleation and subsequent growth of islands on the surface (Fig.

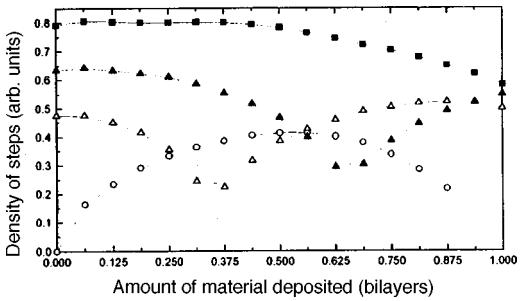

FIG. 3. Density of steps versus the amount of deposited silicon for different substrate porosities: ○ — $P = 0$, △ — $P = 0.18$, ▲— $P = 0.32$, ■ — $P = 0.5$ ($T = 1000$ K, $F = 1.15$ bilayers/s).

2b). The pores become small and they can no longer suppress island growth. In Fig. 3 one can see that the length of the section of decreasing S is proportional to the porosity. This means that the fraction of atoms drifting into pores grows with increasing porosity, i.e., with increasing effectiveness of pores as sinks. The decrease of S observed for $P=0.18$ as the amount of deposited silicon continues to increase is due to the onset of quasiperiodic oscillations of S with a period of one diatomic layer. This corresponds to quasiperiodic changes in surface morphology, which occur during epitaxy of each subsequent biatomic layer. The oscillations of S appear at a larger thickness of the deposited layer than in the case of epitaxy on a smooth substrate ($P=0$). For $P=0.32$ and $P=0.5$ the oscillations start after one biatomic layer has been deposited and for this reason they are not seen in the plot.

When an oxide is present on the walls of the pores, the epitaxy mechanism can change. Taking account of this factor falls outside the scope of our work.

This work was performed on the basis of the Gilmer diffusion model extended to the case of diffusion between layers. For Si(111) modeling revealed a possible detailed mechanism of growth at the initial stage of epitaxy via the formation of a pendant layer. The specific nature of the kinetics of epitaxial growth on porous layers is determined by competition between trapping of atoms in pores and on islands. The approaches developed during the construction of the generalized model are universal and can be use for analysis of processes with the participation of atomic diffusion on a crystal surface with arbitrary morphology.

[1] T. Yasumatsu, T. Ito, H. Nishizawa, and A. Hiraki, Appl. Surf. Sci. **48/49**, 414 (1991).
[2] V. G. Shengurov, V. N. Shabanov, N. V. Gudkova, and B. Ya. Tkach, Mikroélektronika **222**, 19 (1993).
[3] E. Nossarzewska-Orlowska, D. Lipin'ski, M. Pawlowska *et al.*, Electron Technology **29**, 196 (1996).
[4] J. D. Weeks and G. H. Gilmer, Adv. Chem. Phys. **40**, 157 (1979).
[5] D. D. Vvedensky and Sh. Clarke, Surf. Sci. **225**, 373 (1990).
[6] A. V. Latyshev, A. L. Aseev, A. B. Krasilnikov, and S. I. Stenin, Surf. Sci. **213**, 157 (1989).

Translated by M. E. Alferieff

On the relation between conduction and diffusion in a random walk along self-similar clusters

V. E. Arkhincheev

Buryat Science Center, Siberian Branch of the Russian Academy of Sciences, 670047 Ulan-Udé, Russia

(Submitted 26 December 1997; resubmitted 19 February 1998)
Pis'ma Zh. Éksp. Teor. Fiz. **67**, No. 7, 518–520 (10 April 1998)

The relation between diffusion and conduction in the random walk of a particle by means of Lévy hops is investigated. It is shown that on account of the unusual character of Lévy hops, the mobility of a particle is a nonlinear function of the electric field for arbitrarily weak fields. © *1998 American Institute of Physics.*
[S0021-3640(98)01607-7]

PACS numbers: 61.46.+w, 72.20.Ht, 66.30.−h

1. The numerical simulation of hopping by means of Lévy hops has shown that the points visited during diffusion form spatially well-separated clusters. A more detailed analysis shows that each cluster in turn consists of a collection of clusters. Thus a hierarchical structure consisting of self-similar structures is formed.[1] A characteristic feature of Lévy hops is the possibility that at each step a particle is displaced over an arbitrarily long distance, so that the rms displacement per unit time is infinite, while the probability distribution in the Fourier representation has the form

$$P(k,t)=\exp(-A|k|^{\mu}t), \tag{1}$$

where A and μ are positive quantities, $1<\mu<2$. Such distributions are called Lévy distributions. A more detailed discussion of Lévy hops is given in Ref. 2.

In the present letter it will be shown that the Lévy distribution in an electric field can be represented in the form

$$P(k,t;E)=\exp(-A|k|^{\mu}t+ikVt). \tag{2}$$

Then the drift velocity is a nonlinear function of the electric field:

$$V\sim E^{(\mu-1)}. \tag{3}$$

It should be emphasized that this nonlinearity occurs in arbitrarily weak fields and is a consequence of the unusual character of the diffusion. In other words, Ohm's law (linear response to a field) is a consequence of the ordinary character of diffusion. For diffusion of a different character Ohm's law may not apply at all. This result can be elucidated as follows. It is easy to obtain from Eqs. (1) and (2) a continuity for diffusion along self-similar clusters in an electric field

$$[\partial/\partial t+(A|k|^{\mu}+ikV)]N(k,t)=0. \tag{4}$$

Here $N(k,t)$ is the density of diffusing particles in the Fourier representation, the current has diffusion and field components, and the field current $J=NV$ has the standard form.

Next, we employ the well-known Einstein arguments. In equilibrium the diffusion current J_d is compensated by the field current J_f, and the distribution function must have the Boltzmann form

$$J_d+J_f=0, \quad N=\exp(-U/kT), \tag{5}$$

where U is the potential energy. From Eqs. (4) and (5), using the definition for a derivative of fractional order in the form of a series

$$|k|^{\mu}=\lim_{\epsilon\to 0}(\Delta^2+\epsilon)^{\mu}=\sum_{n=0}^{\infty} C_n^{\mu}(\Delta/\epsilon^n),$$

we obtain a general expression for the drift velocity

$$\mathbf{V}=\exp(U/kT)\lim_{\epsilon\to 0}(\Delta^2+\epsilon)^{\mu-2/4}/\nabla\ \exp(-U/kT). \tag{6}$$

In a uniform electric field $U=-qEx$ the result (3) obtains.

2. Let us now examine the one-dimensional discrete analog of Lévy hops.[3] Let the probability that a particle occupies the lth site after n steps be $P_n(l)$ and let $f(l)$ be the probability distribution of hops over lengths:

$$P_{n+1}(l)=\sum_{m=-\infty}^{\infty} f(l-m)P_n(m). \tag{7}$$

Let $f(l)$ be given by

$$f(l)=\sum_{n=0}^{\infty} a^{-n}(\delta_{l,-b^n}+\delta_{l,b^n}), \tag{8}$$

where $\delta_{n,m}$ is the Kronecker delta. Then the structure function for such a random walk is

$$\lambda=\int f(l)\exp(ikl)dl=\sum_{n=0}^{\infty} a^{-n}\cos(kb^n). \tag{9}$$

Note that the structure function λ satisfies the functional relation

$$\lambda(k)=a\lambda(kb).$$

Therefore as $k\to 0$ it must exhibit power-law behavior with exponent $\mu=\ln a/\ln b$. Nonanalytic behavior of the form $|k|^{\mu}$ in the limit $k\to 0$ with exponent μ can be obtained by a Mellin transform or by the Poisson formula for summing series. See Ref. 3 for a more detailed discussion.

Let us now introduce anisotropy into the random walk along self-similar clusters. By virtue of the specific nature of Lévy hops a particle can be displaced in one hop over an arbitrary distance b^n. For this reason a small anisotropy $(1+\alpha)$, where $\alpha=qEs/kT$, for a displacement over a short distance s turns out to be exponentially large at large distances b^n. Since at each step a diffusing particle leaves a site, the sum of the probabilities

W_+ and W_- of motion parallel and antiparallel, respectively, to the field must equal 1: $W_+ + W_- = 1$. Hence we obtain an expression for the probabilities of motion parallel and antiparallel to the field:

$$W_\pm = (1 \pm \alpha)^{b^n} / [(1+\alpha)^{b^n} + (1-\alpha)^{b^n}].$$

Therefore the structure function $\lambda(k;E)$ in the case of diffusion in an electric field by means of Lévy hops equals

$$\lambda(k;E) = \sum_{n=0}^{\infty} a^{-n} [\cos(kb^n) + i \sin(kb^n)(W_+ - W_-)]. \tag{10}$$

Just as in the case of ordinary diffusion, for small $k \to 0$ the second term contains the drift velocity

$$V = i\partial\lambda(k;E)/\partial t|_{k\to 0} = \sum_{n=0}^{\infty} (b/a)^n \{[(1+\alpha)^{b^n} - (1-\alpha)^{b^n}]/[(1+\alpha)^{b^n} + (1-\alpha)^{b^n}]\}$$

$$\cong \sum_{n=0}^{\infty} (b/a)^n \tanh(\alpha b^n), \tag{11}$$

where $\tanh(y)$ is the hyperbolic tangent. To calculate the velocity we employ the Poisson formula

$$\sum_{n=0}^{\infty} f(n) = 1/2 f(0) + \int_0^{\infty} f(t)dt + 2\sum_{m=1}^{\infty} f(t)\cos(2mt). \tag{12}$$

In our case $f(t) = (b/a)^t \tanh(\alpha b^t)$. Making the two substitutions $t' = t \ln b$ and $z = \exp t'$, we obtain $f(z) = z^{-\mu} \tanh(\alpha z)$. Therefore $V(E) = \alpha/2 + \alpha^{(\mu-1)} \times [\Sigma_{m=-\infty}^{\infty} \int_1^{\infty} \tanh(z) z^{-\gamma_m} dz + \int_0^{\alpha} \tanh(z) z^{-\gamma_m} dz]$, where the exponent $\gamma_m = \mu + 2\pi m i / \ln b$. It is easy to see that for small α the second term in brackets is small compared to the first term. Therefore in arbitrarily weak electric fields we obtain for the velocity the nonlinear (in the electric field) function (3).

3. Let us now discuss the results obtained. Both the nonanalytic behavior of the structure function for small $k \to 0$ and the nonlinear electric-field dependence of the velocity in arbitrarily weak fields are asymptotic. A dependence of the form (12) was predicted earlier in a phenomenological description of anomalous diffusion on percolation clusters.[4] However, an attempt to observe this nonlinearity by numerical simulation of drift on clusters was unsuccessful,[5] since in the desired range of fields the electric field itself induces traps. These traps are segments of percolation paths directed antiparallel to the electric field. For this reason, the question of the nonlinear dependence of the velocity on the electric field as a consequence of the anomalous character of the diffusion has remained open, as has the question of the domain of applicability of the phenomenological approach. In the present letter the nonlinear electric-field dependence of the velocity was established for a model of diffusion by means of Lévy hops.

[1] B. Mandelbrot, *Fractals: Form, Chance and Dimension*, Freeman, San Francisco, 1977.
[2] G. Zumofen and J. Klafter, Physica D **69**, 436 (1993); G. Zumofen and J. Klafter, Phys. Rev. E **47**, 851 (1993).
[3] B. D. Hughes, M. F. Shlesinger, E. W. Montroll, Proc. Natl. Acad. Sci. (USA) **78**, 3287 (1981).

[4] V. E. Arkhincheev, É. M. Baskin, and É. G. Batyev, J. Non-Cryst. Solids **90**, 21 (1987).
[5] V. E. Arkhincheev and É. M. Baskin, Zh. Éksp. Teor. Fiz. **100,** 292 (1991) [Sov. Phys. JETP **73**, 161 (1991)].

Translated by M. E. Alferieff